THE ACOUSTIC IMPEDANCE OF LIQUID HELIUM-THREE

by

Kenneth John Butcher, B.Sc.,

Department of Physics

Bedford College

University of London

A thesis submitted for the degree of Doctor of Philosophy

at the University of London

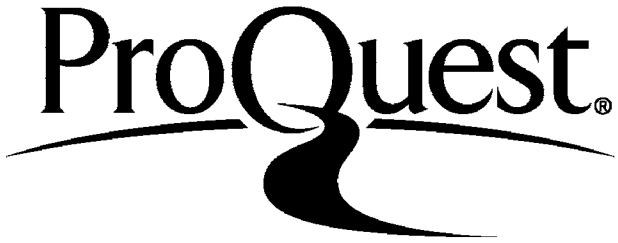

Abstract

Measurements of the transverse acoustic resistance of liquid helium-3 have been made at pressures between 0.3 bar and 28.0 bar in the temperature range 0.015 Kelvin to 1.0 Kelvin using a helium-3/helium-4 dilution refrigerator. The method involved observation of the decay of a series of echos generated in a piezoelectric rod immersed in the liquid, one end of the rod being excited by a resonant cavity. The frequency of this cavity was 242 MHz in the greater proportion of this work but similar measurements were also made at 1048 MHz. The measurements at the lower frequency have confirmed the existence of the collective oscillation known as transverse zero sound in liquid helium-3 at higher pressures, as predicted by the Landau Theory of a Fermi liquid. This has enabled an estimate to be made of the magnitude of the symmetrical Landau parameter, F_2^S. The result obtained was in agreement with those of other experimenters who have used a variety of methods to determine F_2^S.

A similar experimental technique has been used to study the longitudinal acoustic resistance of liquid helium-3 in order to investigate the anomalously high value of F_2^S indicated by previous measurements of this phenomenon. These measurements, both transverse and longitudinal, have mainly been carried out on pure helium-3 (ie. better than 99.9997 per cent) but some data have been obtained for the transverse acoustic resistance of helium-3 in which a small amount of helium-4 (about 1%) was present. These results enabled the determination of the acoustic resistance of an assembly of non-interacting Fermions.

CONTENTS :

LIST OF FIGURES :

Page

CHAPTER ONE

1.0. THE FERMI LIQUID

1.1. Introduction

The Landau theory of superfluidity in a quantum liquid of Bosons was developed to explain the observed behaviour of superfluid liquid helium (ie. HE II). The lack of a complementary theory in the case of particles obeying Fermi-Dirac statistics resulted in the theory of a Fermi liquid, an example of which seemed to be liquid helium-3 in what is now known as the 'normal' regime. It is interesting to note that, in his original paper of 1956, Landau allows for the existence of superfluidity in the case of helium-3 by pointing out that, whilst the theory of a Bose liquid requires superfluid properties to be exhibited, the converse theorem that a Fermi liquid cannot be a superfluid is not generally true. The validity of this far-sighted comment was demonstrated sixteen years later when the superfluid phases of liquid helium-3 were experimentally observed for the first time.

The importance of the behaviour of sound in a Fermi liquid stems from Landau's prediction of new modes of sound propagation at very low temperatures. Fermi liquid theory suggests the existence of a series of modes of which the first is identified as a longitudinal wave, similar to ordinary, hydrodynamic, sound in a conventional liquid; and the second as a transverse oscillation that resembles high-frequency shear waves in a viscoelastic medium. These modes were given the general name

'Zero sound' by Landau since they can, in principle, exist at the absolute zero of temperature. The interaction forces between the quasiparticles that form the Fermi liquid are described by a series of parameters and the Landau theory showed that the properties of the zero sound modes would depend upon the values of certain members of the series. Obviously, a full knowledge of the properties of a Fermi liquid requires a complete knowledge of the Landau parameters. However, if the theory is to be of use in predicting the behaviour of real systems, knowledge of the first few parameters only should suffice to enable good approximations to be made. A study of sound in a Fermi liquid helps in the determination of these parameters which may then be used to build-up a complete picture of the system.

The longitudinal zero sound mode was first observed in 1964 by Keen, Matthews and Wilks, and has since been studied in great detail. Recently this mode has been used to study the superfluid phases of liquid helium-3 and has been particularly helpful in unravelling the complexities of the anisotropic 'A' phase. The history of transverse zero sound is much shorter, being observed for the first time by Roach and Ketterson towards the end of 1975, some time after the commencement of this work. The problems involved in the detection of the transverse mode are formidable due to the extremely high attenuation in the liquid and this will probably limit its usefulness as an experimental probe. In this work, transverse zero sound was detected by observing the change in acoustic impedance between a piezoelectric transducer and the liquid, following the method employed by Wilks and his co-workers in their original work on the longitudinal mode.

The full theory of transverse acoustic impedance is rather complex as recently derived by Flowers and Richardson, and has been included in some detail since a careful quantitative analysis of the experimental data is necessary to clearly establish the existence of transverse zero sound. The important contributions to the theory made by Fomin are also discussed in detail and some attempt has been made to place these in context within the framework of the complete theory. To make this work to some extent self-sufficient, the theoretical discussion starts with an outline of the Landau Theory of a Fermi Liquid and sets down some of the more important results.

1.2. Landau Theory

The theory of a Fermi gas requires the interactions between the particles to be weak. However, the theory has been applied in situations where this requirement is not met and it is then impossible to determine which properties of the gas model correspond to the real situation and which are intrinsic to the model. To overcome this problem Landau formulated the theory of a Fermi liquid (Landau (1957) and (1959)) in which larger interactions could be considered. The model was later extended by Abrikosov and Khalatnikov (1959).

Landau considered a Fermi gas at a temperature below the degeneracy temperature and introduced weak interactions between the particles. In the diffuse zone, near the Fermi surface, the average energy of the thermally excited Fermions is directly proportional to temperature. Therefore at a sufficiently low temperature, known as the Dingle temperature, the energy

indeterminacy due to collisions is small compared to the average energy. Also, at very low temperatures, the damping of the excitations (given by the imaginary part of their self energy) will be small compared to the real part of the energy.

Landau assumed the following; each energy level corresponds to a level in a non-interacting system such that when the interaction is 'turned-on' gradually, the atoms become quasiparticles, each of which possesses a definite energy. The quasiparticles obey Fermi-Dirac statistics and their number always coincides with the number of particles in the liquid. The momenta of the particles is unchanged as the interaction is turned on. This leads to the quasiparticle being considered as a particle in a self-consistent field of particles. In such a field, the energy of the system is not simply the sum of the energies of the individual particles but depends upon the distribution function of the particles. Landau therefore defines the energy of a quasiparticle (ϵ) by the relation :

$$\delta E = \int \epsilon \, \delta n \, d\tau \qquad (1.2.1.)$$

δE is the change in energy density of the whole system resulting from an infinitesimal change in the distribution function (n). The integration is over all momentum space so that ;

$$d\tau = \frac{2 \, dp_x \, dp_y \, dp_z}{(2\pi\hbar)^3}$$

Because the quasiparticles have non-integer spin quantum number the total energy will depend upon the spin states so Landau introduced the spin matrix $\underline{\sigma}$. Bearing in mind that ϵ and n are now matrices,

equation (1.2.1.) is rewritten in a form that includes the spin dependence ;

$$\delta E = \frac{1}{2} S_{p\sigma} \int \epsilon \, \delta n \, d\tau \qquad (1.2.2.)$$

$S_{p\sigma}$ implies summation of the diagonal elements of the matrix product and the factor $\frac{1}{2}$ appears because both spin states are included in the definition of $d\tau$.

Landau determines the distribution function $n(\epsilon)$ by maximising the entropy of the system subject to the conditions that the total energy and total number of quasiparticles is constant. Since there is an exact correspondence between the particles of a perfect Fermi gas and the quasi-particles of a Fermi liquid, the entropy equation for a perfect gas is used to obtain the expression ;

$$n(\epsilon) = \left[\exp\left(\frac{\epsilon - \mu}{kT} \right) + 1 \right]^{-1} \qquad (1.2.3.)$$

where μ is the chemical potential and k is the Boltzmann constant. The difference between this result and the equivalent expression for a Fermi gas is that, in this case, ϵ is a function of n .

The energy spectrum of the quasiparticles near the Fermi surface, $\epsilon(p)$, is obtained by assuming a temperature sufficiently low that $\epsilon \approx \mu$ Landau obtains the result ;

$$\epsilon = \mu + \frac{p_F}{m^*} (p - p_F) \qquad (1.2.4.)$$

where p_F is the Fermi momentum and m^* is the "effective mass" of the quasiparticle which is defined, by analogy with Fermi gas theory, thus ;

$$\left(\frac{\partial \epsilon}{\partial p}\right)_F = \frac{p_F}{m^*} = v_F \qquad (1.2.5.)$$

(The term in parantheses is evaluated at the Fermi surface).

1.3. The Interaction Function

By considering small deviations from equilibrium at temperatures just above T = 0, the quasiparticle energy may be expressed thus ;

$$\epsilon = \epsilon_F(\underline{p}, \underline{\sigma}) + \delta\epsilon(\underline{p}, \underline{\sigma}) \qquad (1.3.1.)$$

where ϵ_F is the Fermi energy.

Landau introduces the interaction function f, an operator dependant upon momentum $\underline{p}$ and spin coordinate $\underline{\sigma}$, by rewriting (1.3.1.) in the form ;

$$\epsilon = \epsilon_F(\underline{p}, \underline{\sigma}) + \frac{1}{2} S_{p\sigma} \int f(\underline{p}, \underline{\sigma}; \underline{p}', \underline{\sigma}') \delta n(\underline{p}', \underline{\sigma}') d\tau' \qquad (1.3.2.)$$

where $\delta n = n - n_F(0)$, that is, the deviation of n from its equilibrium value at T = 0.

To obtain an expression relating the interaction function to the effective mass, Landau uses Galileo's principle of relativity which states that the momentum arriving at unit volume of liquid must equal the mass flow density.

$$\frac{1}{2} S_{p\sigma} \int \underline{p}\, n\, d\tau = \frac{1}{2} S_{p\sigma} \int m \frac{\partial \epsilon}{\partial \underline{p}}\, n\, d\tau \qquad (1.3.3.)$$

By taking the variational derivative of this expression with respect to n, we obtain, at the Fermi surface ;

$$\frac{1}{m} = \frac{1}{m^*} + \frac{p_F}{2(2\pi\hbar)^3} S_{p\sigma} S_{p\sigma'} \int f(\chi) \cos\chi \, d\Omega \qquad (1.3.4.)$$

In this expression $f(\chi)$ is the value of f at the Fermi surface, where $p \approx p' \approx p_F$, and χ is the angle between $\underline{p}$ and $\underline{p}'$ The integral is now taken over real space, $d\Omega$ being an element of solid angle.

1.4. The Landau Parameters

In general, the interaction function f depends upon spin, ie :

$$f = f(\underline{p}, \underline{\sigma} ; \underline{p}', \underline{\sigma}')$$

Landau separates f into two components one of which is independant of spin, the other spin dependant.

$$f(\underline{p},\underline{\sigma};\underline{p}',\underline{\sigma}') = f(\underline{p},\underline{p}') + \zeta(\underline{p},\underline{p}')\,\underline{\sigma}.\underline{\sigma}' \qquad (1.4.1.)$$

We are only concerned with quasiparticles near the Fermi surface, therefore $p \approx p' \approx p_F$ and the two components of the interaction function will depend only upon the angle χ between $\underline{p}$ and $\underline{p}'$.

ie $$f(\underline{p},\underline{\sigma};\underline{p}',\underline{\sigma}') = f(\chi) + \zeta(\chi)\,\underline{\sigma}.\underline{\sigma}'$$

Landau now defines two new functions ;

$$F^S(\chi) = \left(\frac{d\tau}{d\epsilon}\right)_F f(\chi) \qquad ; \qquad F^A(\chi) = \left(\frac{d\tau}{d\epsilon}\right)_F \zeta(\chi) \qquad (1.4.2.)$$

where the density of states is evaluated at the Fermi surface,

ie $$\left(\frac{d\tau}{d\epsilon}\right)_F = \frac{m^* p_F}{\pi^2 \hbar^3}$$

Since the magnitudes of the momenta before and after scattering are roughly equal the invariance of the system under spatial rotation means that F^S and F^A depend only upon the angle χ. Consequently they may be expanded in Legendre polynomials ;

(i) $$F^S(\chi) = \sum_n F_n^S\, P_n(\cos\chi)$$

(ii) $$F^A(\chi) = \sum_n F_n^A P_n(\cos\chi)$$

Landau's original notation was $F(\chi)$ and $G(\chi)$ respectively but it is now more common to refer to F^S and F^A which are known as the symmetric and antisymmetric Landau parameters.

The symmetrical parameter F_1^S can be obtained by substituting for $f(\chi)$ in (1.3.4.) and performing the integration to give ;

$$\frac{1}{m} = \frac{1}{m^*}\left(1 + \overline{F^S \cos\chi}\right)$$

where the bar denotes the average value over the angle.

Finally, since $\overline{F^S \cos\chi} = \frac{F_1^S}{3}$, we have ;

$$\frac{1}{m} = \frac{1}{m^*}\left(1 + \frac{F_1^S}{3}\right) \qquad (1.4.3.)$$

The effective mass may be determined from measurements of the heat capacity, substituting m^* for m in the equation for the heat capacity of a Fermi gas.

The first symmetrical parameter F_o^S is determined by measuring the velocity of ordinary (hydrodynamic) sound in the Fermi liquid and using the relationship derived by Landau ;

$$c^2 = \frac{p_F^2}{3m^2}\left[\frac{1 + \overline{F^S}}{1 + \overline{F^S \cos\chi}}\right]$$

where c is the velocity of sound in the liquid.

Again, since $\overline{F^s} = F_o^s$, we may write :

$$c^2 = \frac{p_F^2}{3m^2}\left[\frac{1 + F_o^s}{1 + F_1^s/3}\right] \qquad (1.4.4.)$$

Both of these expressions (1.4.3.) and (1.4.4.) are exact by virtue of the nature of $\overline{F^s}$ and $\overline{F^s \cos\chi}$ (being averages over the whole solid angle) and do not involve any arbitrary truncation of the infinite series of Landau parameters. Therefore, the first two symmetrical parameters of the series may be determined exactly by relatively precise experimental measurements.

Landau's original paper also shows how the first assymmetric parameter may be determined from measurements of the magnetic susceptibility. By considering the change in energy resulting from the application of a magnetic field, he obtains the expression ;

$$\chi_M = \frac{\beta^2 \left(\frac{d\tau}{d\epsilon}\right)_F}{1 + F_o^A/4} \qquad (1.4.5.)$$

where χ_M is the magnetic susceptibility and β is the magnetic moment of the helium-3 atom. The density of states is again evaluated at the Fermi surface.

These three Landau parameters, F_o^s , F_1^s and F_o^A , have now been determined at pressures from the saturated vapour pressure up to the melting pressure and have been fully tabulated by Wheatly (1975).

We note, in passing, the range of values taken by these parameters :

F_0^S = 10.07 at 0 bar and 94.13 at 34.36 bar

F_1^S = 6.04 at 0 bar and 15.66 at 34.36 bar

F_0^A = -0.67 at 0 bar and -0.74 at 34.36 bar

(NB: Wheatly denotes F_0^A by Z_0 where $Z_0 = 4F_0^A$)

The importance of these values, and their dependence upon pressure, will become clear in the following chapters concerning the propagation of zero sound. In this work the values used in calculation were those quoted in Table V of Wheatley's review paper (1975) which were derived from the values of m^* contained in the same table. However, in a recent publication (Wölfle; 1976) the Landau parameters have been calculated using a different value of m^* and it is unclear at this time which of these values is to be preferred.

CHAPTER TWO

2.0. OSCILLATIONS IN A FERMI LIQUID

2.1. The Kinetic equation and the Fermi Sphere

Having produced the theory of a Fermi liquid, Landau then investigated the nature of oscillations in such a liquid. In the previous section the propagation of sound in the hydrodynamic regime was mentioned in which the product $\omega\tau \ll 1$, where ω is the angular frequency of the disturbance and τ is the average time between quasiparticle collisions. Under these conditions, provided that the temperature is not reduced too far, sound will propagate in the liquid according to the laws of classical hydrodynamics, the damping of the wave being proportional to τ. However, τ is inversely proportional to the square of the temperature so the damping increases rapidly as the temperature falls. Ultimately, a temperature will be reached at which the time between collisions (τ) exceeds the period of the sound wave and the propagation of hydrodynamic sound will cease. This point is roughly equivalent to $\omega\tau = 1$. Landau's theory of a Fermi liquid allows quantum mechanical solutions in this low-temperature region (known as the "collisionless" regime) which show that a different form of wave may be propagated at temperatures down to the absolute zero. For this reason he referred to these modes as "zero sound".

Landau starts by considering spin independent vibrations at absolute zero for which both the equilibrium distribution function (n_F) and the perturbed function (n) are independent of the spin variables

i.e. $$n = n_F + \delta n(\underline{p}) \qquad (2.1.1.)$$

A similar expression gives the energy of the perturbed quasiparticle in terms of the Fermi energy (ϵ_F) and some small deviation from equilibrium, $\delta\epsilon(\underline{p})$. It is assumed that both $\delta n(\underline{p})$ and $\delta\epsilon(\underline{p})$ are periodic in time and space such that they vary as $\exp(i[\underline{k}.\underline{r} - \omega t])$.

For a Fermi liquid, the Boltzmann equation is :

$$\frac{\partial n}{\partial t} + \left(\frac{\partial n}{\partial \underline{r}} \cdot \frac{\partial \epsilon}{\partial \underline{p}}\right) - \left(\frac{\partial n}{\partial \underline{p}} \cdot \frac{\partial \epsilon}{\partial \underline{r}}\right) = I(n) \qquad (2.1.2.)$$

where $I(n)$ is the collision integral.

Now $I(n)$ is proportional to $\delta n / \tau$. Therefore since we are considering the region for which $\omega\tau \gg 1$, $I(n)$ is very small and may be set to zero at this stage. Following the method of Wilks (1967) substitution for n and ϵ yields the expression ;

$$[\underline{k}.\underline{v} - \omega]\, \delta n = [\underline{k}.\underline{v}]\, \frac{\partial n_F}{\partial \epsilon}\, \delta\epsilon \qquad (2.1.3.)$$

where $\underline{v}$ is the velocity of a quasiparticle which is given by

$$\frac{\partial \epsilon_F}{\partial \underline{p}} = \underline{v} \qquad \text{and also} \qquad \frac{\partial n_F}{\partial \underline{p}} = \underline{v}\left(\frac{\partial n_F}{\partial \epsilon}\right)$$

Now, $\delta\epsilon$ may be expressed in terms of the interaction function, F, to give

$$\delta\epsilon = \iint F\,\delta n'\,d\epsilon'\,\frac{d\Omega'}{4\pi} \qquad (2.1.4.)$$

Landau now introduces a new function $\nu(n)$, defined thus ;

$$\nu(n) = \int \delta n(\underline{p})\,d\epsilon \qquad (2.1.5.)$$

Therefore (2.1.3.) becomes ;

$$\left[\underline{k}.\underline{v} - \omega\right]\delta n - \left[\underline{k}.\underline{v}\right]\frac{\partial n_F}{\partial \epsilon}\int F\,\nu'\,\frac{d\Omega'}{4\pi} = 0 \qquad (2.1.6.)$$

The form of this equation implies that δn is proportional to $\left(\frac{\partial n_F}{\partial \epsilon}\right)$ so ν may be expressed as the coefficient of proportionality,

ie $$\delta n = \nu\,\frac{\partial n_F}{\partial \epsilon}$$

which is consistent with the definition of $\nu(n)$, equation (2.1.5.)

Thus ;

$$\left[\underline{k}.\underline{v} - \omega\right]\nu = \left[\underline{k}.\underline{v}\right]\int F\,\nu'\,\frac{d\Omega'}{4\pi} \qquad (2.1.7.)$$

(The interaction function F is taken at the Fermi surface and therefore depends only on the angle χ between $\underline{p}$ and $\underline{p}'$).

Landau then takes the direction of $\underline{k}$ as the polar axis of a set of spherical coordinates in which the angles θ and ϕ define the direction of $\underline{p}$ (and hence, of $\underline{v}$) with respect to this axis. Equation (2.1.7.) then becomes ;

$$\cos\theta \int F(\chi)\, \nu(\theta', \phi')\, \frac{d\Omega'}{4\pi} = \left(\frac{\omega}{kv} - \cos\theta\right) \nu(\theta, \phi) \qquad (2.1.8.)$$

The propagation velocity u is given by : $u = \frac{\omega}{k}$

Therefore, representing the ratio u/v by s, we obtain ;

$$(s - \cos\theta)\, \nu(\theta, \phi) = \cos\theta \int F(\chi)\, \nu(\theta', \phi') \frac{d\Omega'}{4\pi} \qquad (2.1.9.)$$

That δn is proportional to ($\partial n_F / \partial \epsilon$) means that a change in the distribution function will result in a deformation of the Fermi surface with the function ν providing a measure of the amount of distortion. (ν has the dimensions of energy).

The simplest solution of (2.1.9.) is obtained by taking $F(\chi)$ to be a constant, F_0^s. The solution is of the form ;

$$\nu = \frac{A\cos\theta}{(s - \cos\theta)}$$

where A is a constant.

This solution represents a non-symmetric distortion of the Fermi surface along the direction of propagation of the wave. For real solutions, $s > 1$ which means that elongation occurs in the forward direction of propagation and a flattening of the Fermi sphere in the opposite direction. Figure 2.1. represents this solution which corresponds to the longitudinal mode of zero sound.

2.2. General solution of the kinetic equation

Landau did not consider the general solution to the kinetic equation but he recognised that it would permit the existence of different types of zero sound, distinguishable by different velocities and angular dependences, $\nu(\theta, \phi)$. The solution was obtained by Abrikosov and Khalatnikov (1959), by expressing $F(\chi)$ as the sum of spherical harmonics, and has been discussed in detail by Brooker ((1964) and (1967)). Briefly, the solution takes the following form :

Expressing $F(\chi)$ as a series of Legendre polynomials, equation (2.1.9.) becomes ;

$$(s - \cos\theta)\nu(\theta,\phi) = \cos\theta \int \sum_n F_n P_n(\cos\chi)\nu(\theta',\phi')\frac{d\Omega'}{4\pi} \qquad (2.2.1.)$$

Using the addition theorem for spherical harmonics :

$$P_n(\chi) = \sum_{m=-n}^{n} P_n^m(\theta) P_n^m(\theta') \exp\{im(\phi - \phi')\} \frac{(n - |m|)!}{(n + |m|)!} \qquad (2.2.2.)$$

where $P_n^m = P_n^{-m}$, and are associated Legendre polynomials; $|m| \leq n$.

Substituting in (2.2.1.) ;

$$(\cos\theta - s)\,\nu(\theta,\phi) \;+\; \cos\theta \sum P_n^m(\theta)\, e^{im\phi}\; \Phi_{nm} = 0 \qquad (2.2.3.)$$

where

$$\Phi_{nm} = F_n \frac{(n-|m|)!}{(n+|m|)!} \int P_n^m(\theta')\, \nu(\theta',\phi')\, e^{-im\phi'} \frac{d\Omega'}{4\pi} \qquad (2.2.4.)$$

Solving (2.2.3.) for ν, Abrikosov and Khalatnikov obtain the result ;

$$\nu(\theta,\phi) = \frac{-\cos\theta}{(\cos\theta - s)} \sum \Phi_{nm}\; P_n^m\; e^{im\phi} \qquad (2.2.5.)$$

Substituting this into (2.2.4.) and performing the integration with respect to ϕ' gives ;

$$F_n \frac{(n-|m|)!}{(n+|m|)!} \int \sum_k P_n^m(\theta') \frac{\cos\theta'}{(\cos\theta' - s)}\; P_k^m(\theta') \frac{d\Omega}{4\pi}\; \Phi = \sum_k \Phi_{km}\, \delta_{kn} \qquad (2.2.6.)$$

This somewhat unwieldy expression represents a system of equations which determine the quantities Φ_{km}. The system separates into groups of independent equations characterised by different values of m.
Abrikosov and Khalatnikov recognised that each m value would correspond to a particular dependence upon the angles θ and ϕ. The waves with $m = 0$ correspond to an angular dependence such that ν is isotropic in the plane perpendicular to $\underline{k}$ whereas those with $m \geq 1$ are polarized in the plane of $\underline{k}$.

2.3. Physical interpretation of the 'm' values

Landau (1957) shows that the momentum flux tensor for a Fermi liquid is ;

$$\Pi_{ik} = \int n p_i \frac{\partial \epsilon}{\partial p_k} d\tau + \delta_{ik} \left[\int n \epsilon \, d\tau - E \right] \qquad (2.3.1.)$$

Putting in the zero sound solutions, it may be shown that the only non-zero components of this tensor are Π_{33}, to which only the $m=0$ waves contribute, and Π_{13} to which only the $m=1$ waves contribute. We are therefore able to identify the $m=0$ waves with longitudinal waves (ie. pressure variation) and the $m=1$ waves with viscous, or shear, waves. We also note that waves with $m \geq 2$ do not contribute to the transfer of momentum and so cannot be generated nor detected by acoustical methods.

If ν is regarded as a measure of the distortion of the Fermi surface we see that the general solution discussed above gives ν proportional to $\cos m\phi$. Thus, for $m=0$ there is no angular dependence and the distortion of the Fermi surface is the symmetrical elongation predicted by the simple solution in which $F(\chi)$ is taken to be a constant (Figure 2.1.). However, in the case of $m=1$, we have ν proportional to $\cos\phi$ which results in an asymmetrical distortion as shown in figure 2.2.

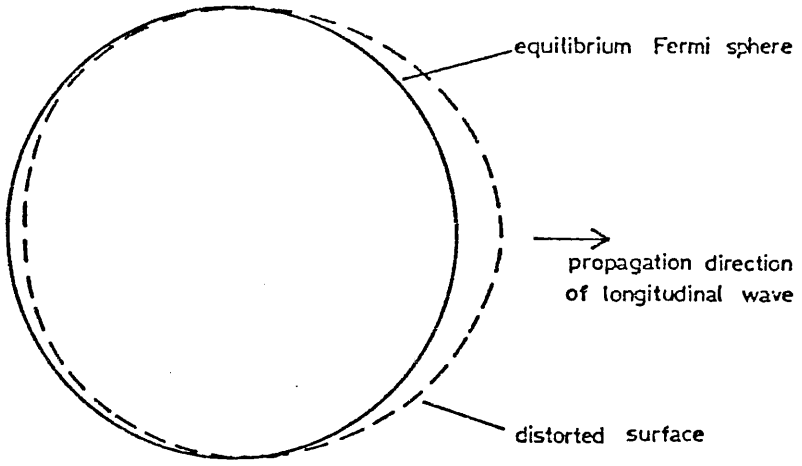

Fig. 2.1 Symmetric distortion of Fermi surface (longitudinal zero sound)

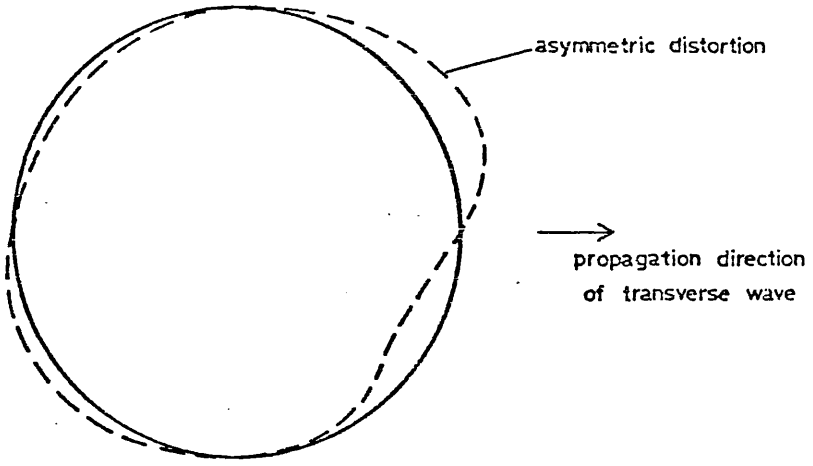

Fig. 2.2 Asymmetric distortion (transverse zero sound)

2.4. Dispersion Equation for Zero Sound

The Boltzmann equation is ;

$$\frac{\partial n}{\partial t} + \frac{\partial n}{\partial \underline{r}} \cdot \frac{\partial \epsilon}{\partial \underline{p}} - \frac{\partial n}{\partial \underline{p}} \cdot \frac{\partial \epsilon}{\partial \underline{r}} = I(n)$$

The more general treatment prevents the collision integral, $I(n)$, being set to zero. Abrikosov and Khalatnikov[1a] (1959) express $I(n)$ in terms of a relaxation time τ defined thus ;

$$I(n) = -\frac{\delta n}{\tau}$$

To ensure a smooth transition from the zero sound region into the hydrodynamic regime, both momentum and energy must be conserved in the quasiparticle collisions. Therefore, it is required that :

$$\int_{\underline{p}} I(n)\, d\tau = 0 \qquad \text{and} \qquad \int \epsilon\, I(n)\, d\tau = 0$$

The number of quasiparticles is also conserved, so that :

$$\int I(n)\, d\tau = 0$$

These conditions imply that the coefficients of the Legendre polynomials $P_0(\cos\theta)$, $P_1^0(\cos\theta)$ and $P_1'(\cos\theta)$ in the expansion of $I(n)$ must be zero. Abrikosov and Khalatnikov define the relaxation time consistent with these requirements by subtracting out the coefficients of the corresponding terms in the expansion of $\delta n(\underline{p})$.

Therefore, expanding $\delta n(\underline{p}) = \delta n(p, \theta, \phi)$ as a series of spherical harmonics ;

$$\delta n(p,\theta,\phi) = \sum_{n} \sum_{m=0}^{n} \delta n_n^m(p,\theta,\phi)\ P_n^m(\cos\theta)\cos m\phi$$

and the collision integral is then written thus ;

$$I(n) = \frac{1}{\tau}\left\{\delta n - (\delta n)_0 - (\delta n)_1^{\circ}\cos\theta - (\delta n)_1^{'}\sin\theta\cos\phi\right\} \qquad (2.4.1.)$$

Introducing this term into the kinetic equation (2.1.6.) we obtain ;

$$(kv\cos\theta-\omega)\nu - kv\cos\theta\int F\nu'\frac{d\Omega'}{4\pi}$$

$$= -\frac{1}{i\tau}\left\{\nu - \nu_0 - \nu_1^{\circ}\cos\theta - \nu_1^{'}\sin\theta\cos\phi\right\} \qquad (2.4.2.)$$

The (δn) terms have been replaced by ν terms because ν is defined thus ;

$$\delta n(p) = \nu\ \frac{\partial n_F}{\partial \epsilon_F}$$

Since $(\partial n_F/\partial \epsilon_F)$ is a delta function at the Fermi surface we have ;

$$\delta n(p) = \nu$$

Equation (2.4.2.) is the general equation for the dispersion of zero sound which may be solved (after insertion of the appropriate value of m) for the propagation constant k, and hence for the velocity of the required wave.

2.5. The dispersion of longitudinal waves ($m = 0$)

Abrikosov and Khalatnikov (1959) solved the dispersion equation for longitudinal waves using only the first two parameters of the Landau series; F_0^s , F_1^s . However Brooker ((1964) and (1967)) has solved the same equation to include the term F_2^s and obtains the result ;

$$\xi^2 = \frac{(1+F_0)(1+F_1/3)}{3(1+\alpha)^2} - \frac{(1+F_1/3)}{3(1+\alpha)} \frac{z}{az+w} \qquad (2.5.1.)$$

where $$\xi = \frac{i\omega\tau - 1}{ik\tau v_F} \qquad \alpha = \frac{1}{i\omega\tau - 1}$$

$$w(\xi) = \frac{\xi}{2} \ln \frac{(\xi+1)}{(\xi-1)} - 1$$

$$z(\xi) = (1 - 3\xi^2) w + 1$$

The superscript 's' has been omitted from the Landau parameters since only the symmetric parameters appear in this equation. The factor 'a' involves the parameter F_2^s , being defined thus ;

$$a = \frac{F_2/4}{1 + F_2/5}$$

In the hydrodynamic limit, as $\omega\tau \to 0$, equation (2.5.1.) reduces to the following :

$$\left(\frac{\omega}{k v_F}\right)^2 = \xi^2 (1+\alpha)^2$$

Therefore,

$$\left(\frac{\omega}{k v_F}\right)^2 = \frac{(1+F_0)(1+F_1/3)}{3} - \frac{4}{15}(1+F_1/3)(1+F_2/5) i\omega^2\tau \qquad (2.5.2.)$$

Taking zero order terms in $\omega\tau$:

$$\left(\frac{\omega}{k}\right)^2 = \frac{v_F^2(1+F_0)(1+F_1/3)}{3} = \frac{p_F^2}{3m^2}\frac{(1+F_0)}{(1+F_1/3)}$$

This equation is Landau's result for the speed of ordinary (hydrodynamic) sound in a Fermi liquid (cf. equation (1.4.4.)) which confirms that, in the limit $\omega\tau \to 0$, the zero sound wave corresponding to $m=0$ may be identified with ordinary sound.

The imaginary component of (2.5.2.) may be used to obtain the absorption, ie :

$$\mathcal{I}_m\{k\} = \frac{2}{15}\frac{v_F^2}{c^3}(1+F_1/3)(1+F_2/5)\omega\tau$$

Comparing this with the classical damping of a wave :

$$\mathcal{I}m\{k\} = \frac{\omega^2}{2\rho c^3}\,\frac{4}{3}\eta$$

we have;

$$\tau = \frac{5\eta}{\rho v_F^2}\,\frac{1}{(1+F_1/3)(1+F_2/5)} \qquad (2.5.3.)$$

For values of $\omega\tau$ not close to zero, equation (2.5.1.) must be solved numerically.

Pethick (1969) has obtained an equation which relates the velocities of zero (c_0) and hydrodynamic (c_1) sound in terms of the Landau parameters ;

$$\frac{c_0^2 - c_1^2}{c_1^2} = \frac{4}{5}\,\frac{(1+F_2/5)}{(1+F_0)}$$

Therefore, the transition from hydrodynamic sound to longitudinal zero sound will be signalled by a change in wave velocity and values of F_2 may be obtained by comparing the sound velocities in the limits $\omega\tau \ll 1$ (for c_1) and $\omega\tau \gg 1$ (for c_0).

2.6. Dispersion of transverse waves ($m=1$)

The case of transverse waves was briefly considered by Brooker ((1964) and (1967)) and studied in more detail by Lea et al (1973)(a).However, the latter author considers only the Landau parameters F_0^s and F_1^s. The following sets down the main results of these authors but incorporates the interaction parameters up to F_2^s.

By simplifying equation (2.~~4~~.~~2~~.) for $m=1$, and carrying out the integration, Brooker obtains the result :

$$w(1-\xi^2) + \frac{1}{3} = \frac{2/3(1+\alpha)}{F_1/3 - \alpha + 4a\xi^2(1+\alpha)} \qquad (2.6.1.)$$

where the terms ξ, w and α are as defined in Section 2.5. and the term a is again defined by the relationship :

$$a = \frac{F_2/4}{1 + F_2/5}$$

In the hydrodynamic limit, as $\omega\tau \to 0$, Brooker reduces this equation to :

$$k = \frac{\omega}{v_F}\left[\frac{5}{2(1+F_1/3)(1+F_2/5)\,\omega\tau}\right]^{1/2}(1+i) \qquad (2.6.2.)$$

If this expression is equated to that for a classical hydrodynamic shear wave, we find that ;

$$k = \left[\frac{\omega\rho}{2\eta}\right]^{1/2}(1+i)$$

Where η is the viscosity of a Fermi liquid, and is given by ;

$$\eta = \frac{1}{5}\rho\tau v_F^2(1+F_1/3)(1+F_2/5) \qquad (2.6.3.)$$

(We note that this equation is a simple rearrangement of equation (2.5.3.) which was obtained from the imaginary component of the longitudinal dispersion relation).

In the "zero sound limit", as $\omega\tau\to\infty$, it is found that the existence of a wave solution depends crucially upon the value of the interaction function. Brooker ((1964) and (1967)) shows that, as $\omega\tau\to\infty$, a real solution, and hence transverse zero sound, will exist only if :

$$F_1^s + \frac{3F_2^s}{1+F_2^s/5} > 6 \qquad (2.6.4.)$$

(It will be noticed that, if F_2^s is set to zero, the condition reduces to $F_1^s > 6$, a result first obtained by Landau (1959)). If the values for F_1 for liquid helium-3 quoted by Wheatley (1975) are taken as correct, ie. $F_1^s = 6.04$ at the saturated vapour pressure, we see that transverse zero sound should be propagated at all pressures provided that

F_2^s is roughly zero. However, if F_2^s is found to be appreciably greater than zero, transverse zero sound will only be possible for liquid helium-3 under pressure. Furthermore, it appears that the properties of transverse zero sound may provide the most reliable method for the determination of F_2^s. (The question of the existence of transverse zero sound will be discussed in detail in the concluding chapter)

The velocity of the zero sound wave, relative to the Fermi velocity may be determined by solving the dispersion relation (2.6.1.) in the zero sound limit. That is, as $\omega\tau \to \infty$;

$$\xi = \frac{i\omega\tau - 1}{ik v_F \tau} \to \frac{\omega}{k v_F}$$

We denote the ratio of zero sound velocity to the Fermi velocity, at $\omega\tau \to \infty$, by s.

Thus;

$$\frac{\omega}{k v_F} = s = \frac{c_t}{v_F}$$

where c_t is the velocity of the transverse zero sound wave.

Also, as $\omega\tau \to \infty$; $\alpha \to 0$ and equation (2.6.1.) reduces to :

$$\left[\frac{s}{2} \ln\frac{(s+1)}{(s-1)} - 1\right](1-s^2) + \frac{1}{3} = 2\left[F_1 + \frac{3F_2 s^2}{1 + F_2/5}\right]^{-1} \quad (2.6.5.)$$

(The superscript has been omitted from F_1 and F_2 since only symmetrical parameters are involved).

The equation (2.6.5.) may be solved numerically for given values of F_2 to provide a relationship between F_1 and s, and figure 2.3. shows the approximate value of s as a function of F_1 for the various F_2 values indicated. We need not be concerned with $F_2 < -2$ since, in liquid helium-3, the value of F_1 is limited to about 15.6 by solidification at a pressure of 34.4 bar. It may be seen from figure 2.3. that, for $F_2 = 0$, the relative velocity of the wave increases from 1.002 at $F_1 \approx 6.2$ to 1.20 at $F_1 \approx 14.3$, as calculated by Fomin (1968).

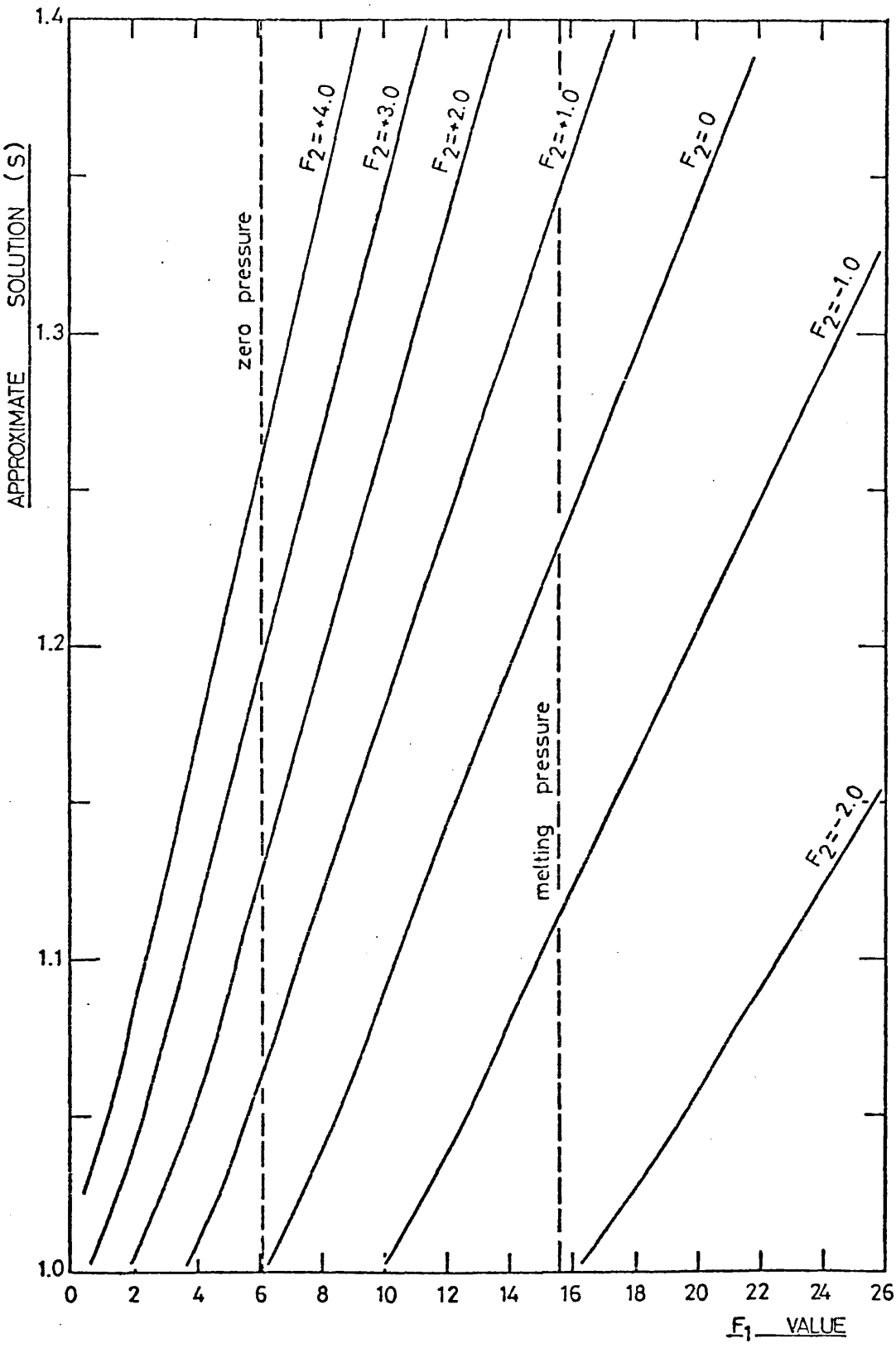

Fig. 2.3 Approximate solutions to the dispersion relation ($\omega\tau \to \infty$)

CHAPTER THREE

3.0. ACOUSTIC IMPEDANCE AND ZERO SOUND

3.1. Introduction

It was shown in the previous chapter how a change in wave velocity would signal the transition from ordinary to zero sound. Classical fluid dynamics relates the speed of sound to the acoustic impedance of a medium, so we may expect a corresponding change in this property at the transition. In fact, the change in acoustic impedance provided the first experimental evidence of the existence of zero sound when it was observed by Keen, Matthews and Wilks (1965) at a temperature of 92 mK using longitudinal waves at 1000 MHz in a piezo-electric quartz rod. A detailed study of the theory of the acoustic impedance of liquid helium-3 has been undertaken by Brooker ((1964) and (1967)), who included a careful analysis of the experimental results of Keen et al, and by Gavoret (1965). More recently, the problem of acoustic impedance in the transverse case has been studied by Flowers and Richardson (1978) and by Fomin ((1968) and (1976)). The following chapter attempts to outline the basic theory of acoustic impedance, for both longitudinal and transverse waves, and sets down the more important results of these authors.

3.2. Fluid dynamics and acoustic impedance

Suppose a fluid is subjected to a periodic disturbance which gives rise to a mass flow represented by the vector $\underline{j}$. Let the momentum transfer tensor be Π_{lm} and the momentum density be $\underline{p}$.

Conservation of momentum requires that ;

$$\frac{\partial \Pi_{lm}}{\partial x_m} + \frac{\partial p_l}{\partial t} = 0 \qquad (3.2.1.)$$

Assuming that both Π_{lm} and $\underline{p}$ vary as $\exp\{i(\underline{k}.\underline{r} - \omega t)\}$ we obtain

$$ik\Pi_{lm} = i\omega p_l$$

If we use the general result that momentum density $\underline{p}$ is equal to mass flux $\underline{j}$ and also that, at the boundary, $\underline{j} = \rho \underline{u}$, where $\underline{u}$ is the velocity of the boundary, we obtain ;

$$\Pi_{lm} = \frac{\omega}{k} \rho \underline{u}$$

The acoustic impedance is defined to be the momentum flow divided by velocity, thus ;

$$Z = \frac{\Pi_{lm}}{\underline{u}} = \frac{\rho \omega}{k} \qquad (3.2.2.)$$

i.e: $$\frac{Z}{\rho} = c_o \qquad (3.2.3.)$$

Where c_o is the wave velocity.

(It is convenient to express the acoustic impedance in this way as the ratio Z/ρ assumes the dimensions of velocity.)

This expression assumes that the disturbance is wholly periodic and whilst this is true in the hydrodynamic regime $(\omega\tau \to 0)$, it is not necessarily true for the zero sound regime, or the transition between, because of the momentum transferred by excitation of individual quasi-particles. The rigorous treatment of acoustic impedance by Brooker (1964) shows that, in general, the dispersion relation may have more than a single solution for a given value of $\omega\tau$. It would be expected (mathematically, at least) that some discontinuity in the measurable properties of liquid helium-3 would be observed whenever a solution appeared or vanished but, experimentally, this is not the case. Brooker resolves the inconsistency by pointing out that in addition to the collective waves propagated, single quasiparticles may be excited by the moving boundary. These quasiparticles then travel their free-path distance and then give up their ordered motion in collisions with other quasiparticles. The contribution of these single particle excitations is such that, although the total measured acoustic impedance is continuous, the separate contributions need not be. The acoustic impedance of equation (3.2.3.) is therefore modified by a factor dependant upon the energy carried away by the excited quasiparticles as they are scattered from the boundary.

A further modification results from the nature of the scattering (ie. pure specular, pure diffuse or mixture). This has been discussed in detail by Bekarevich and Khalatnikov (1961) who show that the scattering mechanism has a profound effect upon the energy transfer. However, the de Broglie wave length for helium-3 quasiparticles near the Fermi surface is of the

order of a few Angstrom units whereas the surface of the oscillating boundary will exhibit irregularities greater in size by at least two orders of magnitude. Therefore, in the practical case, we assume that the scattering will be entirely diffuse. This conclusion is supported by the thermal conductivity experiments of Betts, Brewer and Hamilton (1974) who found that for liquid helium-3 in "Vycor" glass, the specular reflection coefficient is zero.

The modifications due to non-wavelike processes may be expressed as follows :

Let a fraction f of the total mass current j be due to wave motion, ie. $j_0 = fj$. Then, the non-wave component will be :

$$j_1 = (1 - f)\, j$$

If we consider the pressure stress Π to be similarly divided into components Π_0 and Π_1 we have ;

$$\frac{Z}{\rho} = \frac{(\Pi_0 + \Pi_1)}{j} = \frac{\Pi_0}{j_0} f + \frac{\Pi_1}{j_1}(1-f) \qquad (3.2.4.)$$

If c_0 is the wave velocity,

$$\frac{Z}{\rho} = c_0 f + \frac{\Pi_1}{j_1}(1-f) \qquad (3.2.5.)$$

We note that in general Z, c_0, Π_1/j_1 and f are all complex quantities which become real in the limit $\omega\tau \gg 1$ (zero sound regime) and real or zero for $\omega\tau \ll 1$ (the hydrodynamic case).

In the hydrodynamic regime the fraction $f \to 1$, and only wavelike processes contribute to the acoustic impedance. Therefore we obtain the classical result :

$$\frac{Z}{\rho} = c_o$$

In the zero sound limit $(\omega\tau \to \infty)$ the measured acoustic impedance/ρ will be less than the zero sound wave velocity as a result of the single quasiparticle contributions.

Bekarevich and Khalatnikov (1961) calculated the effect on the distribution function of a disturbance composed of both wavelike and non-wavelike processes and obtained expressions of the form ;

$$\delta n(\theta) = A(\theta)\exp\{(i\omega\tau - 1)\zeta \sec\theta - i\omega t\} + \int_0^{\pi/2} B(\theta,\theta')\exp\{(i\omega\tau-1)\zeta\sec\theta' - i\omega t\}\,d\theta' + C(\theta)\exp\{i(kz-\omega t)\} \qquad (3.2.6.)$$

where $\zeta = \frac{z}{\tau v_F}$

The first term is non-zero only for $\theta < \pi/2$. The phase velocity is $v_F \cos\theta$ and the attenuation length is $\tau v_F \cos\theta$. Brooker (1964) identifies this term with quasiparticles reflected from the boundary at an angle θ to the normal to the boundary. They then travel through the liquid, carrying information about the motion of the boundary, at a velocity v_F for a mean time τ. On collision with another quasiparticle, the information is divided between the two mutually scattered quasiparticles which then both contribute to δn. The second term in (3.2.6.) is identified with this contribution. The final term is the contribution due to

wave motion which is the only significant term at high temperatures, the first two terms becoming negligible due to the decrease in τ.

3.3. Longitudinal Acoustic Impedance

In the case of longitudinal waves, the boundary oscillating in a direction parallel to the propagation direction of the wave, the Fermi velocity is small compared to the wave velocity in the zero sound regime ($\omega\tau \gg 1$). Consequently almost all of the disturbance set up by the oscillating boundary is observed as zero sound waves. The acoustic impedance of helium-3 in the longitudinal case may then be expressed simply as

$$Z = \rho c$$

where ρ is the density of liquid helium and c is the velocity of sound in the liquid.

In the experiment of Keen, Matthews and Wilks (1965) a pulse of longitudinal ultrasound was generated in a piezo electric rod. This pulse experienced multiple reflection from the polished ends of the rod, giving up a small amount of energy to the liquid at each reflection. The fraction of wave energy lost into the liquid per reflection depends upon the acoustic impedances of the quartz rod and the liquid.

Therefore;

$$\text{energy lost per reflection} = 1 - R^2$$

where R is the reflection coefficient.

R is normally given by ;

$$R = \left| \frac{Z_l - Z_s}{Z_l + Z_s} \right|$$

where Z_l and Z_s are the acoustic impedances of the liquid and solid respectively.

(Although the experiment was performed under conditions in which classical hydrodynamics may not be applicable, this expression has been shown by Brooker (1964) to be valid without assuming a wavelike transmitted mode. The only assumption required in this case is that the liquid medium is semi-infinite which is satisfied in the case of liquid helium-3 by virtue of its high attenuation.)

Therefore, energy lost per reflection is given by ;

$$\beta = 1 - \left| \frac{Z_l - Z_s}{Z_l + Z_s} \right|^2$$

For $Z_l \ll Z_s$

$$\beta \approx \frac{4 Z_l}{Z_s}$$

More correctly, since Z_l may be complex, we have, in general ;

$$\beta \approx 4 \, Re \left[\frac{Z_l}{Z_s} \right]$$

where Re denotes the real part only.

Keen, Matthews and Wilks (1965) measured the reflection coefficient by observing the change in the rate of decay of the train of echoes produced in the piezoelectric crystal when liquid helium-3 was allowed to cover either one or both faces of the crystal. At about 92 mK, the acoustic resistance/ρ was found to change quite rapidly by about 19 ms^{-1} and this result has been taken as the first experimental observation of the transition from hydrodynamic to zero sound. The results of this experiment were analysed by Brooker ((1964) and (1967)) who showed that, whilst qualitatively in agreement with the theory, the measured change in acoustic impedance was somewhat larger than predicted.

Three possible areas of doubt are considered in an effort to explain the discrepancy between theory and experiment. These are :

(i) the termination of the series of Landau parameters after only two terms,

(ii) the approximation of the collision integral to a relaxation time,

(iii) the validity of Landau theory at temperatures above 0.05 Kelvin.

The points (i) and (ii) both require careful mathematical treatment in the region of the transition but in the low-temperature limit $(\omega\tau \gg 1)$ the collision integral is tending to zero so that (ii) is not significant. Also, the conditions required by the Landau theory are well satisfied at the low-temperature limit so that (iii) may also be disregarded. The remaining area of doubt was the magnitude of F_2^s and succeeding parameters about which little was known at that time. Brooker used F_2^s as a variable

parameter and found that the theory and experiment were in agreement when F_2^s was given the value 14.8 at the saturated vapour pressure. However, doubts were later cast upon this value by the results of the direct measurement of the attenuation and velocity of longitudinal zero sound by Abel, Anderson and Wheatley (1971). Three independent estimates of F_2^s were obtained from their results, being calculated from the peak attenuation, velocity change and relaxation time. Each of these indicated $F_2^s \approx 0$.

3.4. Transverse acoustic impedance

The work of Bekarevich and Khalatnikov (1961) included calculations of the acoustic impedance in the transverse case but without considering the effect of the parameters beyond F_1^s. Recently, a detailed theory of the transverse acoustic impedance has been produced by Flowers and Richardson (1978) in which the parameter F_2^s is included.

The experimental study of transverse zero sound is rather more difficult than that of the longitudinal mode due to the extremely high attenuation of transverse waves. Corruccini et al (1969) has shown that the attenuation length of the wave is roughly the same as the single particle mean free path length, and inversely proportional to the square of the temperature.

ie : attenuation coefficient, $\alpha \sim l^{-1} = (\tau v_F)^{-1} \sim T^2$

The attenuation coefficient for the transverse mode is about 10^3 times greater than that of longitudinal zero sound which implies that direct observation of the propagation of such a wave is very difficult. Furthermore, because of the similarity between the attenuation length and the mean free path length of the quasiparticles, any experiment designed to observe the zero sound wave will detect a contribution due to the incoherent single particle excitations of similar magnitude to that of the wave. As has been mentioned in section 3.2., the total disturbance of the liquid will be a continuous function although the zero sound contribution need not be therefore we may not expect to observe a sudden transition as in the longitudinal experiments. Fomin (1976) has pointed out that the frequency and temperature dependences of the acoustic impedance are similar for both wave and single particle contributions and if measurements of impedance are to be taken as evidence for the existence of transverse zero sound, a quantitative correspondence between experiment and theory must be established. The full theoretical treatment of transverse acoustic impedance, due to Flowers and Richardson (1978) is very complex and only a brief outline will be presented here.

The theoretical method follows that of Bekarevich and Khalatnikov (1961) but uses a two-time relaxation time approximation for the collision integral in place of the single relaxation time of the earlier work. (The two-time approach had previously been used in the theory of the attenuation of longitudinal waves in a Fermi liquid by Pethick (1969).) In the generalised expression for the collision integral, the terms involving $l = 0$ and $l = 1$ vanish in order to conserve quasiparticle number and total momentum in collisions so that only distortions of the Fermi surface corresponding to $l \geq 2$ need to be considered.

The $\ell = 2$ distortions from local equilibrium are characterised by a relaxation time τ_2. For simplicity, the relaxation times associated with higher values of ℓ (ie. τ_3 , τ_4 ...etc)are taken to be equal and are denoted by the second of the two relaxation times, τ. The time τ_2 is obtainable from the hydrodynamic viscosity η;

$$\eta = \frac{1}{5} n m^* v_F^2 \tau_2$$

and τ is related to τ_2 by a parameter ξ_2 such that;

$$\frac{1}{\tau_2} = \frac{\xi_2}{\tau}$$

(see Section 3.7.)

Flowers and Richardson derive a linearised form of the Boltzmann equation for the system which they solve subject to the boundary conditions appropriate to pure diffuse scattering. The solution enables the component of the stress tensor corresponding to transverse waves (Π_{xz}) to be determined from which the acoustic impedance is evaluated using the definition;

$$Z = \frac{\Pi_{xz}(z=0)}{u}$$

where the boundary is in the xy plane, the oscillations being polarized in the x direction. Furthermore, by considering the spatial dependence of the Laplace transform of the stress tensor, Flowers and Richardson separate it (and hence, the acoustic impedance) into two components; a discrete term representing the transverse zero sound and a continuum due to the excitation of single quasiparticles.

For the total transverse acoustic impedance, they obtain the expression :

$$Z = -n p_F \frac{(b-1)}{s_1 b} \left[\frac{A-B}{A+B}\right] \qquad (3.4.1.)$$

and for the contribution from transverse zero sound only ;

$$Z^c = -2n p_F \frac{(b-1)^2}{b} \frac{(1-s_o)}{(s_1^2 - s_o^2)} \left[\frac{g_-(-s_o)}{(A+B)}\right] \qquad (3.4.2.)$$

In these expressions ;

$$A = \frac{(s_1 + s_o)}{(s_1 + 1)\, g_-(s_1)} \qquad B = \frac{(1-b)(s_1+1)}{(s_1+s_o)\, g_+(-s_1)}$$

But $g_-(s)$ and $g_+(s)$ are functions defined such that :

$$g_+(-s) = \frac{1}{g_-(s)}$$

Therefore,

$$B = \frac{(1-b)}{A}$$

The function $g_-(s)$ is given by the expression ;

$$g_-(s) = \left[G(s)\right]^{1/2} e^{-s\psi(s)}$$

where ;

$$\psi(s) = -\frac{1}{2\pi i} \int_0^1 \frac{\ln \Delta_+(\frac{1}{u}) - \ln \Delta_-(\frac{1}{u})}{1-(us)^2}\, du \qquad (3.4.3.)$$

This integral may be evaluated numerically, $\Delta_{\pm}(\frac{1}{u})$ being obtained from :

$$\Delta_{\pm}(\tfrac{1}{u}) = 1 - bs_1^2u^2 - \frac{3}{4}b(1-s_1^2u^2)\left\{2u^2 + u(1-u^2)\left[\ell n\left(\frac{1+u}{1-u}\right) \pm i\pi\right]\right\} \quad (3.4.4.)$$

The function Δ arises out of the Laplace transform of the linearised Boltzmann equation obtained by Flowers and Richardson. (The phases of the logarithms in (3.4.3.) are defined to be zero for $u = 0$).

The function $G(s)$ is related to $g_{\pm}(s)$ as follows ;

$$G(s) = g_+(s) \Big/ g_-(s)$$

and is defined by the expression ;

$$\Delta(s) = \frac{(s^2 - s_0^2)}{s^2 - 1} G(s) \quad (3.4.5.)$$

s_1 is given by :

$$s_1 = \sqrt{\frac{c(b-1)}{b}} \quad ; \quad Re\left[s_1\right] > 0 \quad (3.4.6.)$$

where : $a = 1 - i\omega\tau \quad ; \quad b = \dfrac{1/a + F_1/3}{1 + F_1/3}$

$$c = \frac{F_2}{1 + F_2/5} + \frac{5}{a}\left[\frac{1}{1 + F_2/5} - \xi_2\right]$$

S_o is the root of the dispersion relation with positive real part and is obtained ~~from~~ in the following way:

The propagation vector for the collective mode is ;

$$k = \frac{i s_o a}{v_F \tau}$$

Where s_o is a root of the equation $\Delta(s) = 0$, and $\Delta(s)$ is given by :

$$\Delta(s) = 1 - \frac{b s_1^2}{s^2} - \frac{3b}{2s^2}\left(1 - \frac{s_1^2}{s^2}\right)\left[\left(1 - \frac{1}{s^2}\right)\frac{s}{2}\ln\left(\frac{1+s}{1-s}\right) + 1\right] \qquad (3.4.7.)$$

This equation always has a root in the hydrodynamic limit but the existence of a root in the zero sound limit $(\omega\tau \to \infty)$ is found to depend upon ;

$$F_1 + \frac{3F_2}{1 + F_2/5} > 6$$

which is in agreement with the condition obtained by Brooker (1967) in this limit, see Section 2.6.

3.5. Total acoustic impedance, Z.

Flowers and Richardson use the relationship

$$B = \frac{(1-b)}{A}$$

to obtain the following expression for the total transverse acoustic impedance :

$$\frac{Z}{\rho v_F} = \frac{i\omega\tau(3+F_1)}{(3+aF_1)s_1} \frac{\left[(s_1+1)(s_1-s_0)e^{-s_1\psi_1} - (s_1-1)(s_1+s_0)e^{s_1\psi_1}\right]}{\left[(s_1+1)(s_1-s_0)e^{-s_1\psi_1} + (s_1-1)(s_1+s_0)e^{s_1\psi_1}\right]} \qquad (3.5.1.)$$

3.5.1. Zero sound and hydrodynamic limits for $F_2 \to 0$.

As $F_2^s \to 0$, a single relaxation time approximation may be substituted for the two-time approach in the zero sound limit so that $\xi_{s_2} \to 1$. Therefore $s_1 \to 0$ and equation (3.5.1.) reduces to :

$$\frac{Z_\infty}{\rho v_F} = \frac{-i\omega\tau(3+F_1)}{(3+aF_1)}\left[\frac{1}{s_0} - 1 + \psi(0)\right] \qquad (3.5.2.)$$

where $\psi(0)$ is calculated from (3.4.3.) for $s_1 = 0$ (The subscript '∞' denotes the value of impedance at the limit, $\omega\tau \to \infty$.)

This important result is equivalent to that obtained by Fomin (1976) for the real part of the acoustic impedance (R) in the zero sound limit ;

$$\frac{R_\infty}{\rho} = \frac{3p_F}{mF_1}\left[\eta - 1 + \Phi\right] \qquad (3.5.3.)$$

where m is the mass of the helium-3 atom and η is the real part of the reduced velocity. The term Φ is defined by Fomin thus ;

$$\Phi = \frac{1}{\pi}\int_0^1 \tan^{-1}\left[\frac{\pi}{2}\frac{u(1-u^2)}{(1-u^2)(1-u\tanh^{-1}u)-\left(\frac{F_1-6}{3F_1}\right)}\right]du \qquad (3.5.4.)$$

It may be shown by straightforward, though tedious, rearrangement that Φ is identical to the term $\psi(0)$ in the equation of Flowers and Richardson. Then, by substituting the effective mass equation for m and replacing η by s_o^{-1}, Fomin's equation (3.5.3.) may be shown to be equivalent to equation (3.5.2.).

In the hydrodynamic limit ($\omega\tau \to 0$) equation (3.5.2.) reduces to the classical result for acoustic impedance :

$$Z = \rho\frac{\omega}{k}$$

where k is the propagation vector of the collective mode and is defined by :

$$k = \frac{i\,s_o}{v_F\,\tau}$$

3.5.2. Zero sound and hydrodynamic limits for $F_2 \neq 0$.

By rearranging the exponential terms in the form of hyperbolic functions, Flowers and Richardson express equation (3.5.1.) in the zero sound limit ($\omega\tau \to \infty$) in two parts ;

(i) For $-5 < F_2 < 0$;

$$\frac{Z_\infty}{\rho v_F} = \frac{3+F_1}{F_1}\frac{1}{\sigma_1}\tanh\left(\sigma_1\psi_1 + \alpha_1\right) \qquad (3.5.5.)$$

where $$\sigma_1 = \left[\frac{|3F_2|}{F_1(1 + F_2/5)}\right]^{1/2}$$

and $$\alpha_1 = \tanh^{-1}\left[\frac{(1-s_0)\sigma_1}{s_0-\sigma_1^2}\right]$$

(ii) For $F_2 > 0$;

$$\frac{Z_\infty}{\rho v_F} = \frac{3+F_1}{F_1}\ \frac{1}{\sigma_1}\ \tan(\sigma_1 \psi_1 + \alpha_2) \qquad (3.5.6.)$$

where $$\alpha_2 = \tan^{-1}\left[\frac{(1-s_0)\sigma_1}{s_0+\sigma_1^2}\right]$$

Flowers and Richardson note that if these equations are expanded in terms of σ_1 for small values of F_2, a linear dependance of Z_∞ upon F_2 is found to dominate. Consequently, the zero sound limit of acoustic impedance provides a sensitive measure of F_2.

In the hydrodynamic limit $(\omega\tau \to 0)$, $s_1 \to 0$, so the limiting impedance is the same as that obtained in the $F_2 = 0$ case,

ie ; $$Z = \frac{\rho\omega}{k}$$

where, $k = \frac{i s_o}{v_F \tau}$

However, in this case, s_o is determined by the dispersion relation (3.4.7.) for $F_2 \neq 0$. Flowers and Richardson show that, by expanding equation (3.4.7.) in powers of s and $\omega\tau$, the root of the dispersion relation is given by :

$$s_o^2 = -\frac{5 i \omega \tau \xi_2}{(1 - F_1/3)}$$

3.6. The collective contribution, Z^c

3.6.1. $F_2 \to 0$ limit.

Again, as $F_2 \to 0$, $s_1 \to 0$ and equation (3.4.2.) may be expressed in simpler form ;

$$\frac{Z^c}{\rho v_F} = \left(1 + \frac{F_1}{3}\right) \frac{(1-b)^{3/2}(1-s_o)}{b s_o^2} \left(\frac{e^{s_o \psi(s_o)}}{[Q(s_o)]^{1/2}}\right) \qquad (3.6.1.)$$

where $Q(s_o) = \frac{1}{2 s_o^2}\left[3(b-1) + s_o^2\right]$

3.6.2. Zero sound limit for $F_2 \neq 0$.

The limiting value of the zero sound contribution to the acoustic impedance does not simplify greatly but may be expressed in terms of hyperbolic and trigonometric functions, as follows :

(i) For $-5 < F_2 < 0$.

$$\frac{Z^c_\infty}{\rho v_F} = \frac{3+F_1}{3}(1-s_0)\left[\frac{3}{F_1(s_0^2-s_1^2)}\left(\frac{1-b}{G(s_0)}\right)^{1/2}\right]\frac{e^{s_0\psi(s_0)}}{\cosh(\sigma_1\psi_1+\alpha_1)} \quad (3.6.2.)$$

(ii) For $F_2 > 0$, as above, but $\cos(\sigma_1\psi_1+\alpha_2)$ is substituted for the term involving 'cosh'

In these equations, α_1 and α_2 have the same meaning as in equations (3.5.5.) and (3.5.6.) and $G(s_0)$ is given by

$$G(s_0) = \frac{(s_0^2-1)}{2s_0}\left[\frac{d\Delta}{ds}\right]_{s=s_0}$$

which yields, on evaluation of the bracketed term using equation (3.4.6.) the rather cumbersome expression ;

$$G(s_0) = \frac{3}{8}b(s_0^2-1)\left\{\left(6+\frac{8s_1^2}{3}\right)s_0^{-4} - 10s_1^2 s_0^{-6} + \left[s_0^{-3} - 3(1+s_1^2)s_0^{-5} + 5s_1^2 s_0^{-7}\right]\ln\left(\frac{1+s_0}{1-s_0}\right)\right\} \quad (3.6.3.)$$

N.B. Richardson (private communication) has recently developed a simpler theory of transverse acoustic impedance based upon a variational principle. No details of this method are available at this time, but using a simple plane-wave trial function, the variational principle yields the following expression for the transverse acoustic impedance :

$$\frac{Z}{\rho v_F} = \frac{3+F_1}{8(1+\sqrt{X})} \qquad (3.6.4.)$$

where $$X = \frac{1}{4}\left\{4+F_1-\left(\frac{3+F_1}{i\omega\tau}\right)\right\}\left\{\frac{1}{(1+F_2/5)}+\left(\xi_2-\frac{1}{(1+F_2/5)}\right)\frac{1}{1-i\omega\tau}\right\}$$

In the zero sound limit, the real part of the impedance is given by :

$$\frac{R_\infty}{\rho v_F} = \frac{(3+F_1)}{8\left[1+\frac{1}{2}\left(\frac{4+F_1}{1+F_2/5}\right)^{1/2}\right]} \qquad (3.6.5.)$$

It is suggested that equation (3.6.4.) is accurate to better than one half of one per cent in the zero sound regime, although the errors in the hydrodynamic regime may be of the order of a few per cent. This new theory is apparently being extended to include the longitudinal acoustic impedance.

3.7. The parameter ξ_2.

The parameter ξ_2 is not directly obtainable from experiment although estimates are possible by consideration of the quasiparticle scattering amplitude and a value of 0.35 has been suggested by Dy and Pethick (unpublished; as quoted by Lawson et al (1974)). More recently, Wölfle (1976) has suggested that $\xi_2 \approx 0.28$, this value being obtained from studies of the superfluid phases of helium-3. However, the importance of a precise value for ξ_2 has been investigated by Flowers and Richardson and they have found that the effect of ξ_2 upon the transverse acoustic resistance (that is, the real part of the complex acoustic impedance) is very small. Numerical calculations have shown that the acoustic resistance changes by less than one per cent when ξ_2 is changed by a factor of 3. Consequently, in shear acoustic resistance calculations, the actual value chosen is not significant and it is often convenient to set ξ_2 to unity, which is equivalent to a single relaxation time approximation in terms of the departure of the distribution function from local equilibrium.

In contrast to this, the attenuation of transverse zero sound (which is related to the imaginary part of the acoustic impedance) is found to be strongly dependent upon ξ_2. Numerical calculations of the imaginary part of the solution to the dispersion relation show that, in the zero sound regime, the attenuation coefficient is roughly proportional to $(\xi_2)^{-1}$. Clearly, a single relaxation time approximation is not justified in attenuation calculations. Fortunately, in the work presented here, we are concerned only with the transverse acoustic resistance so that any dependence upon ξ_2 may be ignored.

Furthermore, in the zero sound limit, the term involving $\mathcal{F}_{s_2}$ approaches zero so that the limiting values of the acoustic resistance do not depend upon the parameter $\mathcal{F}_{s_2}$ (see equation (3.4.6.)).

3.8. The acoustic impedance of a Fermi gas

An assembly of non-interacting Fermions cannot support shear stress and therefore no transverse waves can be propagated. However, a finite value of acoustic impedance may still be obtained by treating the Fermi gas as the limiting case of a Fermi liquid as the interaction function approaches zero.

If we consider Fomin's equation for the real part of the acoustic impedance in the limit $\omega\tau \to \infty$, we have ;

$$\frac{R_\infty}{\rho} = \frac{3 p_F}{m F_1}\left[\eta - 1 + \bar{\Phi}\right] \qquad (3.8.1.)$$

where $$\bar{\Phi} = \frac{1}{\pi}\int_0^1 \tan^{-1}\left[\frac{\pi}{2}\frac{u(1-u^2)}{(1-u^2)(1-u\tanh^{-1}u) - \left(\frac{F_1-6}{3F_1}\right)}\right] du$$

There is no transverse wave propagated, and the term $(\eta - 1)$ disappears from the equation. Now, in the definition of $\bar{\Phi}$, as $\omega\tau \to \infty$, the second term in the denominator becomes dominant ;

ie : $$\bar{\Phi} = \frac{1}{\pi}\int_0^1 \tan^{-1}\left[-\frac{\pi}{2}u(1-u^2)\ \frac{3F_1}{(F_1-6)}\right] du$$

Thus, as $F_1 \to 0$;

$$\Phi = \frac{1}{\pi}\int_0^1 \tan^{-1}\left(\frac{\pi}{2}u(1-u^2)\frac{F_1}{2}\right)du$$

Also, as $F_1 \to 0$; $\tan^{-1} F_1 \to F_1$, therefore ;

$$\Phi = \frac{1}{\pi}\int_0^1 \frac{\pi}{2}\frac{F_1}{2}u(1-u^2)\,du = \frac{F_1}{16}$$

Thus, for acoustic resistance, we find ;

$$\frac{R}{\rho} = \frac{3}{16}\frac{p_F}{m} = \frac{3}{16}\frac{m^*}{m}v_F$$

As the interaction function vanishes, $m^* \to m$;

ie:
$$\frac{R}{\rho} = \frac{3}{16}v_F \qquad (3.8.2.)$$

This same result may be obtained by considering the rate of transfer of momentum from the oscillating boundary to the quasiparticles by diffuse scattering. Transverse acoustic impedance is defined thus :

$$Z = \Pi_{ik} / v_i \qquad (3.8.3.)$$

where Π_{ik} is the (ik) component of the momentum transfer tensor and v_i is the velocity of the boundary (Polarization of the oscillations is assumed to be in the i direction).

The momentum transferred to a single quasiparticle = $m^* v_i$. At any instant, the number of quasiparticles moving away from the boundary will be roughly $n/2$, where n is the number density of quasiparticles. Therefore, total momentum transferred in unit time is given by:

$$\text{Momentum transfer / unit time} = \frac{n}{2} m^* v_i$$

The rate at which this transfer occurs is the average of the velocity components v_k of the quasiparticles ($\underline{k}$ being the direction of the normal to the oscillating boundary). Now the Fermi sphere is not distorted but simply displaced by v in the direction $\underline{i}$, so the average of the v_k components will be that for a half Fermi sphere. Therefore, average velocity in direction $\underline{k}$ is given by:

$$\overline{v_k} = \frac{3}{8} v_F$$

Rate of transfer of momentum;

$$\Pi_{ik} = \frac{n}{2} m^* v_i \frac{3}{8} v_F$$

Therefore:

$$Z = \frac{3}{16} n m^* v_F$$

or,

$$\frac{Z}{\rho} = \frac{3}{16} \frac{m^*}{m} v_F$$

Again, since $m^* \rightarrow m$ as $F_1 \rightarrow 0$;

$$\frac{Z}{\rho} = \frac{3}{16} v_F$$

CHAPTER FOUR

4.0. EXPERIMENTAL TECHNIQUES

4.1. Pulse-echo techniques

The basic techniques of reflection mode pulse-echo studies are well established and figure 4.1. shows a block diagram of the arrangement used in this work. A high-intensity pulse of radio-frequency energy is applied to the electrode which induces a short pulse of high-frequency ultrasound in the piezoelectric rod. (The details of ultrasonic generation by surface excitation have been described by Lea et al (1973) (b). If the rod has end faces that have been polished flat and parallel, the pulse will be reflected many times as it gradually loses energy. Each ultrasonic pulse will therefore generate a train of echoes, the amplitude of which decreases exponentially as the number of echos increases. The loss of energy is due to two main processes,

(i) attenuation in the material of the rod due to scattering processes,

(ii) losses due to energy transmission at each reflection.

Therefore any change in the decay pattern of the echo envelope may be related to these losses.

In the experimental work described here, the piezoelectric rod was surrounded by liquid helium and the shape of the echo envelope was observed over the range of temperatures from 2.0 Kelvin to about 15 mK.

After correcting for the temperature-dependent losses due to attenuation in the rod, the energy losses due to transmission into the liquid may be determined from which the acoustic impedance is obtained as a function of temperature. The experiments were carried out using a helium-3/helium-4 dilution refrigerator constructed by the Oxford Instrument Company Limited. At the start of this work the refrigerator was fitted with a dilution unit having a nominal base temperature of 25 mK but this was later replaced by a new unit capable of reaching temperatures down to about 12 mK.

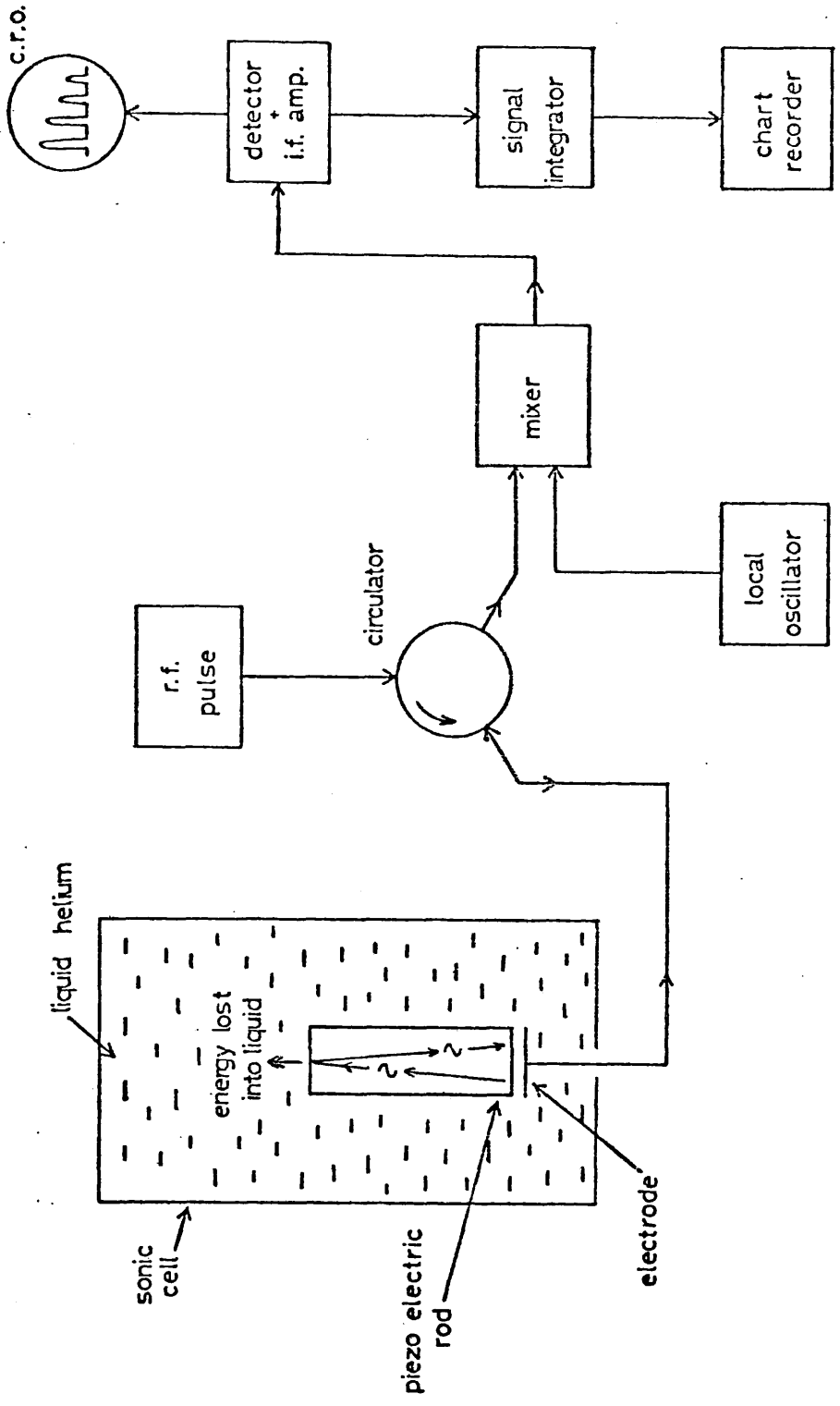

Fig. 4.1 Block diagram of pulse-echo technique

4.2. The sonic cells

The original sonic cells, constructed to designs by Dr MJ Lea, are shown in diagrams 4.2. and 4.3. Their resonant frequencies were 242 MHz and 1048 MHz respectively. The piezoelectric rod was supported just above the electrode which was fed by a resonant cavity attached to the base of the cell. Resonance was achieved by a helical coil in the low frequency cavity and by a quarter-wave post in the high frequency unit. In both cases, coupling was by a capacitive loop since this method ensured thermal isolation between the electrode (in contact with the liquid helium sample) and the r.f. feed line (at a considerably higher temperature than the sample). The resonant frequency was determined by the length of the helix, and the Q-factor by the size and position of the coupling loop. Both were the result of trial and error, various loops being tested until a suitable resonance characteristic was obtained. Both the resonant frequency and the Q-factor differed appreciably from their room temperature values when cooled to liquid helium temperatures but there was no significant change in the resonance over the temperature range of the experiment. In the high-frequency cavity, a closed loop was found to overcouple the cavity and this was later replaced by an incomplete loop. The resonance characteristic of the low-frequency (Mark I) cavity, at 0.5 Kelvin, is shown in diagram 4.4. The inner surfaces of both cavities, the coupling loops and the resonant helix were electroplated with superconductive tin to reduce eddy current heating.

The piezoelectric rod was originally separated from the electrode by a disc of porous paper but this was later replaced by a grid of human hair supported by a ring of paper. This method ensured that the rod was completely

surrounded by liquid helium and also reduced the gap between the rod and the electrode , resulting in a high coupling factor. However, some problems were encountered due to the rod rocking from side to side since it no longer had a flat surface on which to stand. This caused small changes in the capacitance between the rod and the cell which were observed as variations in echo amplitude. The problem was simply overcome by placing thin strips of paper between the rod and the sides of the holder to prevent sideways movement of the crystal. The echo train was then unaffected by vibration of the sonic cell.

Both cells shared the same top section since this avoided disturbing the resistance thermometer contained in the cell. This thermometer was not anchored to the cell but had strips of copper foil soldered to its contact wires to improve thermal contact with the liquid helium. In addition to the thermometer, a small resistive heater was mounted in the top section of the cell so that thermal response times could be measured. The connecting wires to both these devices were sealed-in with "Epibond" heat-cured epoxy resin. The top section and main body of the cells were sealed together with an O-ring of clean indium wire.

The major fault common to both these early cells was the limited surface area of copper in contact with the liquid helium. In the Mark I cell, the contact surface area was about 5 cm^2 but considerably less than this for the high-frequency (Mark II) cell. If the thermal relaxation time, that is, the time required for the liquid helium to come to thermal equilibrium with the cell, is τ then this is given by the expression :

$$\tau = CR$$

where C is the net thermal capacity of the system and R is the thermal boundary resistance. Using, for R , the Kapitza boundary

resistance over the contact surface area, ie. $R = R_k A$, we find that for the Mark I cavity, $\tau \approx 0.84$ second at 1.0 Kelvin. This time is short compared to that required to make any observation on the sample so it is reasonable to assume that the liquid helium is in good thermal contact with its surroundings. However, as the temperature falls, the Kapitza resistance increases as T^{-3} and we find that, at low temperatures, the thermal relaxation time has increased such that τ is about 55 minutes at 0.02 K. Obviously with relaxation times of this order, thermal equilibrium cannot be assumed and, as the cell is cooled, the temperature of the liquid helium sample increasingly lags behind that of the cell. The implication of this problem will be discussed further in section 4.7.

A new sonic cell (figure 4.5.) was designed with the aim of considerably reducing this thermal relaxation time. The use of copper sinter increased the surface area to such an extent that the surface area of the rest of the cell was insignificant. The ratio of surface area to volume was roughly $\pi\sqrt{2}/d$ where d is the diameter of the copper particles. In our case, using 40 micron particles, the surface area of the sintered copper was about 9.6×10^2 cm^2; a factor of 200 greater than the Mark I cell. This implies a reduction in the thermal relaxation time by the same factor to give;

$\tau \approx 4.2\,ms$ at 1.0 Kelvin and

$\tau \approx 16s$ at 0.02 Kelvin

Bearing in mind that the rate of cooling produced by the refrigerator at the lowest temperatures is, typically, 1 mK $hour^{-1}$ at 30 mK, these relaxation times are quite acceptable and the sample may be taken to be in thermal

equilibrium with the sonic cell at all temperatures. The fabrication of the sintered copper section was kindly undertaken by the Oxford Instrument Company Limited. The hole into which the rod was placed was cut using a spark erosion machine to avoid damage to the sinter. This hole was stepped , having a diameter of 3 mm at one end and 5 mm at the other, so that, by inverting this section, the cell could accommodate rods of either 3 mm diameter or 5 mm diameter.

The resonant cavity was basically the same as in the earlier designs except that the resonant helix may be replaced by a quarter-wave post so that the same cavity may be used over a larger range of frequencies. A new top-cap was designed for this cell to include provision for a CMN thermometer in addition to the resistance thermometer. For this reason, the cap was machined from "Epibond" epoxy resin,bonded to a copper flange. The shape of the cap was designed to incorporate a right circular cylinder of pressed cerium magnesium nitrate powder, and a shallow groove was machined onto the outside of the cap to locate the necessary detection coil. Again, indium O-rings were used to seal the three sections together. Considerable force was required to ensure that the cell was leaktight after assembly and for this reason stainless-steel bolts were used.

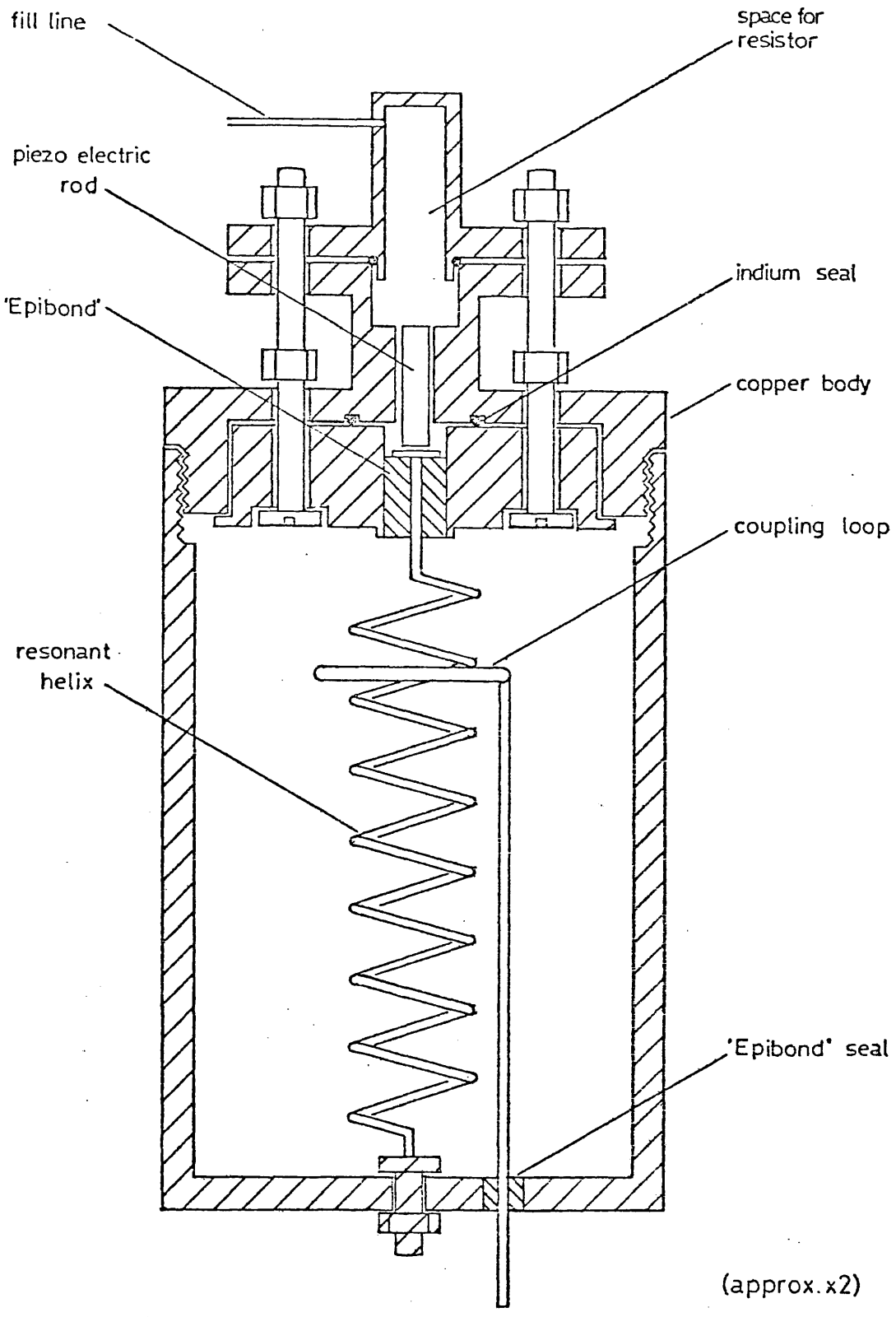

Fig.4.2 Mark 1 Sonic cell (242 MHz)

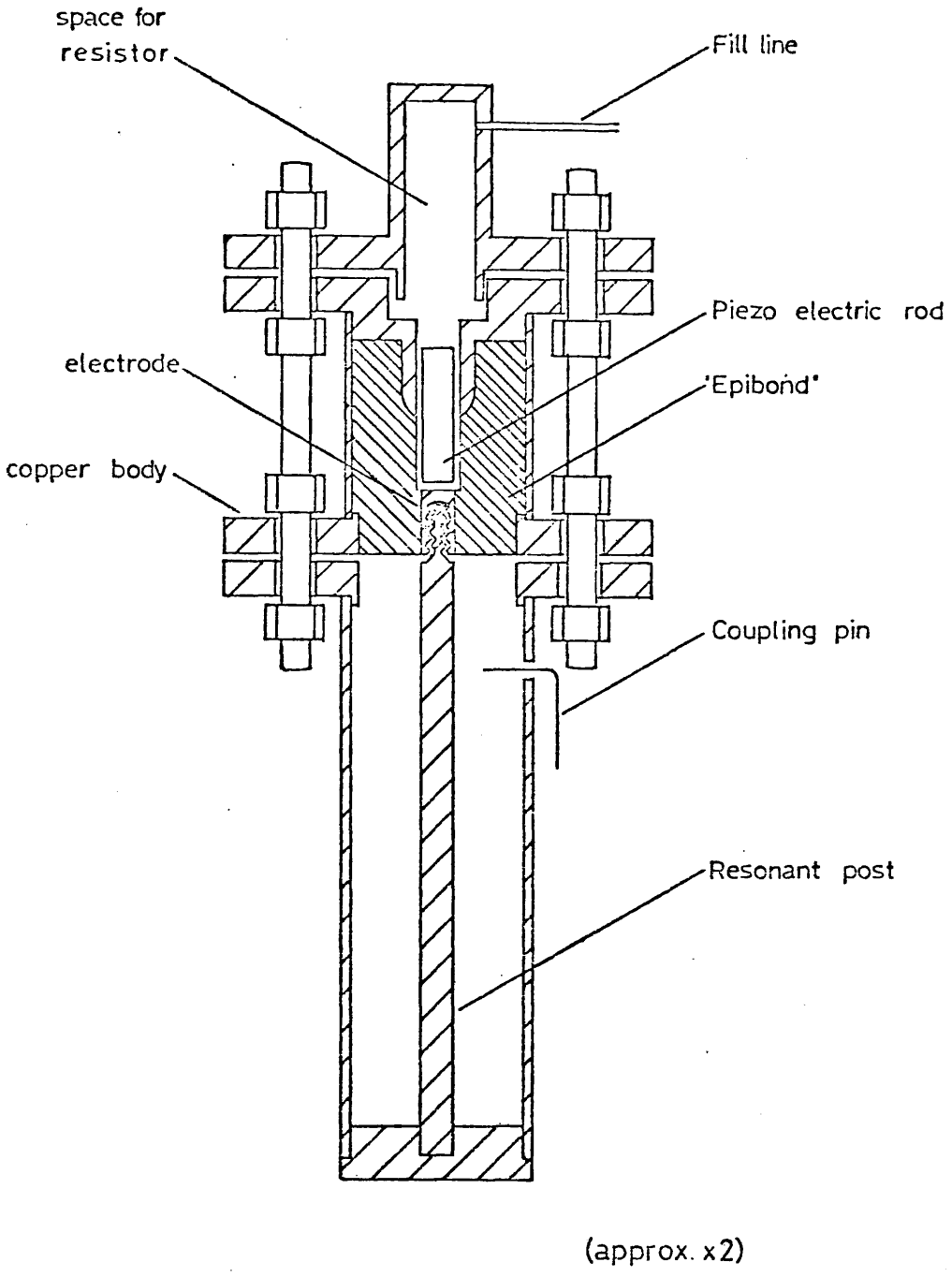

Fig.4.3 Mark 2 Sonic cell (1048 MHz)

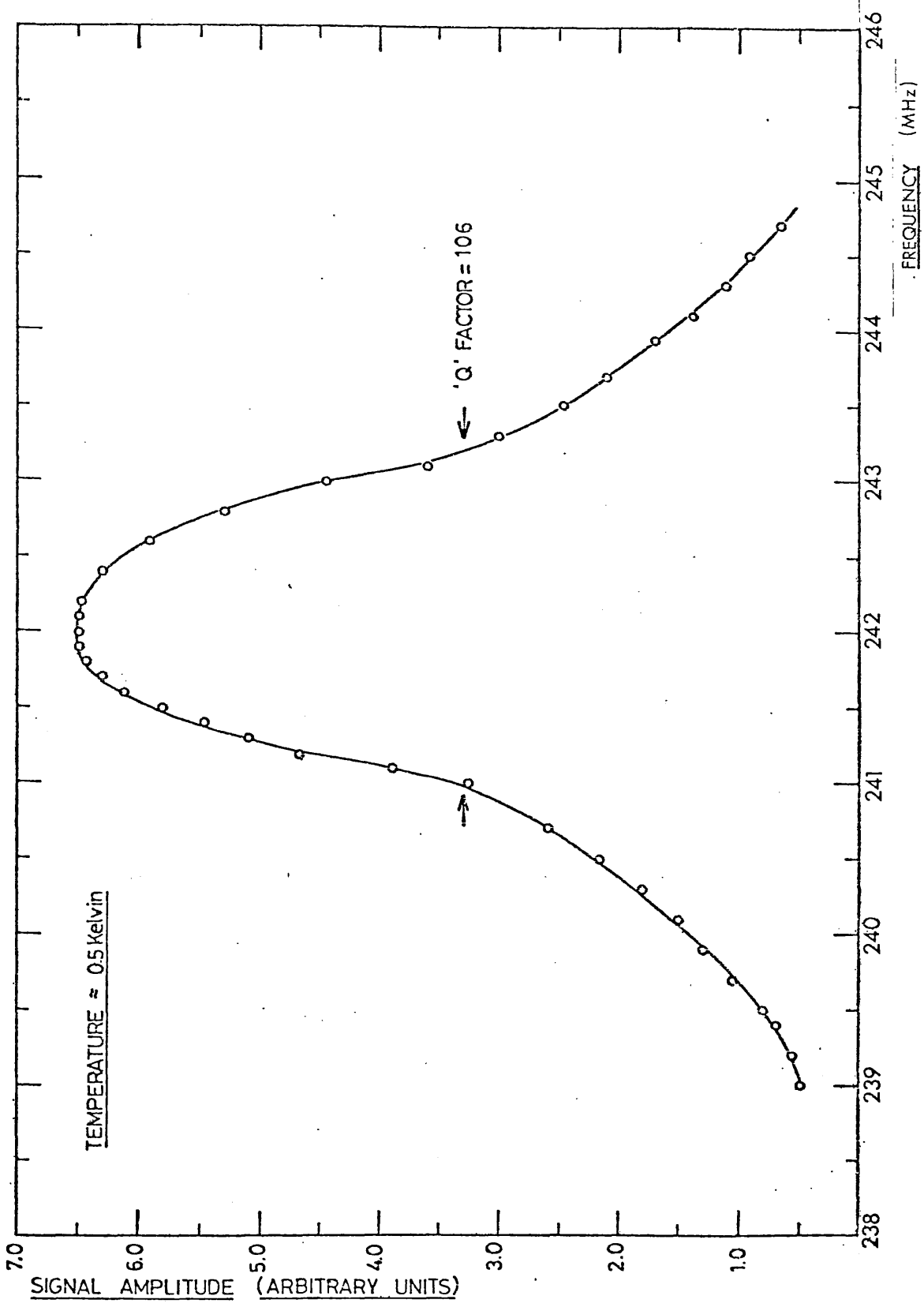

Fig. 4.4 RESONANCE CHARACTERISTIC (Mk.1 CAVITY)

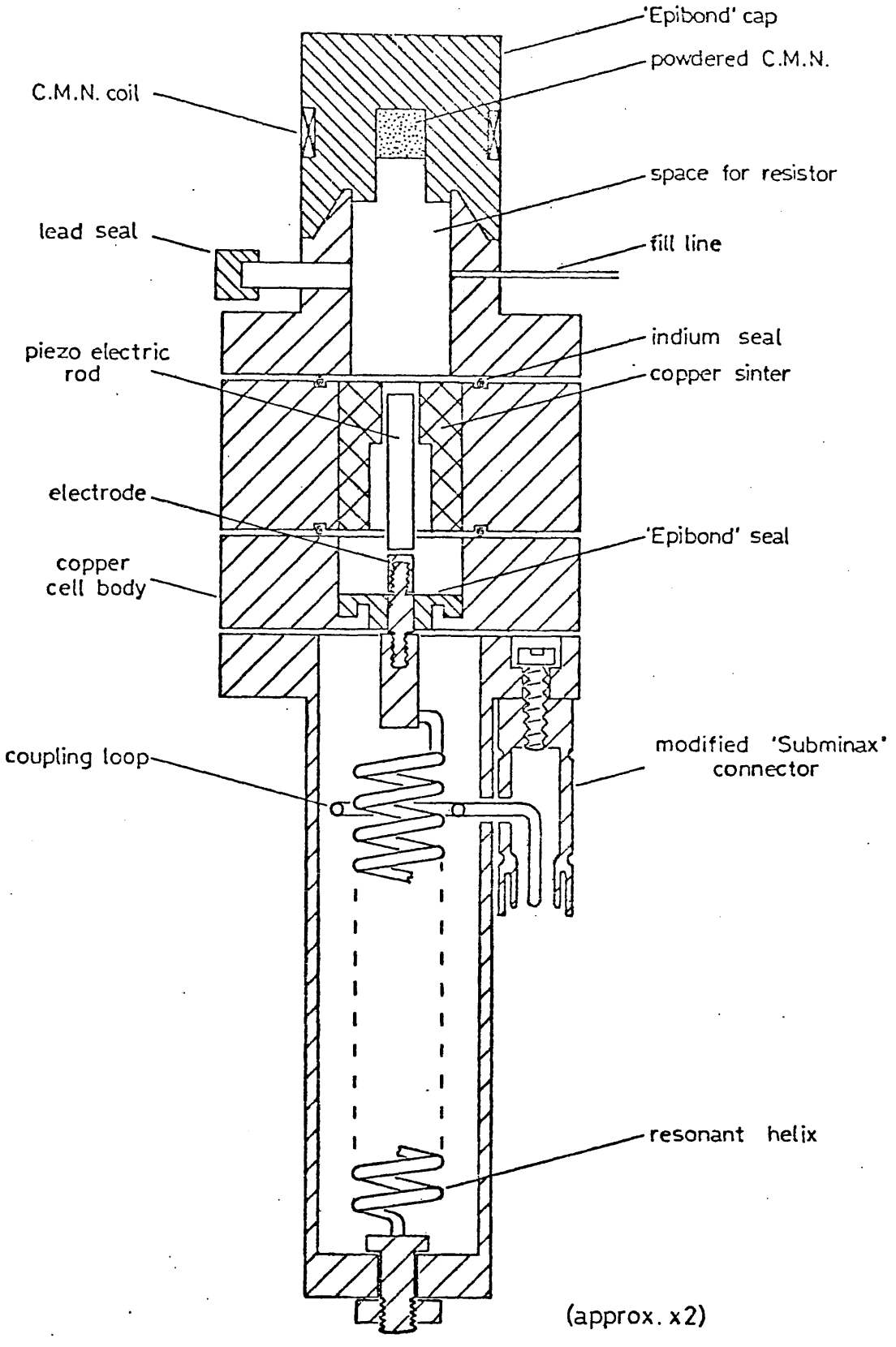

Fig.4.5 Mark 3 Sonic cell (250 MHz)

4.3. Piezoelectric rods

4.3.1. Transverse mode experiments

The most frequently used material in pulsed ultrasonic studies is quartz. (see, for example, the work of Matthews, Keen and Wilks (1965) and of Abel, Anderson and Wheatley (1971).) However, this material is unsuitable for transverse acoustic impedance work because the coupling constants into the shear modes are very low (0.08 and 0.14 for the AC and Y directions, respectively; see Neppiras (1973)). An alternative appeared to be lithium niobate ($Li\ Nb\ O_3$) which has very high coupling constants to the two shear modes of oscillation (0.62 and 0.68). However, the attenuation does not fall below 2.0×10^{-2} dB cm^{-1} at 500 MHz (Spencer et al (1967)) even at temperatures below 4.2 Kelvin and this limited the useful echo train to about two hundred transits beyond which the echos were lost in electrical noise. Calculations had shown that about three hundred transits were required to produce a change in signal height of about 0.5 dB, which was considered to be the smallest clearly observable change with the apparatus available at that time. Some early experiments confirmed the unsuitability of this material.

The search for a piezoelectric material having a lower attenuation coefficient for the transverse mode was rewarded when reports (Neppiras (1973), Spencer et al (1967), Rehwald (1973)) describing the properties of bismuth germanium oxide ($Be_{12}GeO_{20}$) were studied. Although the coupling constant into the singleshear mode is, at 0.24, lower than that for lithium niobate, the attenuation at temperatures below 4.2 Kelvin is extremely small. Spencer et al (1967) quotes a value for the attenuation at 4.2 Kelvin of

0.14×10^{-2} dB cm^{-1} at 118 MHz; a considerable improvement on lithium niobate. When a suitable rod of BGO was tested it was found to be capable of producing a train of more than three thousand echos (at 240 MHz) below 4.2 K although fewer than fifty were observed at room temperature. Another advantage of this material was that, since its crystal structure was cubic, pure elastic modes of propagation could be obtained which would not be sensitive to crystallographic orientation. Furthermore, it has been shown by Spencer et al (1967) that the application of an electric field in any major crystallographic direction will couple only into the pure elastic shear mode, making BGO an almost ideal material for transverse wave studies.

For this work, a rod orientated with the direction of propagation of the wave [110] parallel to the axis of the crystal (to an accuracy of better than five minutes of arc) was used, the rod being 12.5 mm in length and 3.0 mm in diameter. The end faces were required parallel to within five seconds of arc and were polished to optical flatness ($\lambda/10$).

4.3.2. Longitudinal mode experiments

Bismuth germanium oxide is not a suitable material for longitudinal studies because of the difficulty of generating a pure mode; the only longitudinal mode is propagated in the [111] direction which also supports shear wave propagation. To obtain a pure longitudinal mode along a principal axis, a rod of X-cut quartz seemed the most suitable since this material offered a reasonable compromise between the various piezoelectric parameters. The rod was cut and polished to the same specification as the BGO rods used in the transverse experiments.

The echo envelope produced in both transverse and longitudinal cases was not a simple exponential decay but revealed regularly-spaced maxima and minima (see figure 4.6.). If the heights of the maxima are plotted as a function of echo number the expected exponential decay is apparent. Many experimenters have commented upon the modulation of the echo envelope and several theories have been proposed to account for this effect. Bömmel and Dransfeld (1958) have studied the effects of off-axis propagation and a computer simulation of echo patterns, taking into account the results of axis misalignment and non-parallelism of the end faces, has been published by Gates (1964). The theory of wave propagation in piezoelectric rods has been studied in some detail by McSkimmin (1956) and Redwood (1959) and the nulls in the decay pattern have been accounted for by interference between the initial wave and a series of secondary waves produced by 'mode - conversion'.

In the longitudinal case, the reflection of the wave at the walls of rod causes some energy to be converted into a transverse mode which then travels across the rod at a lower velocity than the longitudinal wave. On reflection from the opposite wall a similar mode conversion produces a secondary longitudinal wave which travels with the same speed as the original wave, but out of phase with it. The net effect is an interference pattern superimposed upon the exponential decay due to scattering . For transverse waves, McSkimmin (1956) has shown that the simultaneous excitation of several transverse modes of vibration will result in interference due to the slightly different propagation velocities of these various modes. The use of a circular driving electrode, which excites the whole face of the rod, will inevitably generate several such modes and this is probably the major cause of the modulations to the echo envelope.

To excite a single transverse mode, McSkimmin suggests the use of an elliptical driving electrode that favours excitation of the central area at the expense of excitation at the edges of the crystal. Fortunately none of these mechanisms are temperature dependent so that, provided the frequency of the wave is constant and that all the measurements are taken using a particular group of echoes, the actual shape of the decay pattern is unimportant. Figure 4.7. shows a typical group of echos in BGO, at 242 MHz.

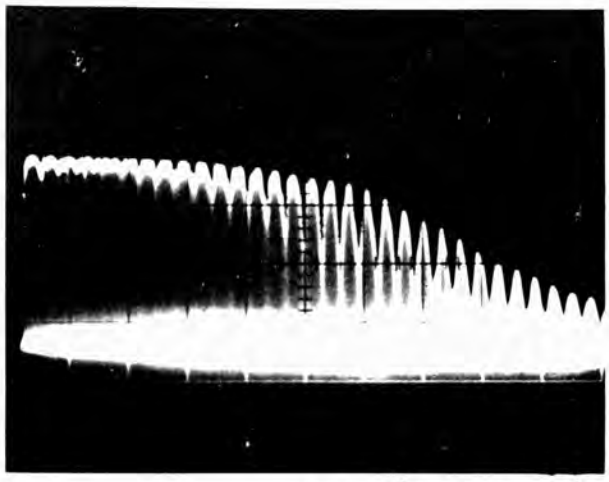

(2ms cm^{-1} ≡ 200 echo cm^{-1})

Fig 4.6 Echo envelope for transverse waves (242MHz) at 4.2K in BGO

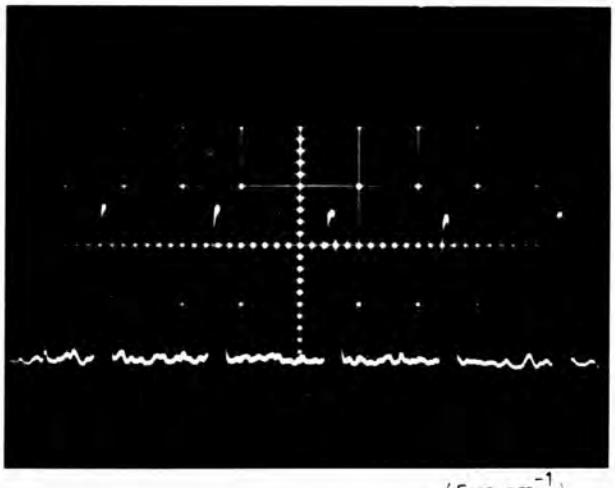

(5μs cm^{-1})

Fig 4.7 Detail of echo train (as above) centered at 2800th echo

4.4. Electronics

4.4.1. Introduction.

The early experiments were carried out using an analogue data recording system consisting of Brookdeal "Boxcar" integrators driving an X-Y chart recorder. The resonant cavity was driven by a cavity oscillator which was repetitively triggered (at about 10 Hz). The resulting echo train was gated such that the height of a particular echo could be integrated by the signal averager to give a d.c. level proportional to the average height of the echos in the gate. Thus any change in echo height would be reflected in the d.c. level and observed on the chart recorder. A similar system was used to monitor the first echo so that any voltage drift or change in the amplifier gain could be taken into account. Synchronisation was achieved by using the trigger output of a 'MATEC' pulse comparator as the master trigger and the delayed trigger output of a Tektronix 585 oscilloscope to gate the Bookdeal integrator after an appropriate delay time. The system worked quite well and some useful results were obtained. However, two serious disadvantages soon became apparent:

(i) The position of the integrator gate needed constant adjustment to ensure that the same echos were integrated throughout the experiment.

(ii) The fairly high pulse repetition frequency required by the integrator caused considerable heating in the sonic cell which prevented the refrigerator from reaching its base temperature.

The first of these problems, whilst inconvenient, was not insurmountable and the task was made easier by fitting a second helical potentiometer to the oscilloscope to improve control of the delay time. The second problem was much more important in that it prevented data collection in the most interesting range of temperatures. To reduce the heating effect of repetitative running, a single-shot method of operation was devised in which a single pulse was applied to the cavity. The resulting echo train was momentarily displayed on the oscilloscope where it was recorded by means of a Polaroid-Land camera. The present electronic arrangement, shown in figure 4.8., uses this same basic method but with digital triggering to improve stability and a more sophisticated data-acquisition system based upon a transient recorder and digital store. The most important features of the system will be described in the following sections.

4.4.2. Pulse generation.

The driving r.f. pulse was provided by a tuneable cavity oscillator. In the lower frequency experiments a J.V.M. type 7600/1 oscillator was used which covered the frequency range from 225 to 400 MHz. This cavity, when driven by its maximum permitted modulation pulse (3 kV), was capable of producing an output power of about 2 kW but for the experiments described here such power was unnecessary and the modulator level was never set at greater than 1 kV. The high-frequency experiments used a similar cavity oscillator, J.V.M. type 7440/1, which covered the frequency range from 960 to 1120 MHz. Both cavities were fitted with decade counters to ensure precise and reproduceable frequency selection. The stability of the oscillators, both in frequency and output amplitude, was found to be excellent showing negligible drift over an operating period of several hours.

The output pulse was fed via a calibrated (0 to 25 dB) barrel-type attenuator to a ferrite-ring circulator and then to the driving electrode in the sonic cell through a rigid coaxial feed line.

The design of the coaxial feed line to the cell was important since it was a potential source of heat leaks into the refrigerator. Materials having very poor thermal conductivity were required so thin-walled cupro-nickel tube was used; 5mm diameter for the outer conductor and 2mm diameter for the inner. This ratio of conductor radii gave an impedance of about fifty ohms, thereby roughly matching the impedance of the other components. The outer conductor was thermally anchored at 1.2 Kelvin, 800 mK (the still) and 20 mK (the lowest heat exchanger) by copper screw-threads, soldered to the tube, which mated with copper bushes attached to the refrigerator. The inner conductor must also be thermally anchored and this was accomplished by the use of glass-to-metal seals. These consist of inner and outer coaxial conductors bonded to a glass disc which electrically insulates the two conductors whilst thermally connecting them. One of these seals at each of the thermal anchor points ensured that the inner and outer conductors were thermally linked. The importance of thermal anchors was dramatically demonstrated during one experimental run in which the seal at 1.2 Kelvin had broken, leaving the inner conductor thermally isolated. The result was a heat leak which prevented the refrigerator from cooling below 50 mK. Outside the refrigerator, conventional fifty-ohm coaxial cable was successfully used at both 242 and 1048 MHz.

Each arm of the circulator was matched to its particular load by means of Weinschel double-stub tuners and a fourth set of tuners was placed between the cavity oscillator and the calibrated attenuator. Once these tuners had

been set further adjustments were not necessary during the course of an experimental run.

4.4.3. Amplification.

The echo pulses were detected by means of a superheterodyne system using a Hewlett-Packard (10514A) matched-diode mixer. The r.f. signal from the sonic cell was first amplified by a high-gain, low-noise Avantek amplifier before being fed to the mixer where it was combined with a local oscillator signal to produce a 60 MHz intermediate-frequency signal. Amplification of the complete echo train resulted in gross saturation of the amplifier and distortion of the base line, therefore a radio-frequency switching circuit was placed before the amplifier so that only the tail of the echo train would be amplified. Typically, in the transverse experiment, the switch was timed to open at roughly the twelve hundredth echo. The point at which the switch opened was originally controlled by the delayed-trigger output of the oscilloscope but this was later replaced by a digital delayed trigger which will be described later. The time for which the switch remained open was determined by a variable delay, controlled by a helipot.

It was necessary to record the first few echos (the amplitude of which would vary little with temperature) so that corrections for variations in the driving pulse amplitude could be carried out during analysis. This was achieved by dividing the signal before the r.f. switch and heavily attenuating the unswitched signal to reduce the amplitude of the first few (unamplified) echos to match that of the gated (amplified) echos towards the end of the train. The two signals were then combined before being

fed to the mixer. Although the whole echo train was combined with the gated echos, the unamplified signal is so small at, say, the twelve hundredth echo, that compared with the amplified echos, its contribution to the combined signal could be ignored. Figure (4.9.) should make clear the operation of the r.f. switch and combiner.

4.4.4. Data acquisition

A MATEC PR 201 pulse comparator was used to detect the i.f. signal since this instrument incorporated an excellent low-noise i.f. amplifier. The output was fed to a Datalab 920 transient recorder where it was converted to digital form and then stored in a Datalab 4000-series memory. The memory could be read out as analogue data onto a chart recorder, or as a set of two thousand pure binary numbers onto magnetic tape.

This particular transient recorder was chosen because it offered a facility by which the input signal could be sampled at two different rates, the instrument switching rates at a predetermined point. In this mode of operation, designated A/B, the first twelve hundred echos, for example, could be sampled at slow rate 'A' after which the recorder switches to its fastest rate 'B' to analyse the next few echos in detail. In practice, this was achieved by using an external trigger pulse to coincide with the peaks of the first 1200 echos which resulted in a digitised record of the echo envelope, stored in the first 1200 channels of the memory. When the 1200th pulse was received, the transient recorder automatically switched to its fastest sampling rate so that the remaining 800 channels could be used to store a detailed digital record of the next few echos. This operation is shown schematically in figure 4.10. Diagram (a) shows the echo train as

observed on the oscilloscope (ie. the MATEC output) and (b) shows the start of the train on an expanded scale.

The trigger pulses were arranged to coincide with the peaks of the first 1200 echos and diagram (c) shows the full sweep, the sampling rate switching at the 1200th pulse. In fact, the r.f. switch was set to open about fifty echos before the sample rate changed so that the actual echo pattern stored in the memory appeared as in diagram (d). Figure 4.11. shows a copy of a chart recorder plot of the contents of the store after accumulating 512 shots taken at constant temperature. The echo heights may be measured directly from charts such as this, or deduced from the pure binary data read from the store onto the Perex "Perifile" magnetic tape recorder.

4.4.5. Triggering and synchronisation

As the detection system became more sophisticated, the need for fast and stable triggering became increasingly important and our requirements were finally met by two instruments built to specifications prepared by Dr MJ Lea. The design and construction of these units was expertly carried out by Mr AK Betts.

The first of these devices is known as the "Digital Echo Synchroniser" and it performs two independent functions. The most complex task carried out by this machine is the synchronisation of the transient recorder trigger pulses with the individual echos. A 10 MHz crystal clock and a system of digital pulse counters enables the selection of a clock pulse that exactly coincides with each echo peak. The operator is therefore able to set an initial delay time (using thumbwheel switches) to bring the first echo into

coincidence with a trigger pulse, and then select the period required to bring trigger pulses into coincidence with the remaining echo peaks. This operation is shown in figure 4.10.(b). The initial delay is variable in steps of 0.1 μsec from zero to 99.9 μsec. The period between successive pulses is variable from zero to 100 μsec in steps of 0.0001 μsec, its stability being limited only by that of the crystal clock, which was quoted as 1 part in 10^8.

A separate function of this machine is that of master trigger for the synchronisation of the rest of the electronics. For this purpose a separate crystal clock emits trigger pulses at a continuously variable repetition rate between 0.5 pulse sec^{-1} and 10^5 pulse sec^{-1}. A refinement of this is the "Preset" mode which allows a set number of trigger pulses, from 1 to 999, to be generated at any required rate in this range. These pulses are used to synchronise the modulator, the transient recorder and the "Digital Delay Trigger". The latter instrument is a digital delay designed to replaced the delayed-trigger output of the oscilloscope. It is again based upon a 10 MHz crystal clock and emits a single trigger pulse after either a preset time (between zero and one second) or after a set number of pulses have been received. The delayed trigger was used to open the r.f. switch and to trigger the oscilloscope so that the amplified echos could be observed on an expanded timebase.

4.4.6. Control system.

The final specialised unit is an automatic control system, also designed by Mr AK Betts, to coordinate the operation of the data collection apparatus. This device, by means of a single push-button, initiates the following

sequence of events :

(i) DL 4000 store is cleared

(ii) A preset number of r.f. pulses (typically 512) are fed to the sonic cell at a preset repetition rate

(iii) The transient recorder scales and converts to digital form the echo pattern resulting from each r.f. pulse.

(iv) The store accumulates the data from all 512 echo trains.

(v) The contents of the store are output to the magnetic tape recorder in the form of a discrete 'subfile'.

A time-switch was incorporated into the control system to enable the cycle to be initiated automatically, at preset intervals, so that data could be collected during overnight operation of the refrigerator. A digital counter indicated the number of subfiles transferred to magnetic tape during automatic running.

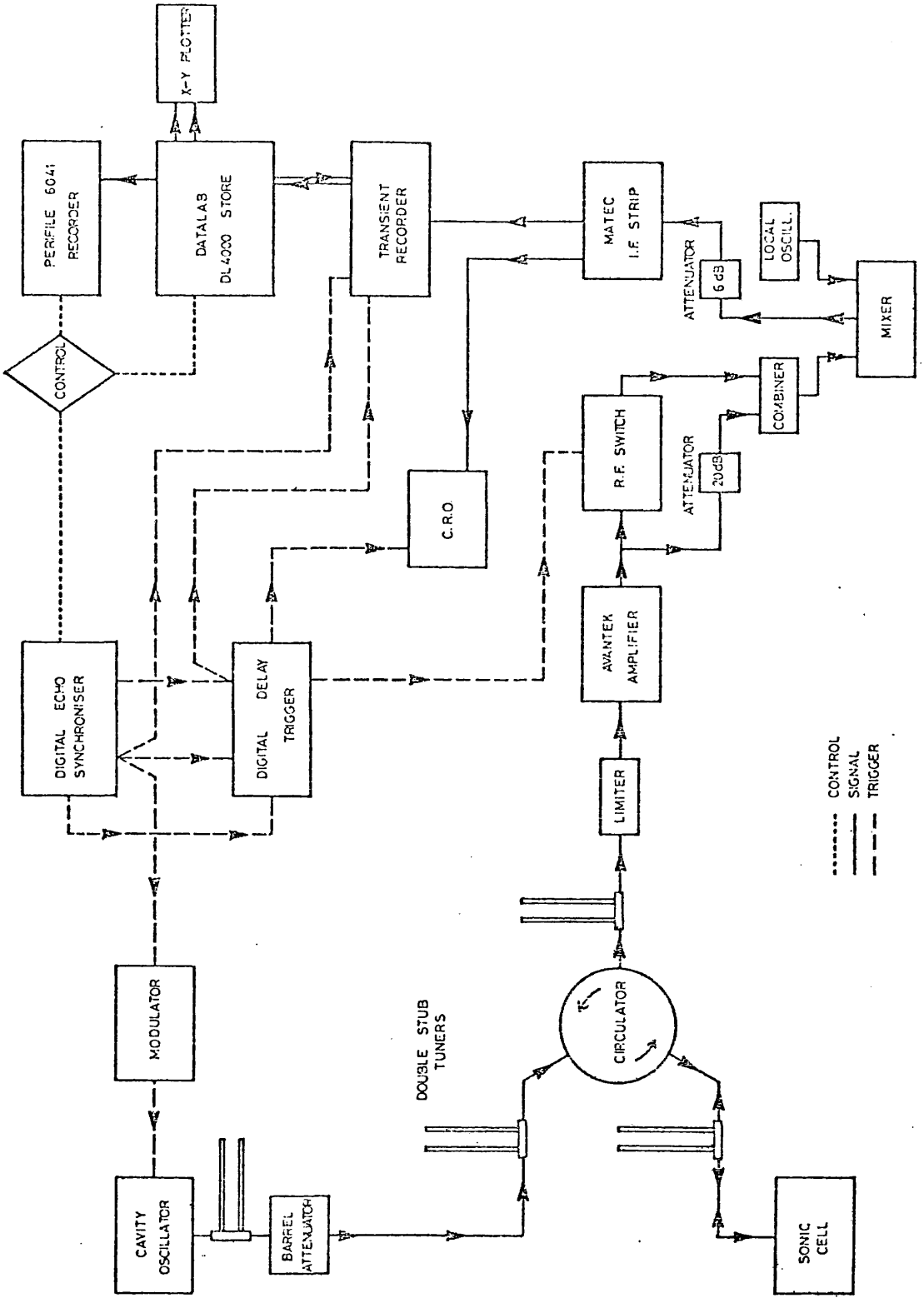

Fig.4.8 SCHEMATIC DIAGRAM OF ELECTRONICS

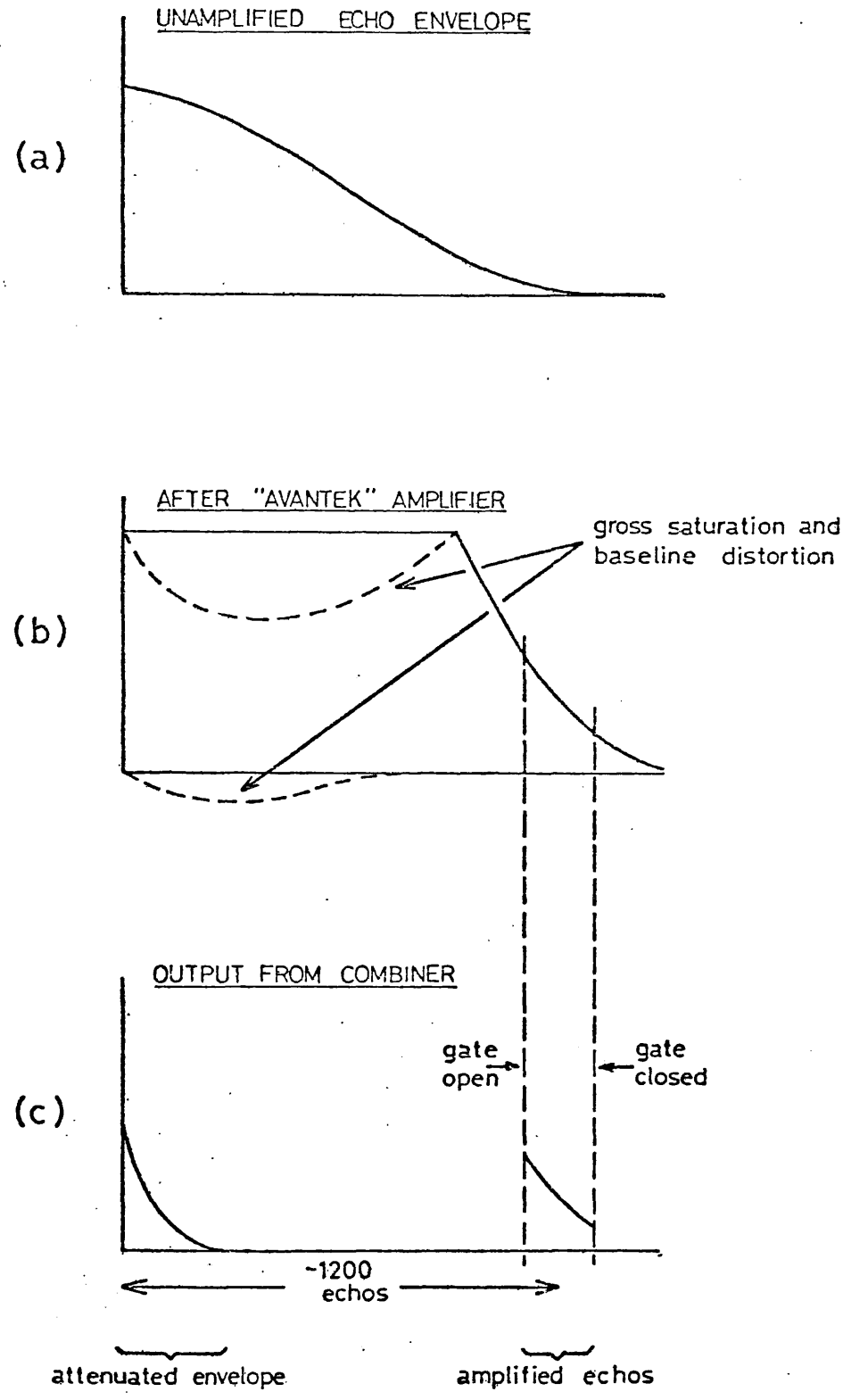

Fig.4.9 OPERATION OF R.F. SWITCH

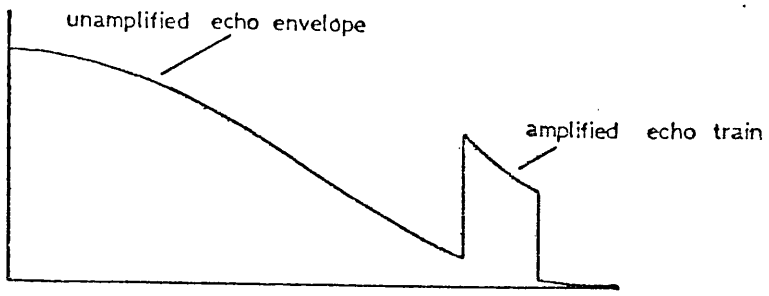

(a) As observed on oscilloscope.

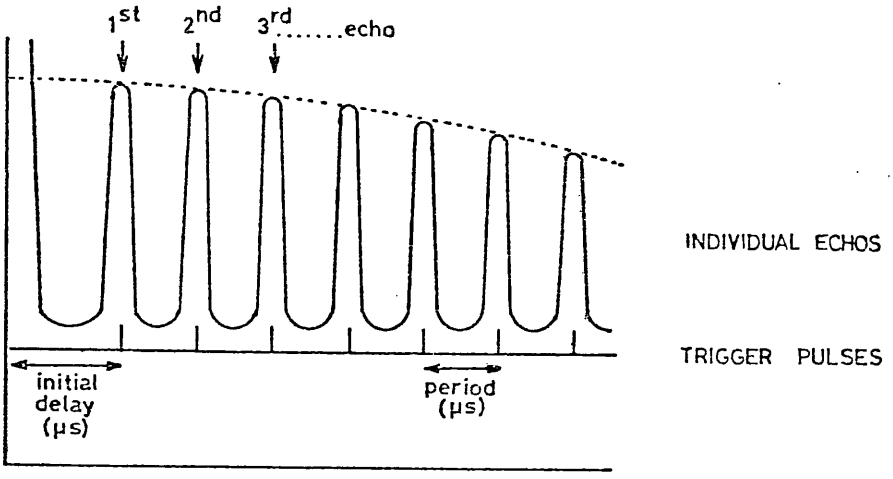

(b) First echos on expanded scale.

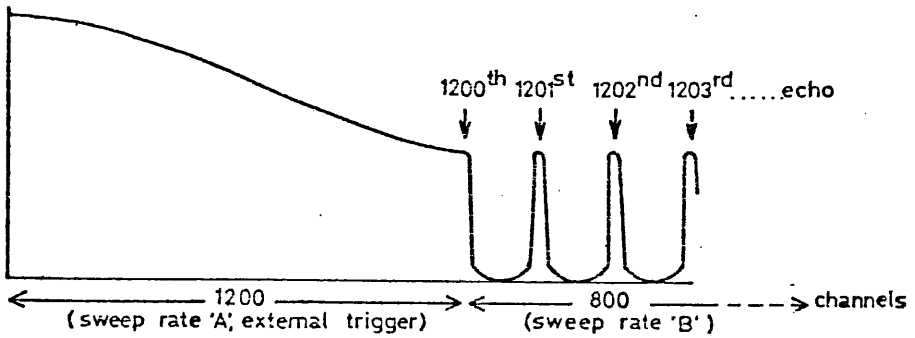

(c) Transient recorder output (r.f. switch open for whole sweep).

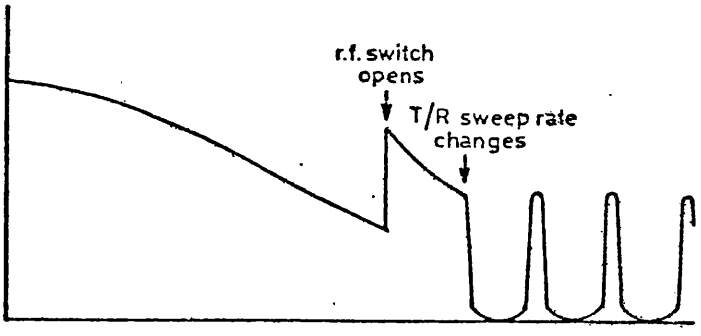

(d) Transient recorder output (normal mode of operation).

Fig.4.10 Operation of transient recorder in A/B mode

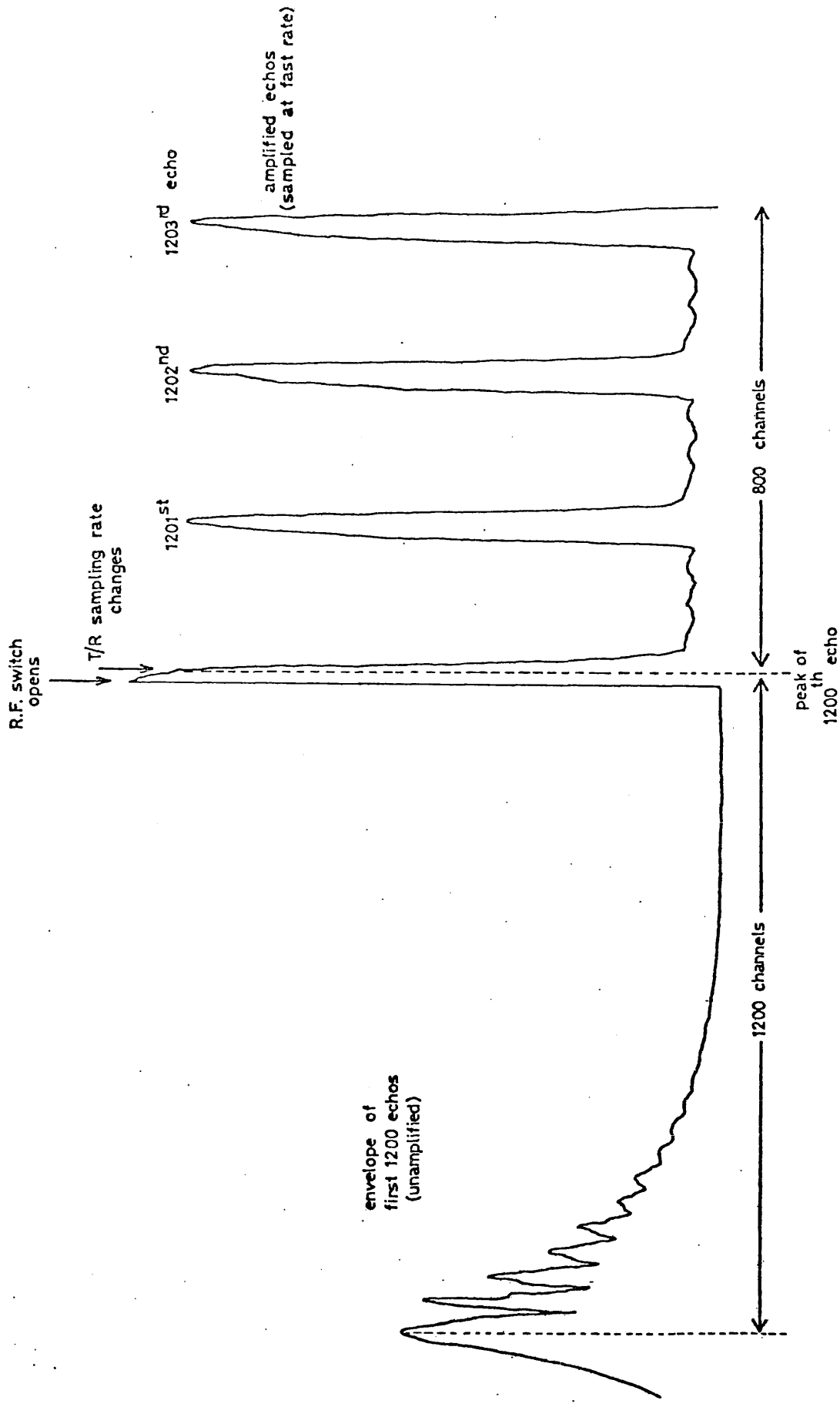

Fig.4.11 Tracing of typical chart recorder output (transverse waves).

4.5. The Helium sample

The helium-3 obtained for these experiments was not particularly pure as supplied (roughly 99.99% helium-3). The most serious contaminant would be helium-4 since this could condense out to form a superfluid film over the piezoelectric rod. This would reduce the energy losses into the liquid to almost zero so that a helium-4 impurity, in a quantity sufficient to form a monolayer, could completely obscure the viscous losses into liquid helium-3. Keen et al (1965) had suggested that phase separation would occur at some temperature depending upon the concentration of the mixture, and the heavier helium-4 would sink to the bottom of the cell. However, in our experimental configuration, this meant that the lower end of the rod would be in contact with helium-4 which would eventually cover the whole rod under the action of superfluid film creep. This would be avoided by ensuring that the surface area of the system was sufficiently large to prevent the formation of a monolayer of superfluid helium-4. Several experimenters had used a highly porous glass, known as Vycor, to trap the normal component of superfluid helium-4 in studies of fourth sound. A small cell containing a piece of this material (kindly provided by Dr DS Betts) was mounted in the helium fill-line, in thermal contact with the mixing chamber, to increase the surface area available for helium-4 condensation.

A more satisfactory solution to the problem of helium-4 contamination was to improve the purity of the sample by distillation. A number of separate processes have been reported but the apparatus described by Sherman (1966) shown in Figure 4.12., which uses a continuous reflux process, seemed to be the most attractive, being simple to construct whilst producing a very

pure distillate. A batch-processing technique was used in which the still was cooled to about 2.0 Kelvin (that is, slightly below the lambda-point) in a helium-4 cryostat and charged with impure helium-3 from the store. The temperature of the still was then raised by the heater so that the helium-3 would be preferentially boiled off. This gas was collected in the cryopump and later transferred to the "pure helium-3" store. The impure residue was then pumped away and a new batch was condensed into the still. The purity of the resulting helium-3 was measured using a M.A.T. "Varian" mass spectrometer and, after distillation at about 2.5 Kelvin, the helium-4 impurity was undetectable using the spectrometer at its highest sensitivity. This was estimated to correspond to an impurity of less than three parts per million.

The sample was pressurized using the system shown in figure 4.13. The cryopump was opened to the helium-3 reservoir and then cooled to 4.2 Kelvin by immersion in liquid helium-4. After closing valve 1, the cryopump was removed from the helium-4 Dewar vessel and the helium-3 contained was allowed to expand into the experimental cell. This expansion was carefully controlled to avoid imposing a sudden pressure change on the indium seals in the sonic cell . When the pump was completely warm and the pressures were equalised, the pressure of the helium-3 in the cell could be observed on the Bourdon gauge, G1. To obtain the highest pressures required,the cell was isolated by the valve V4 and a new charge of helium-3 gas was drawn from the reservoir by the cryopump. This procedure was repeated until the required pressure was obtained in the cell. The range of pressures available was limited by the minimum in the melting pressure curve which has a value 28.9 bar and occurs at 0.32 Kelvin. Any pressure applied in excess of this value would simply result in a plug of solid helium-3 being

formed in the fill line at the point where the temperature was equal to 0.32 K. Consequently, the highest pressure applied during these experiments was 28.0 bar.

When performing experiments on liquid helium-4, a rather different sample handling technique had to be used. A preliminary experiment showed that below the lambda transition, a superfluid film would form on the walls of the fill line which extended to the point at which the temperature was about 2.2 Kelvin. The superfluid film therefore provided a thermal link between the experimental cell and a heat reservoir at the lambda temperature. This heat leak was balanced by the cooling power of the refrigerator which limited the minimum temperature to about 0.6 Kelvin. One possible solution was to insert a coil of capilliary tube, several metres long, to inhibit the film flow but this was impractical due to the limited space available in the refrigerator. An alternative to this was a pressure 'bomb' as described by Abraham et al (1969). The arrangement is shown in Figure 4.14. It was constructed very simply by using a 15 cm length of 2.5 cm diameter copper tube. End caps were soldered in place, the upper cap having a soft copper tube fitted for filling the bomb and the lower cap having a stainless steel tube for connection to the cell. The bomb was mounted vertically, above the sonic cell so that the liquid helium would fill the cell completely.

The bomb was pressurized with helium-4, using the system described above after which the soft copper fill line was crimped and cut to isolate the bomb/sonic cell system. The crimped end of the fill line was sealed with soft solder to prevent leakage on cooling.

The pressure of the gas in the bomb at room temperature was sufficient to ensure that, at 4.2 Kelvin, the sonic cell would be completely filled with liquid helium at the saturated vapour pressure.

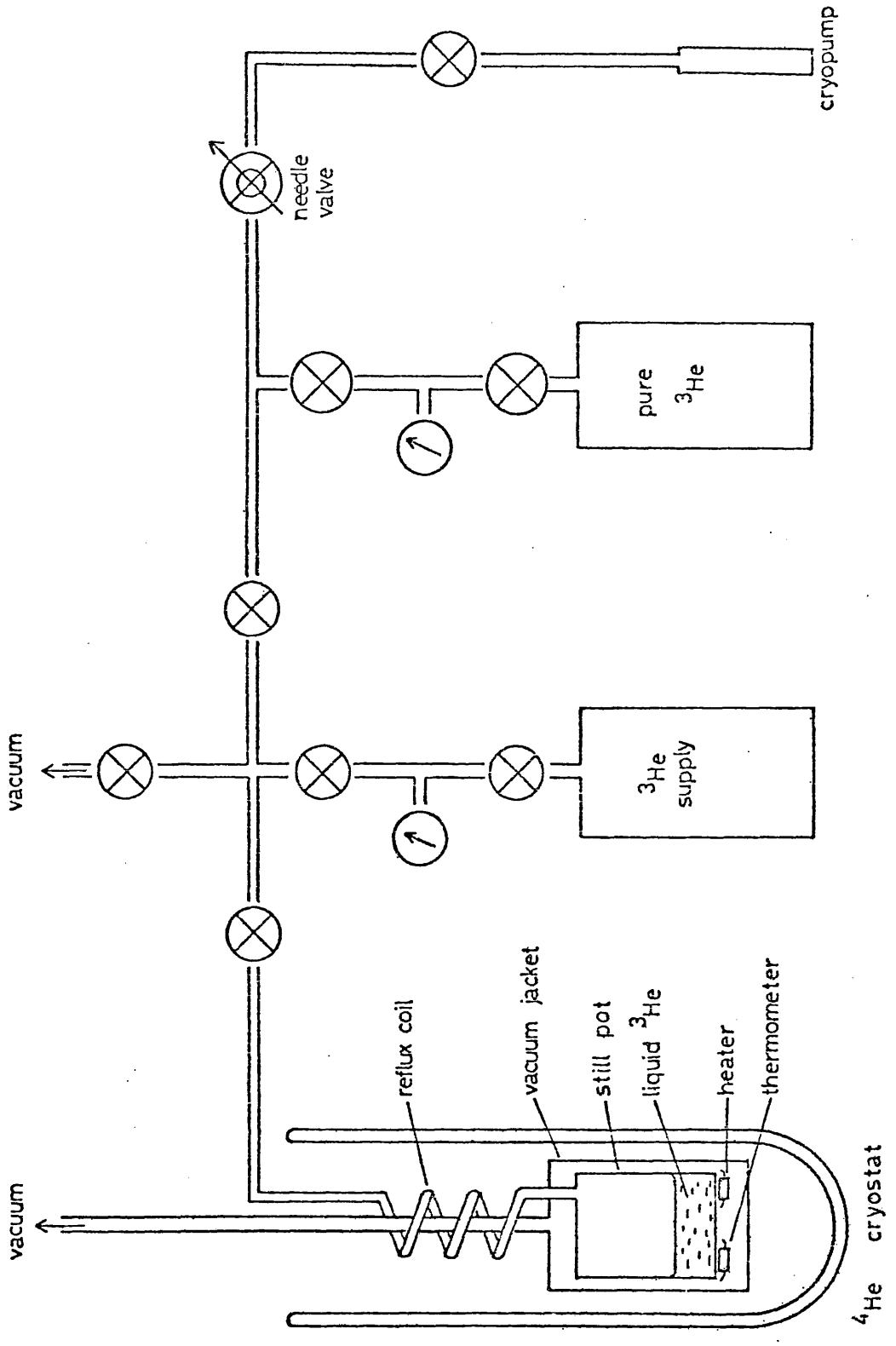

Fig.4.12 Reflux purification of liquid helium-3

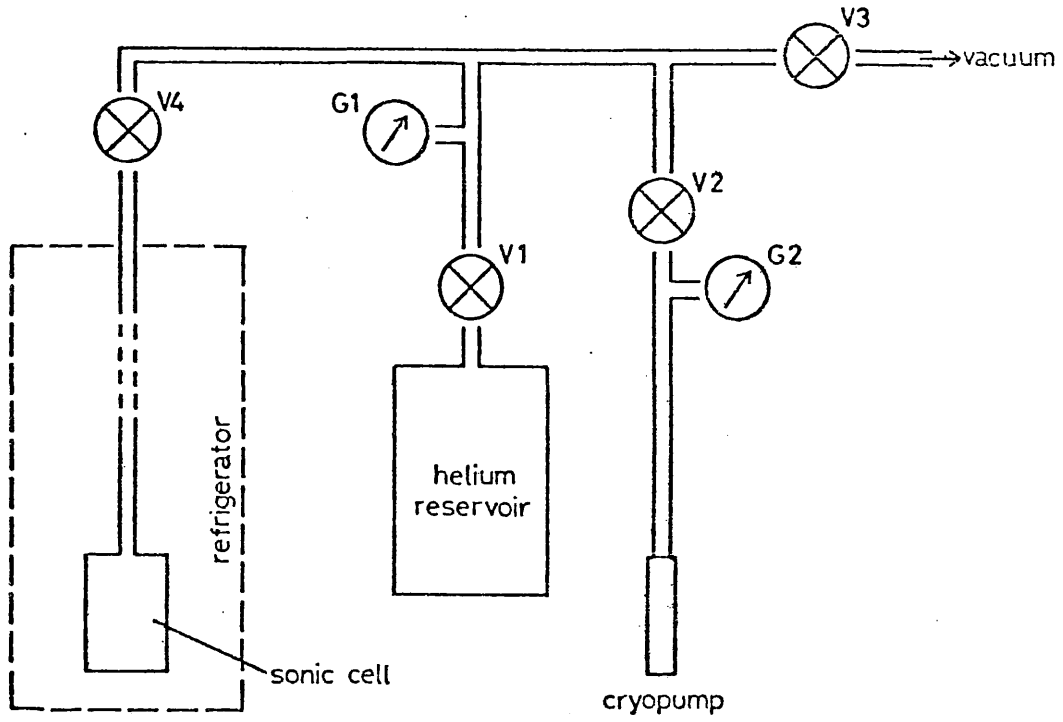

Fig. 4.13 Pressurization of liquid helium-3

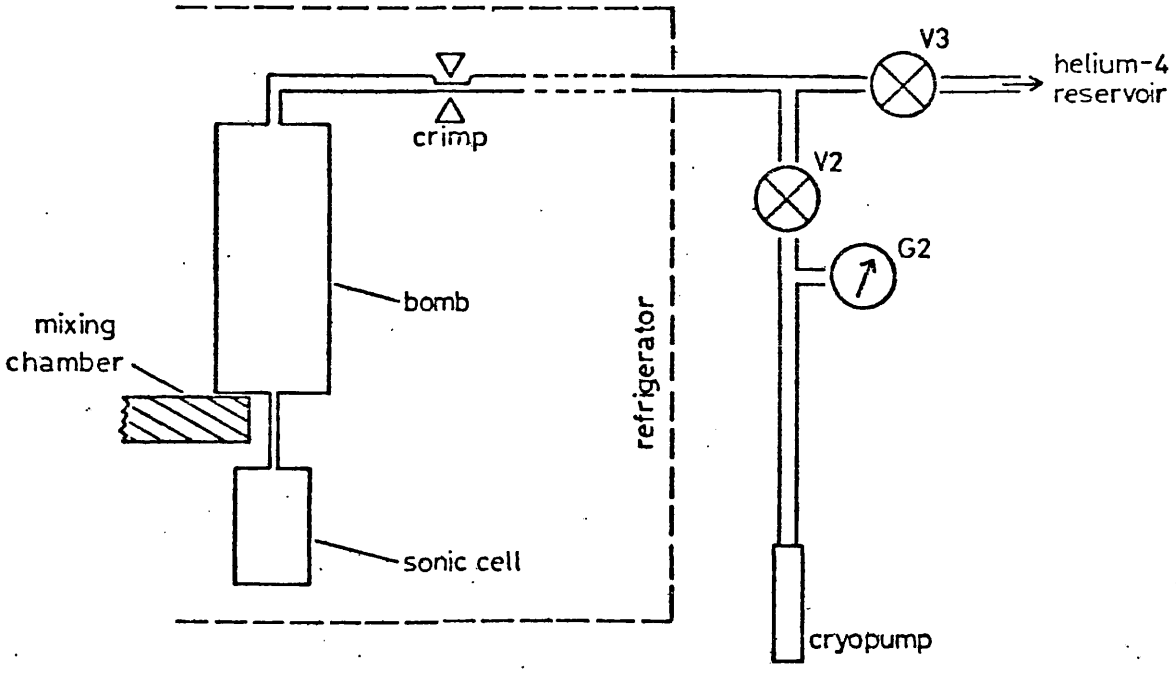

Fig. 4.14 Arrangement for helium-4 experiments

4.6. Heat dissipation in the sample

When pulses of r.f. energy are applied to the sonic cell some degree of heating may result. In our early experiments, in which the pulses were applied continuously, the heat input was sufficient to prevent the refrigerator from attaining its lowest temperature. Under such conditions a considerable heat flow from the sonic cell to the mixing chamber of the refrigerator must have existed thereby possibly setting up a temperature gradient across the sample. Although the use of sintered copper in the Mark III cavity considerably improved thermal contact, much of the data presented here was obtained using the earlier cells. It is therefore important to ensure that the thermal time constants involved are sufficiently short to prevent the establishment of a temperature gradient across the sample.

In the 'single-shot' mode of operation, a number of pulses are fed to the sonic cell at a predetermined rate and the resulting echo trains are accumulated by the transient recorder as explained in section 4.4.3. This procedure (involving, typically, 512 pulses) is referred to as a 'single shot'. To avoid local heating of the helium near the surface of the piezo electric rod, the pulse repetition rate must be sufficiently slow to ensure that the heat resulting from a single pulse is completely dissipated into the bulk liquid before the next pulse is received. The time required for dissipation will depend upon the time constant for heat flow from the rod into the sample, and the rate at which the heat is transferred through the bulk liquid. These two periods limit the rate at which the individual pulses of a 'shot' should be fed to the sonic cell. In the following calculations quartz is taken as the rod material since thermal data is readily available from many sources.

The time constant (τ_R) for the rod to attain thermal equilibrium with the sample is given by $\tau_R = CR$ where C is the heat capacity of the rod and R

is the thermal boundary resistance between the rod and liquid helium-3. The specific heat of quartz has been given by Zeller and Pohl (1971) as $5.7 \times 10^{-7} T^3$ (Joule $g^{-1} K^{-4}$) so for a rod of mass 0.233 g the heat capacity is found to be $1.33 \times 10^{-7} T^3$ (Joule K^{-4}). The thermal boundary resistance is given by :

$$R = R_k / A$$

where R_k is the Kapitza boundary resistance and A is the surface area of the rod. No data on the Kapitza resistance between quartz and liquid helium has been published but Lounasmaa (1974) provides a table of values for various materials in contact with liquid helium. Taking the upper limit of this table, $R_k T^3$ is about 0.1 ($K^4 m^2 W^{-1}$). Therefore for a rod 12.5 mm long and 3.0 mm in diameter :

$$R \approx \frac{8.5 \times 10^2}{T^3} \; K J^{-1} s$$

giving a time constant τ_R of about 1×10^{-4} second. That is, the time required for the rod to return to thermal equilibrium with the helium sample is about 0.1 millisecond, and is independent of temperature.

An alternative approach is to assume that the energy remains in the form of thermal phonons which reflect within the rod, losing energy at each reflection. This energy loss into the helium may be calculated using the theory of acoustic impedance and an appropriate time constant obtained. If Z_s and Z_l are the acoustic impedances of the solid and liquid respectively, and if $Z_s \gg Z_l$ then;

fractional energy loss per reflection, $x \approx \frac{4 Z_l}{Z_s}$

For quartz, $Z_s = 15.1 \times 10^5 \, g cm^{-2} s^{-1}$ and for liquid helium-3, $Z_l = 1.66 \times 10^3 \, g cm^{-2} s^{-1}$. Therefore, fractional energy lost per reflection, x, is about 7.6×10^{-3}.

Now, power loss into the liquid = $e^{-x\dot{n}t}$

where $\dot{n}$ is the number of reflections per second, or if τ is the thermal time constant ; power loss = $e^{-t/\tau}$

$$\therefore \quad \tau = \frac{1}{\dot{n}\, x}$$

Now, the number of reflections per second is given by ;

$$\dot{n} = \frac{v_s}{\ell}$$

Where v_s is the speed of sound in quartz and ℓ is the average distance between reflections. Taking the average of the rod dimensions, $\ell \approx$ 0.7 cm and the thermal time constant (τ) is found to be about 2.8×10^{-4} second. Therefore, using acoustic mismatch theory, we find that the thermal relaxation time for the quartz rod in helium-3 is about 0.3 millisecond, in reasonable agreement with the previous estimate.

We now consider the time required to dissipate the heat from the rod into an absorption layer of helium of thickness δ . The rate of flow of heat across the layer depends upon the thermal conductivity (K) and the temperature differential (ΔT) and we have

$$\dot{Q} = \frac{KA}{\delta} \Delta T$$

where A is the surface area. But thermal boundary resistance is given by:

$$R = \frac{\Delta T}{\dot{Q}}$$

$\therefore$ we have;

$$R = \frac{\delta}{KA}$$

The heat capacity of the absorption layer ; $C = c_v A\delta$.

where c_v is the specific heat at constant volume. Therefore the thermal time constant , τ , is given by :

$$\tau = RC = \frac{c_v \delta^2}{K}$$

For liquid helium-3 , K is largely independent of temperature and is of the order $10^{-2} WK^{-1} m^{-1}$, and the specific heat at 20 mK is about $12.7\ Jm^{-3}K^{-1}$. Thus, $\tau = 12.74 \times 10^2\ \delta^2$ second.

The absorption length δ is inversely proportional to the absorption coefficient for thermal phonons , α . The peak absorption in liquid helium-3 is proportional to frequency so, using the value obtained by Kirby and Wilks (1971) we have, at 240 MHz; $\alpha = 1400\ cm^{-1}$

Thus, $\delta \approx 7.14 \times 10^{-6}$ m.

We find that the thermal time constant for dissipation of heat into the absorption layer is about 6.5×10^{-8} second at 30 mK and is therefore quite negligible compared to the time constant for the quartz rod. Allowing an uncertainty of an order of magnitude, the period between pulses should not be less than about 3 millisecond. In practice, the period used was typically of the order 90 ms.

4.7. Input power level

The insertion loss into the cavity was measured and found to be about 43 dB. The output power of the cavity oscillator was measured by comparison with a calibrated r.f. signal generator and was, typically, about +30 dBm. The power input to the rod was therefore -13 dBm, or about 50 μW. The pulse width was 2 μs, so that the energy coupled into the rod per pulse was about 1×10^{-10} Joule. We now consider the implications of this power input at very low temperatures.

The short thermal time constant obtained above implies that the heat will be quickly dissipated into the liquid helium sample. However, if a temperature rise is produced in the piezoelectric rod, it must be ensured that the maximum temperature reached does not exceed that at which attenuation in the rod material becomes significant (about 0.35 Kelvin). In their detailed study of ultrasonic attenuation in quartz, Nava and Rodriguez (1971) found that for longitudinal waves acoustic attenuation is the result of interactions with both transverse and longitudinal phonons. However, the latter process becomes increasingly dominant as the temperature is reduced and, below about 10 Kelvin, attenuation of the longitudinal mode is due almost entirely to collinear processes of the form : $L + L \rightarrow L$. At these temperatures, this attenuation is independent of frequency and an expression for the attenuation coefficient is obtained which indicates a temperature dependence to the seventh power; that is, the attenuation coefficient for this mode is given by :

$$\alpha_L \approx 8.90 \times 10^{-15} (aT^6 + bT^7) \text{ dB } \mu s^{-1}.$$

where a and b are empirical constants. Now, the time constant for thermal relaxation may be approximated to the time required to attenuate the wave to one half of its original power and, at 1 Kelvin, this is found to be about 6×10^3 second. This indicates the time required for the acoustic energy to be converted into lattice vibrations and at very low temperatures, 20 mK for example, the time constant becomes too long to be physically meaningful. We therefore conclude that the temperature of the rod will not increase as a result of the acoustic power input because the acoustic phonons will be boundary scattered into the surrounding liquid before lattice excitation can occur.

As an absolute upper limit to the possible temperature rise we may briefly consider the classical heat capacity argument. Under conditions of constant pressure we identify the heat input with an increase in the enthalpy of the system and we have ;

total enthalpy increase, $$\Delta H = \int_{T_0}^{T_1} C(T)\,dT$$

where T_0 and T_1 are the initial and final temperatures, respectively. The heat capacity varies as T^3 ; that is $C_v(T) = C T^3$. $(C = const.)$

therefore; $$\Delta H = \frac{C}{4}(T_1^4 - T_0^4)$$

The total heat input to the system, ΔH, is 1×10^{-10} Joule.

Therefore, inserting the heat capacity $C_v = 1.33 \times 10^{-7}$ Joule K^{-4} and the value of ΔH, we obtain ;

$$T_1^4 - T_0^4 = 3.01 \times 10^{-3} \ K^4.$$

If we take $T_0 = 0.02K$ then T_0^4 becomes negligible and we see that the temperature increase due to a single input pulse, provided that all the energy of the pulse contributes to the temperature rise, is about 0.2 Kelvin. We note that even in this unrealistic case the temperature rise is not sufficient to introduce the effects of temperature dependent attenuation by the rod material.

To consider the possibility of temperature gradients across the helium sample, we regard the sample as a cylindrical layer of liquid helium-3 of thickness δ, the phonon absorption length. The temperature difference across this layer due to the r.f. power input may be calculated using the expression for thermal conduction across a cylindrical layer, ie :

$$\Delta T = \frac{\dot{Q}}{4\pi K}\left(\frac{1}{r_1} - \frac{1}{r_2}\right)$$

$r_1 \approx r_2 = 0.15 \times 10^{-2}$ m.

$(r_1 - r_2) = \delta$

K = thermal conductivity

Taking the absorption length δ to be 7.14×10^{-6} m, as before, and assuming that all the power input is converted into heat, we obtain the result ; $\Delta T = 1.26 \times 10^{-3}$ K.

Consequently, the temperature of the liquid helium sample may differ from that of the bulk liquid by approximately one milliKelvin.

The time required for the liquid helium to come to thermal equilibrium with the sonic cell was discussed in Section 4.2. and found to vary between about one second at 1 Kelvin and almost one hour at 20 mK. Therefore it is inevitable that the heat resulting from the individual pulses that constitute a single shot , will accumulate in the liquid helium to some extent and an appropriate period must elapse between shots to ensure that this heat has been removed by the refrigerator. In practice, this delay occurs naturally since, as the temperature falls, the rate of cooling decreases until, at the lowest temperatures (that is, below about 30 mK) the rate of cooling is of the order of 1 mK hour^{-1}. At such a rate of cooling, the time between shots will be about one hour; this time is sufficient to ensure that the rod, helium sample and sonic cell have returned to thermal equilibrium.

CHAPTER FIVE

5.0. THERMOMETRY

5.1. Carbon resistance thermometers

5.1.1. Preparation and mounting.

The use of carbon radio resistors for temperature measurement has been widely studied and a review is to be found in the recent book on refrigeration and thermometry by DS Betts (1976). In particular, the resistors manufactured by Speer Electronic Components (USA) have been the subject of many investigations including a very detailed study by Black,Roach and Wheatley (1964). These resistors have been found to be particularly suitable and the general concensus is that, in the temperature range from 2.0 Kelvin to about 0.02 K, Speer carbon resistors provide a responsive,reasonably sensitive thermometer that is reproducible from run to run to better than one per cent. For the purposes of this work, high precision in temperature measurement was not particularly important and 100 ohm (nominal) Speer resistors, suitably calibrated, were used both for measuring the sample temperature and for general monitoring of the refrigerator performance.

Many sophisticated methods of preparation have been suggested for these resistors such as grinding away the protective insulation from the resistor body and the removal of the superconducting tin-lead solder from the connecting leads. However, none of these procedures have been shown conclusively to improve performance and preparation of the resistors used in this work was limited to the removal of the paint from the insulator body with acetone.

The most important thermometer, designated R3, was contained within the experimental cell, totally immersed in liquid helium. Thermal contact to resistance thermometers is thought to be mainly via the connecting wires (see, for example, Black et al (1964)). For this reason, the surface area of the leads was increased by soldering to them strips of copper foil which were then wrapped around the body of the resistor, separated by strips of insulating paper. The whole assembly was then enclosed in heat-shrink sleeving to electrically insulate the resistor from the walls of the cell. The thermal response time was measured at 40 mK by observing the change in resistance when a pulse was applied to a bismuth-film heater situated nearby. Heater power levels of approximately 0.2, 2 and 20 nanoWatt were applied in turn, and in each case, the thermal response time was found to be less than 0.5 second, indicating adequate thermal contact between the liquid helium and the resistor.

For the other resistors, outside the experimental cell, copper turrets were constructed having at one end a screw clamp to accommodate the resistor in such a way that the whole surface area of the insulator was in contact with copper. After removal of the paint from the resistor a thin film of Apiezon "N-grease" was applied and the resistor was tightly rolled in gold foil to ensure a good fit when the retaining clamp was secured. However, the main thermal link was again through the resistor leads so these were attached to lengths of 30 s.w.g. enamelled copper wire which were then non-inductively wound around the base of the turret, having first been smeared with "N-grease" to ensure good thermal contact.

Electrical contact to all the resistors (and to the bismuth-film heater) was by superconducting Niomax "CN" wire (type A61/05). This is composed of

sixty-one filaments of niobium-titanium wire in a cupro-nickel matrix and has an overall diameter of only 0.05 mm. Between the mixing chamber and the 4.2 Kelvin level, the wires were thermally anchored, by winding around copper posts, at 1.2 K, ~~0.00~~ 0.8 K (the still) and at each heat exchanger. From 4.2 K to room temperature, ordinary enamelled copper wire was used.

5.1.2. Power dissipation in resistors

At low temperatures, the deterioration of thermal contact may result in self-heating of the resistors and rapid loss of sensitivity. Some degree of Joule heating will always be present and the power dissipation in the resistor must therefore be kept well below the rate at which heat can be dissipated into the surrounding liquid. Several relationships between power input to resistor and temperature have been proposed and an expression has been obtained experimentally for Speer resistors by Oda, Fujii and Nagamo (1974) which defines a power level, P_m, which is the power input to the resistor for which the resistance falls by one per cent. For a 220 ohm, Speer resistor, in the temperature range from 30 mK to 1 K, P_m is given by

$$P_m = 2T^{4.3} \ \mu W.$$

At 20 mK this gives a power of about 1×10^{-7} μW and this may be taken as the maximum permissible power input to the resistor at that temperature. Although resistance thermometers have been used successfully at considerably higher input power levels (eg. Black et al (1964) used powers as high as 10^{-6} μW at 20 mK) a reduction in the power level of at least one order of magnitude

will further reduce the possibility of loss of sensitivity due to self-heating.

In practice, the power level at which self-heating occurs at a particular temperature may be easily determined by observing the resistance whilst the input power is slowly increased. The resistance remains steady until the power input exceeds the maximum power dissipation from the resistor into its surroundings, at which point the resistance suddenly falls due to self-heating. This is a simple check that may be performed at low-temperatures to confirm that the power level during temperature measurement is not excessive.

5.1.3. Resistance measurement

The resistance of the various thermometers was measured using an A.C. bridge known as the "Cryobridge S72" produced by the Czechoslovak Academy of Sciences and available in this country through the Oxford Instrument Company Limited. This instrument operates at 237 Hz using a Wheatstone bridge with a phase-sensitive detector. The range of measurable resistance, using the built-in comparison resistors, was from 1 ohm to 112.211 ohm and the accuracy quoted by the manufacturers is 0.1% at a power level of 10^{-12} Watt. The bridge voltage was variable in steps from 2 mV (r.m.s.) down to 20 μV. At 20 mK, the resistance of the main resistance thermometer (R3) was 23.0 KΩ, which gives a power input (at the lowest bridge voltage setting) of about 2×10^{-8} μW ; well within the power criterion suggested by Oda et al (1974) corresponding to this temperature. At this power level, it was possible to measure the resistance to better than 0.5%. To avoid the possibility of errors due to earth-loops, neither the resistor

nor the bridge were earthed and electrical connection was made using screened cable, compensated for capacitance and kept as short as possible.

For the monitor resistors at higher temperatures (for example, the still and 1.2 K pot thermometers) a simple d.c. system was found to be adequate. This consisted of a 1.0 μA constant current source and a Keighley "155" microvoltmeter, the output of which was displayed on a digital voltmeter. At these temperatures (that is, above about 0.1 Kelvin) the power dissipated is negligible and the convenience of a direct-reading instrument is more important than precision of measurement.

5.2. C.M.N. Thermometers

The susceptibility (χ) of cerium magnesium nitrate (CMN) has been shown to obey Curie's Law down to temperatures of the order of a few milliKelvin and therefore provides an excellent thermometric material at these temperatures. The validity of Curie's Law, $\chi = \Lambda/T$ where Λ is the Curie constant, over a large temperature range enables calibration to be performed at high temperatures against, for example, the saturated vapour pressure of liquid helium-4. Having obtained the value of the constant Λ, an extrapolation to milliKelvin temperatures may be made with confidence. The measurement of the susceptibility χ has been the subject of a vast amount of published work and the most common method is by some form of mutual inductance bridge. For the purposes of this work a simpler and more direct method was required since the thermometer was intended for use within the experimental cell to ensure intimate thermal contact with the liquid helium sample.

A thermometer had been proposed by Betts et al (1964) in which a pill of CMN was used as the core of an inductance coil which then became the inductive element of an LC resonant circuit, driven by a marginal oscillator. Susceptibility changes in the CMN results in a shift of the resonant frequency from its high temperature value, f_o. Betts et al showed that the change in frequency (Δf) is given by the expression ;

$$\frac{\Delta f}{f_o} = \frac{A\eta}{T}$$

where A is a constant and η is the packing factor of the salt pill. This formula should be valid provided that the period of oscillation (ω^{-1}) is less than the spin-lattice relaxation time of the salt (τ); ie. $\omega\tau \gg 1$. The condition is satisfied for CMN below 4.2 Kelvin for frequencies of the order of 1 MHz.

The frequency shift of the tank circuit may be measured with a suitable frequency meter although the low level of oscillation requires an amplifier to be inserted between the meter and the tank circuit. Many variations of this thermometer have been published and it was decided to adopt the system used by Harley, Gustafson and Walker (1970), as shown in figure 5.1.(a). The circuit is derived from the oscillator designed by Robinson (1959), for use in nuclear resonance experiments, but drastically simplified by the use of a tunnel diode submerged in liquid helium. The oscillator was built on a printed circuit board about 25 mm square which was thermally anchored to the 1.2 K bath of the refrigerator to improve the temperature stability of the circuit and to ensure that the distance between it and the probe coil was kept to a minimum. Electrical connection between the coil and the oscillator was by "Niomax" superconducting wire. The power supply, which used a 1.35 volt

mercury cell, was mounted at the top of the cryostat, at room temperature, and connection to the oscillator was by means of coaxial cable.

The Mark III sonic cell, described in section 4.2., was designed to include provision for a built-in CMN thermometer of this type but the earlier cells had no such provision. Therefore a calibration cell was constructed to enable resistor R3 to be compared with a CMN thermometer without having to remount the resistor. This cell is shown in figure 5.2. The calibration cell was designed to fit the top-cap of the Mark I sonic cell so that the CMN pill and the resistor would be close together and thermally linked by liquid helium-3. The "Epibond" body of the cell was cast onto the copper flange using "Teflon" moulds and machined to shape after heat curing. The cylindrical inner mould was later used to tamp the powdered CMN into place so as to produce a right circular cylinder of 0.5 cm diameter and 0.5 cm height. Moderate hand pressure was applied to compress the powder which resulted in a filling factor of about 75%. Roughly 150 mg of crystalline CMN was used which had first been ground by hand into a fine powder and passed through a 50 μm sieve. Laboratory grade CMN was used and this was obtained from Fluka AG of Buch, Switzerland. A probe coil consisting of ninety turns of superconducting wire (Niomax CN, A61/05) was carefully wound around the sample in a shallow groove machined on the cell body. This gave a resonant frequency of about 450 kHz. The cell was sealed to the top-cap using an O-ring of indium wire.

At very low temperatures some self-heating of the coil was evident and at such times the power supply was disconnected from the oscillator to prevent heating of the mixing chamber, to which the calibration cell was attached. The self-heating may be reduced by decreasing the level at which the

oscillator operates by means of a feedback loop. Figure 5.1.(b). shows the variation of the marginal oscillator circuit used by Andres and Bucher (1974) which includes a feedback loop controlled by a potentiometer. It is hoped that this circuit, with its improved control over the oscillation amplitude, will remove the problem of self-heating down to at least 15 mK.

An important point to note concerning the use of this type of thermometer is that the frequency of resonance is affected by stray capacitance in the probe-coil leads. The difficulties involved in keeping this capacitance constant if the thermometer is remounted between runs, means that run-to-run reproducability cannot be assumed. For this reason the thermometer was calibrated during each run by comparison with resistance thermometer values at high temperatures (that is, between 1.0 Kelvin and 0.1 Kelvin) and was then used mainly as a secondary thermometer to cross-check the resistor values at lower temperatures.

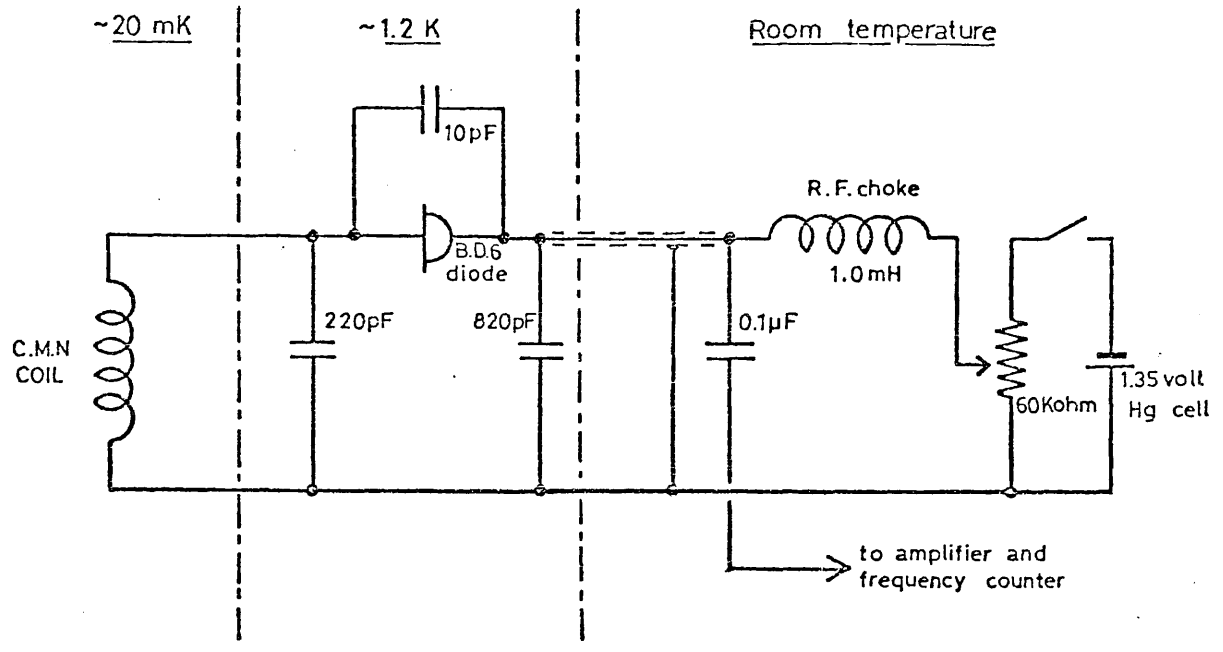

(a) Marginal oscillator circuit due to Hartley et al.

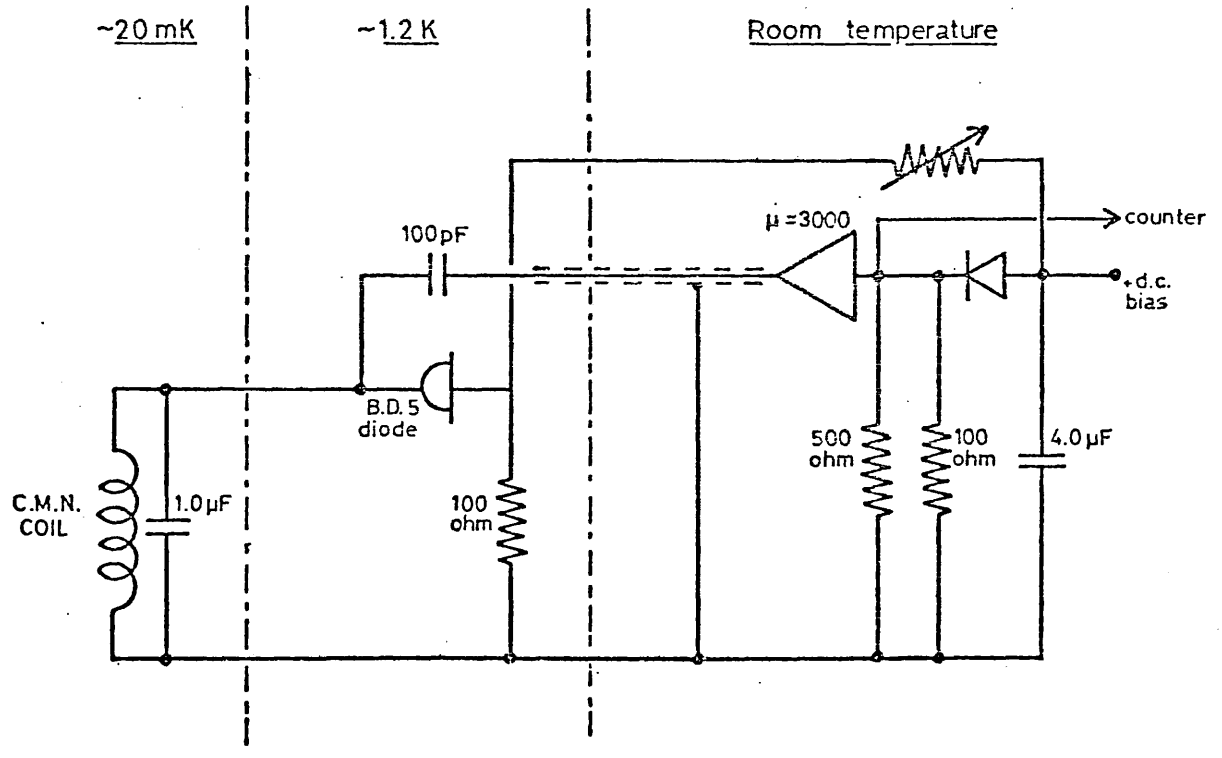

(b) Marginal oscillator circuit due to Andres and Bucher.

Fig. 5.1 Marginal oscillator circuits for C.M.N. thermometry

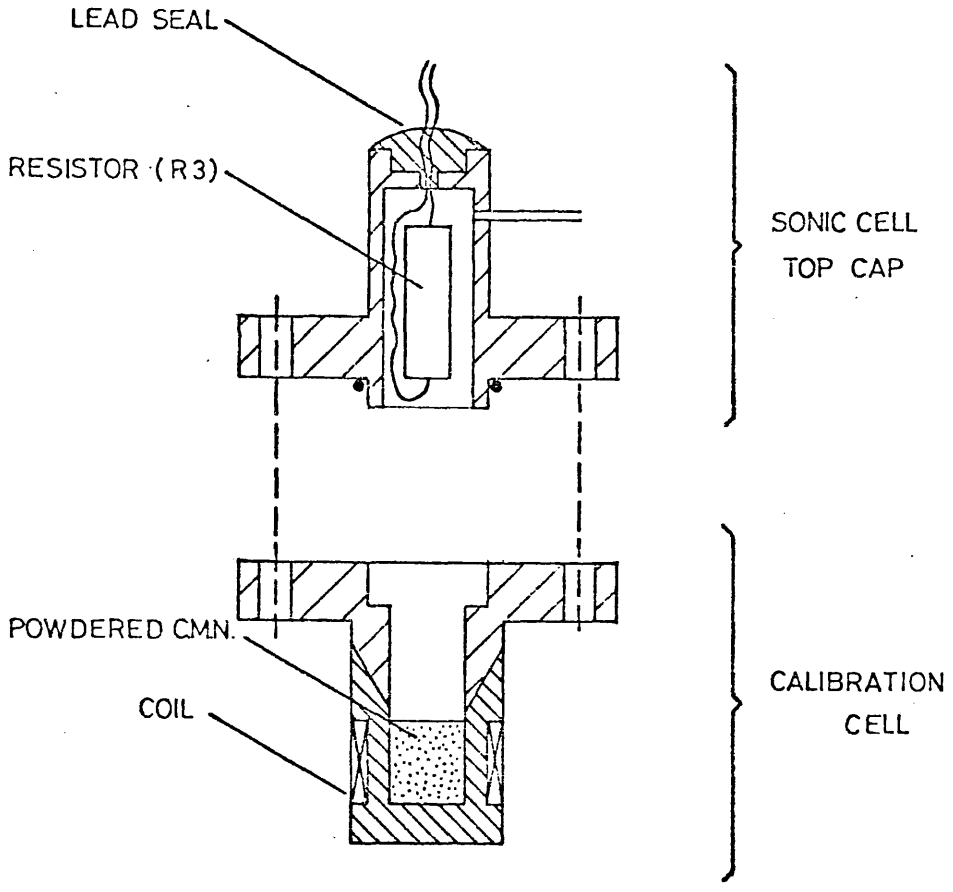

Fig.5.2 C.M.N. CALIBRATION CELL

5.3. Nuclear orientation thermometer

A further check on resistance thermometry at low temperatures was provided by a nuclear orientation thermometer. The theory and practice of this form of thermometry has been described in the review paper by Berglund et al (1971). Briefly, the principle of the thermometer is as follows :

If a nucleus decays by radioactive emission in the presence of a steady magnetic field, the direction of emission of radiation is not random with respect to the axis of precession of the nucleus. Each nuclear hyperfine sub-level has a particular anisotropic probability distribution of emission direction associated with it. The population of these sub-levels for a collection of nucleii will be determined by the Boltzmann equation and the directions of emission of radiation from the collection will therefore take up a pattern that represents the weighted average of the individual patterns. At high temperatures (above, say, 100 mK) the sub-levels will be equally populated and there will be no resultant anistropy of emission direction. However, as the temperature falls the relative populations of the sub-levels will change and a net anisotropy will become apparent. At the lowest temperatures this anisotropy will depend wholly upon the nuclear properties of the decaying isotope but, in the intermediate range, it may be related, via the Boltzmann factor, directly to the absolute temperature. It follows that, over this range of temperatures, the direction of emission of radiation from the decaying nuclei will depend only upon the absolute temperature of the material and may therefore provide a self-calibrating primary thermometer. The range over which the anisotropy is temperature dependent is, typically, from a few milliKelvin up to about 0.1 K.

If θ is the angle between the direction of emission of the radiation and the orientation axis of the nucleii, then the normalised intensity of emission is given by :

$$W(\theta) = \sum_{k=0}^{k(max)} B_k(T)\, U_k\, F_k\, P_k(\cos\theta)$$

The summation extends over even values only of k (because only the direction of the radiation emission is important, not its polarization) between zero and $k(max)$, where $k(max)$ is the lesser of $2I$ (I being the nuclear spin quantum number) and $2L$ where 2^L is the maximum multipolarity of the observed radiation. (For quadrupole radiation, $L = 2$ and therefore values of k will be limited to $k=2$ and $k=4$.) The factors involved in the expression are explained below .

(i) The temperature dependence is wholly contained in the statistical tensors $B_k(T)$ which are defined by :

$$B_k(T) = \left[(2I+1)(2k+1)\right]^{1/2} \sum_{m=-I}^{+I} (-1)^{I-m} \begin{pmatrix} I & I & k \\ m & -m & 0 \end{pmatrix} p(m)$$

where $p(m)$ is the probability of finding the parent nucleus with spin component (m) along the orientation axis. The value of $p(m)$ depends upon the hyperfine splitting Δ_{hf}, that is ;

$$p(m) = \frac{\exp\left\{\frac{-m\Delta_{hf}}{kT}\right\}}{\sum_{m=-I}^{I} \exp\left\{\frac{m\Delta_{hf}}{kT}\right\}}$$

Therefore, $p(m)$ will depend not only upon the decaying nucleii but also upon the nature of the nuclei of the host material. The values of the hyperfine splitting exhibited by the various combinations of source and host materials used in N.O. thermometry are to be found in Berglund et al (1971), as are the values of B_k tabulated as a function of Δ_{hf}/kT.

(ii) U_k are the angular momentum reorientation parameters which account for all the transitions preceding the detected transition. This can be calculated exactly provided that the angular momentum properties of the transitions are known and that the lifetime of the decaying state is sufficiently short ($< 10^{-10}$ s) to ensure that the nucleus cannot reorientate itself before the transition occurs.

The parameters F_k are angular momentum coupling coefficients which depend only upon the multipolarity (L) of the observed radiation, and the spins of the initial and final states. For the two most common gamma-emitters used in N.O. thermometry, ^{60}Co and ^{54}Mn, the decay schemes are well known and the products $U_k M_k$ are easily determined. This has been done by Berglund et al (1971) in the two cases mentioned and yields the simple numbers :

	U_2F_2	U_4F_4
^{60}Co:	-0.42056	-0.24280
^{54}Mn:	-0.49486	-0.44669

(iii) The angular dependence of the emission is expressed by the normalised Legendre polynomials $P_k(\cos\theta)$.

The expression $W(\theta)$ assumes a point detector of radiation which will not, of course, be the case in any practical thermometer. Thus, a further factor Q_k is introduced into the sum which accounts for the solid angle subtended by a detector of finite dimensions. The correction is generally small and tables of values have been produced by various authors for both $NaI(Tl)$ and $Ge(Li)$ detectors. Berglund et al (1971) have interpolated the data available for $NaI(Tl)$ detectors of various sizes in the case of ^{54}Mn gamma radiation of 0.84 MeV energy and have produced a graph of correction factors Q_2 and Q_4 as a function of subtended angle. The corresponding corrections for ^{60}Co are slightly greater on account of the higher energy associated with this emission but, for practical purposes, the differences may be ignored. The theoretical angular distribution $W(\theta)$ for the 1.33 MeV gamma emission from ^{60}Co at the two temperature extremes $T=0$ and $T=\infty$ is shown in figure 5.3. The angular sensitivity is a minimum for the directions $\theta = 0°$ and $\theta = 90°$ and the most common experimental arrangement is a counter situated at $\theta = 0°$. The use of a single counter does mean, however, that the count rate at a particular temperature must be related to the 'warm' count rate (taken at T = 1 Kelvin, say) and the anisotropy is then expressed as a percentage of this count rate.

The source used in this work was ^{60}Co in a single, needle-like crystal of hexagonal cobalt. In such a crystal, provided that the needle axis is parallel to the crystallographic c-axis, the magnetic domains spontaneously align themselves to produce a well defined orientation axis without an externally applied magnetic field. The maximum value of k is four for this source so that the values of U_2F_2 and U_4F_4 given by Berglund et al (1971) were used in the expression for $W(\theta)$, as were the tabulated values of B_2 and B_4

by the same authors. The scintillation counter used was a 5 cm x 5 cm crystal of $NaI(Tl)$ which was mounted at an angle $\theta = 0°$ to the source axis at a distance of about 10 cm. This gave correction factors $Q_2 = 0.97$ and $Q_4 = 0.95$. Taking the hyperfine splitting to have the value quoted by Berglund et al, that is, $\Delta_{hf}/k = 6.23$ mK, a table of percentage anisotropy as a function of temperature (T) was produced from which the curve, figure 5.5., was plotted.

The experimental arrangement is shown in figure 5.4. It is obviously vital that the 'warm' count rate, to which the anisotropy is compared, does not change during the course of the experiment as a result of electronic drift in the counter or amplifier. Consequently, the window of the analyser must always be kept aligned with the peak of the radiation spectrum. If a multi-channel analyser is available, the count rate corresponding to the radiation peak may be determined by selecting the appropriate channel. If not, then a stabilised single channel analyser, such as the "Elscint" SCA - N - 3, must be used. This instrument has an energy window that is divided into two equal subchannels. The 'baseline' and 'window' controls are set such that the peak coincides with the centre of the analyser window. The lower subchannel then counts the pulses resulting from one half of the peak whilst the upper sub-channel counts those due to the other half. If the two subchannel counting rates are equal, the peak is properly aligned within the window. However, if the peak drifts to one side of the window the count-rates from the two subchannels will differ and a signal is produced proportional to the difference in rates, which automatically adjusts the baseline and the window width to compensate for the drift. Therefore the single-channel analyser is 'locked-on' to the photopeak and the count-rate is stabilised against long-term drift in the counter and analyser.

The counting time depends largely on the strength of the source and a compromise must be made since the heating effect of a very strong source (due mainly to the absorption of associated β- decay and X-ray emission) may be significant at very low temperatures. In this work, a source strength of about 5 μCi produced about 9×10^4 counts in a counting period of 400 s which represented a statistical uncertainty $(\sqrt{N})$ of about 0.3%.

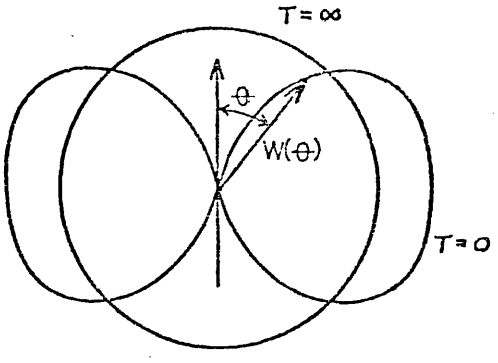

Fig.5.3 ANISOTROPIC EMISSION FROM COBALT-60

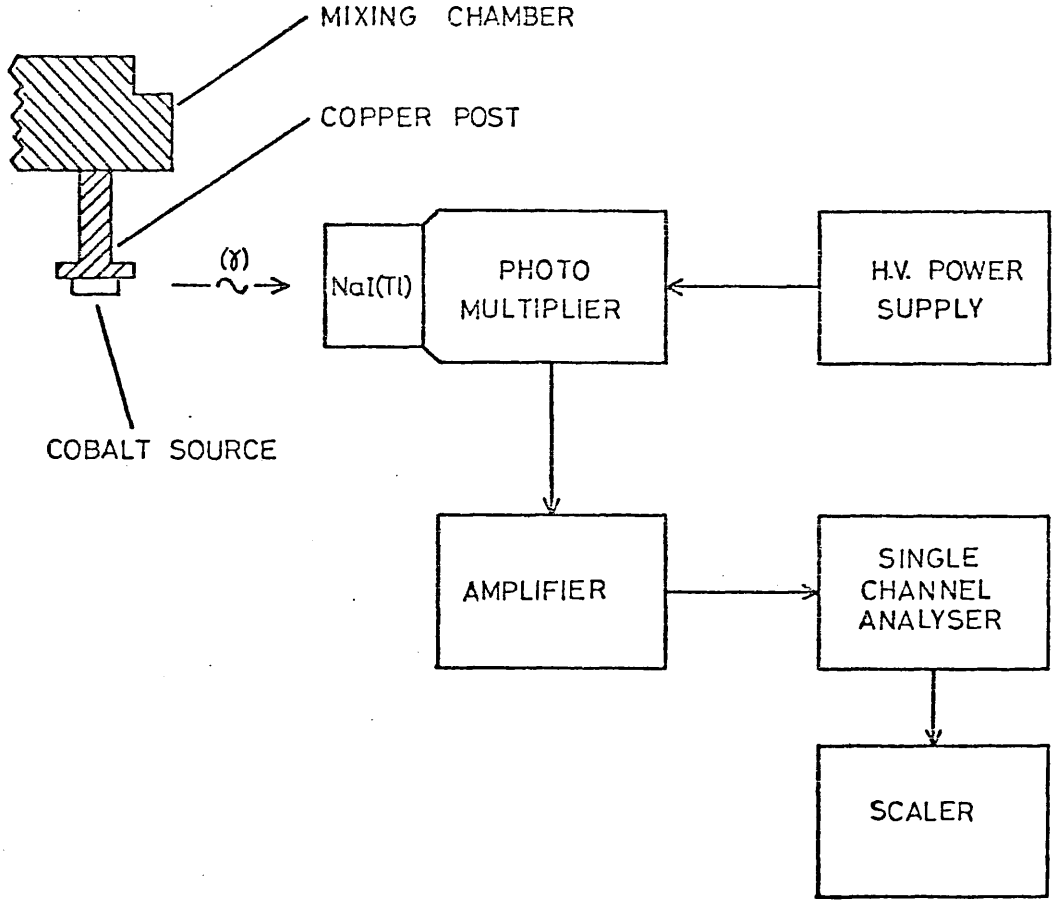

Fig.5.4 NUCLEAR ORIENTATION THERMOMETRY

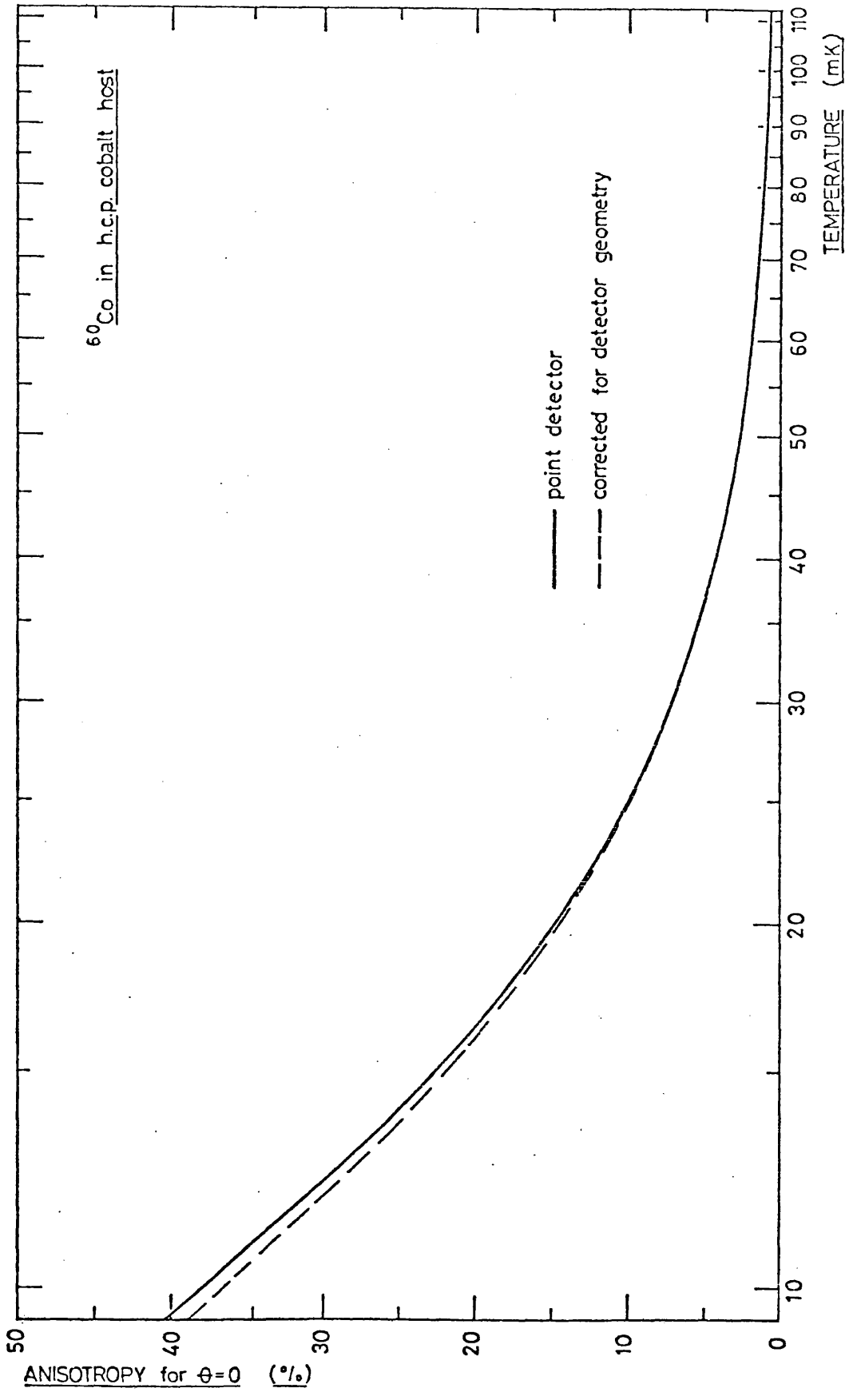

Fig.5.5 Anisotropy against temperature for Cobalt-60

5.4. Calibration of resistance thermometers

The main thermometer used throughout this work was a Speer 100 ohm carbon resistor, designated R3. As mentioned in section 5.1., this resistor was totally immersed in the liquid helium sample in preference to being thermally anchored to the copper body of the experimental cell. It was hoped that the intimate thermal contact achieved in this way would ensure a more precise correspondence between the temperature of the liquid helium and the measured resistance. The rapid response to heat pulses, applied directly to the sample by a small heater, appeared to confirm this thermal behaviour, as noted in section 5.1. However, the accurate calibration of this resistor proved to be a problem that remained unsolved at the termination of the experimental work and this created some difficulties in the analysis of the data collected at the lowest temperatures.

At the start of this work, the only thermometry available in the low-temperature regime (below, say, 1.5 Kelvin) was two Speer resistors, known as R3 and R4, which had been calibrated at the University of Lancaster in 1972. In the case of R4, this had been performed with the resistor mounted on a copper post, by comparing the resistance with the susceptibility of cerium magnesium nitrate (CMN) using a pair of inductive coils and a mutual inductance bridge. At higher temperatures a comparison had been made with the saturated vapour pressure of liquid helium-3 and, at still higher temperatures, with the s.v.p. of liquid helium-4. A combination of these methods enabled R4 to be calibrated against temperature in the range from 4.2 Kelvin to 24 mK. This was extended at Bedford College using the CMN thermometer described in Section 5.2. and this low-temperature calibration was fitted to the Lancaster data to provide a smooth calibration curve down to about 16 mK. This had

been checked from time to time, both at Lancaster and Bedford College, in the 100 mK region by noting the indicated temperature of the transition to superconduction in a sample of Iridium and no significant change had been observed.

The basic calibration for R3 between about 2.0 Kelvin and 30 mK was obtained at Lancaster University by direct comparison with R4, both resistors being mounted on copper posts, in vacuum. A plot of $\log_{10} R3$ against $\log_{10} R4$ produced a good straight line so that when R4 had been extended to 16 mK, an extrapolation of the R3 calibration to this temperature was carried out. This enabled a working calibration of R3, down to 16 mK, to be plotted and it was this provisional calibration that was used in the analysis of the experimental data. This calibration will in future be referred to as R3 (1972). The inadequacies of this calibration, due to the indirect methods employed were appreciated but little could be done to improve the situation as no other method of temperature measurement below 100 mK was available with which to check the calibration. The most doubtful aspect of the R3 (1972) calibration was that it depended upon the resistance characteristic when in thermal contact with copper whereas, in the experiment, the resistor was immersed in liquid helium. A direct calibration of R3 in liquid helium was therefore required and the calibration cell described in section 5.2. was constructed. Unlike the CMN sample used in the calibration of R4, in which the powder was assumed to be in thermal contact with a mass of copper wires, the sample in the calibration cell was in direct contact with the liquid helium which, it was hoped, would fully permeate the loosely-packed pill.

The calibration cell, containing R3, was mounted on the mixing chamber of the dilution chamber along with a 470 ohm Speer resistor (R8), a germanium resistance thermometer (both of which were uncalibrated) and the other calibrated resistor, R4. With the cell open to a reservoir of helium-3, simultaneous measurements of these various resistances and the resonant frequency of the marginal oscillator were made during several slow sweeps over the temperature range from 4.0 Kelvin, to about 30 mK. Each sweep was treated as a separate run due to uncertainty in the reproducibility of the CMN thermometer. However, over a period of two days, the change in resonant frequency at 4.2 Kelvin was only 2 Hz in 450 MHz.

To obtain the calibration, the germanium resistor and the 470 ohm Speer resistor (R8) were mounted in a helium-4 cryostat and calibrated against the saturated vapour pressure of liquid helium-4, using the standard T_{58} calibration, in the temperature range from 4.2 Kelvin to about 1.4 K, and a curve of R8 against inverse temperature (T^{-1}) was produced. The earlier calibration runs in the refrigerator had yielded a straight line relationship between the resonant frequency of the CMN circuit and R8 in the range 2.0 K to 0.9 K so that, by combining these results a relationship between resonant frequency and T^{-1} was obtained. This proved to be a good straight line so that extrapolation down to 20 mK was possible and the full relationship between resonant frequency and inverse temperature was determined. This relationship was then used to convert the R3 versus resonant frequency information into a calibration of R3 across the complete temperature range from 4.2 Kelvin to 20 mK. This calibration became known as R3 (1977).

5.5. Comparison of calibrations : R3 (1972) and R3 (1977)

The two calibration curves R3 (1972) and R3 (1977) in the low temperature region are shown together in figure 5.6. At temperatures above 100 mK there is no significant difference between them but below this temperature a discrepancy appears which increases to about 7.5 mK at the lowest temperatures. A discrepancy of this magnitude was unexpected and disappointing and it was decided that a calibration run to compare R3 with the nuclear orientation thermometer should be carried out in an attempt to resolve the conflict. Unfortunately, this was not achieved due to serious problems with the dilution refrigerator which prevented further experimental work from being carried out.

It was suspected that the difference between the low temperature resistance values was due to the 1972 calibration being carried out with the resistor in vacuum whilst R3 (1977) had been produced with R3 immersed in liquid heliun-3. However, without an independent check on the 1977 values, carried out both in liquid helium and in vacuum, it would have been premature to rely upon the R3 (1977) calibration alone. It was therefore decided to complete the analysis of the experimental data using the 1972 calibration, which had been independently checked several times (although not with the resistor in liquid helium), whilst being fully aware of the large uncertainty that had appeared in the low-temperature region. In some cases the data were analysed using both calibrations to indicate the differences that emerge in the final results. This will be discussed in detail in the next chapter.

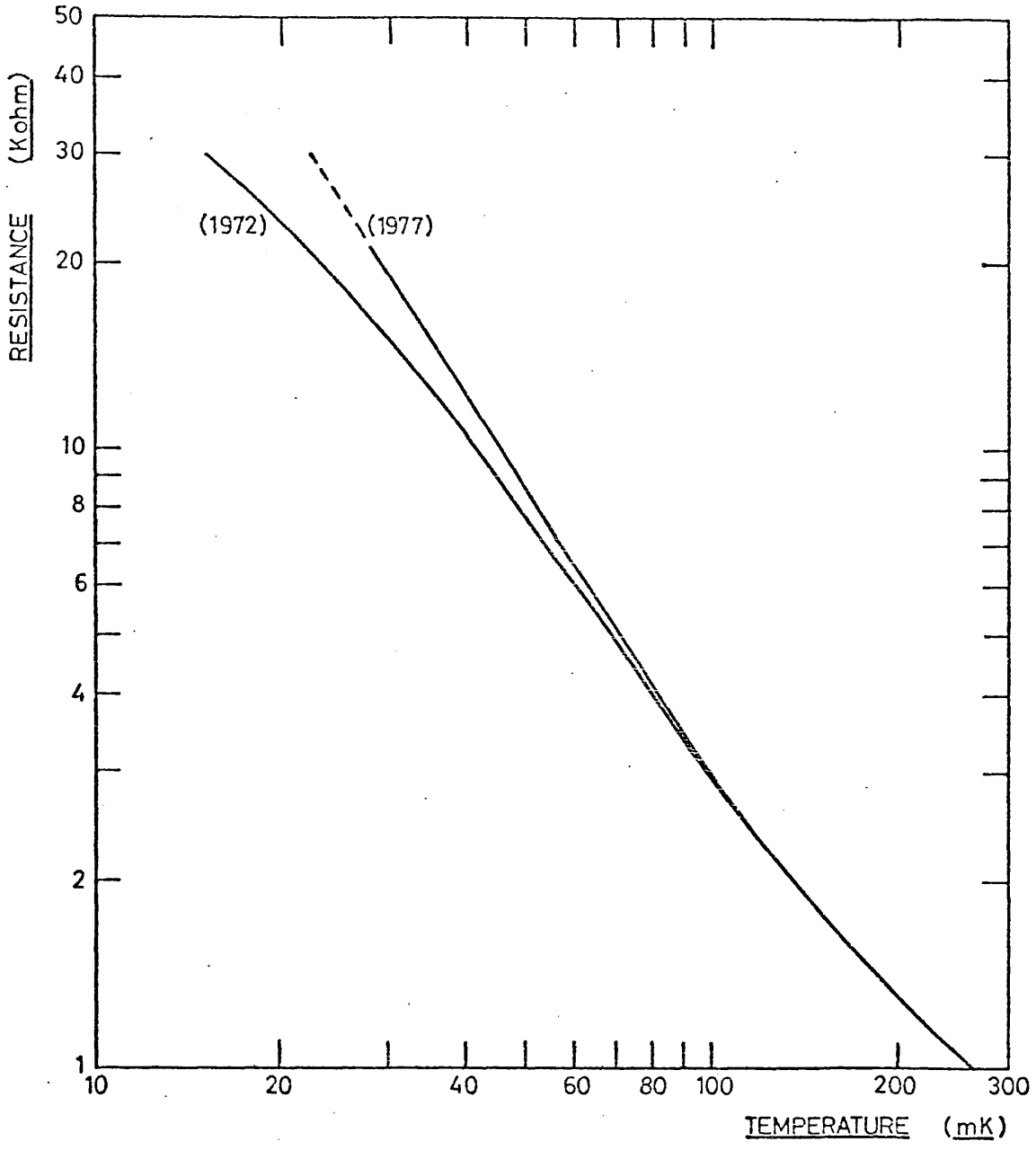

Fig. 5.6 RESISTOR CALIBRATIONS R3(1972) & R3(1977)

CHAPTER SIX

6.0. ANALYSIS AND CALCULATIONS

6.1. Data Collection and Analysis

6.1.1. Introduction

The basic data consisted of a series of measurements of echo height as a function of temperature. The measurement was made in three ways, at different stages during the course of the experimental work, and these methods have already been described in section 4.4. The data collected by the single-shot methods (either by photographs of the oscilloscope screen or by digital storage) differed from that collected in the early runs using the "Boxcar" integrators, and required rather different methods of analysis. For this reason the two techniques will be described separately.

6.1.2. Repetitive-pulse data.

The raw data in the early experimental runs was in the form of a continuously varying d.c. output from the "Boxcar" integrator as described in section 4.4. This output was used to drive the vertical axis of a chart recorder whilst the horizontal axis was driven by the output from the resistance bridge to provide a temperature scale. The chart resulting from a typical temperature sweep is shown in figure 6.1. In this case the data was collected during a warming-up period of about two hours, the value of the resistor R3 being shown along the bottom edge of the chart. The vertical scale (in decibels) was obtained by introducing known attenuation into the signal line, at constant temperature,

by means of a calibrated attenuator. A calibration curve, derived from this scale, was used to enable the data to be replotted in terms of signal amplitude and, by dividing this by the number of reflections suffered by the chosen echos, yields the loss of energy into the liquid helium at each reflection. Figure 6.2. shows this energy loss (in dB reflection^{-1}) as a function of temperature for the same sweep as the raw data plot (figure 6.1.) combined with similar data from another sweep, carried out at higher temperatures during the same experimental run. The fall in signal with increasing temperature at high temperatures (above about 600 mK) is due to temperature dependent losses in the piezoelectric rod. These losses were measured by observing the change in echo height when the experimental cell contained only a small amount of helium-3 gas (to ensure thermal contact between the rod and the cell). It was then possible to correct the data to account for the temperature dependent losses at high temperatures and the corrected curve is also shown, by the filled circles (•), in figure 6.2. The zero on the vertical scale is arbitrary at this stage since we are concerned with the change in energy loss into the liquid.

6.1.3. Discrete-point data.

The analysis of the single-shot data was more direct in that the raw data consisted of oscilloscope photographs of a particular group of echos (as shown in figure 4.7.) or , in the major proportion of the work, a chart recorder plot of the echo pattern obtained from the digital store as described in section 4.4.3. (A typical output chart, showing the echo height at about 30 mK, is shown in figure 6.3.) Each datum point therefore consisted of the measured average of the heights of the echos, from either the photographs

or the chart recorder plots, at the particular temperature at which the shot was fired. The advantage of accumulating a large number of echo trains (typically 512) at a particular temperature in the DL 4000 store, is illustrated by the noise level between the echos in the photographic data (figure 4.7.) compared with that shown on the chart recorder plot (figure 6.3.).

To ensure that the measured echo heights could be easily related to an energy loss in decibel, the output characteristic of the diode detector was plotted by measuring the height of a 240 MHz calibration pulse, from a Marconi 801 B/1 pulse generator. In this case the height of the pulse as received was determined as an integer (h), from the digital store, and compared with the input pulse amplitude as indicated by the calibrated attenuator setting on the pulse generator (in dBm). The results are shown in figure 6.4. The straight line is a square-law, representing the expression $20 \log_{10} h$, where h is the measured signal height in arbitrary units. The law is closely followed down to a signal level of about -99 dBm at which point the sensitivity of the detector begins to diminish. However, the echo height was normally somewhat greater than this, usually in the range from -70 to -80 dBm, in which region the detector output conformed well to the square law. The change in echo height could therefore be expressed in decibel simply by taking the logarithm of the measured height and multiplying by twenty. In practice, several adjacent echos were measured and the signal level was taken to be the average of the individual echo heights. Again, the data were corrected for temperature dependent losses and expressed in terms of energy loss per reflection by dividing the signal height (now in decibel) by the number of reflections experienced by the middle echo of the chosen group (ie. divided by $(2n-1)$ where n is the echo number).

6.2. Calculation of acoustic impedance

If the fractional loss of energy across a solid/liquid interface is β, then the energy reflected back into the solid is $(1-\beta)$. The measured echo height is this quantity expressed in decibel, that is ;

$$\Delta S = 10 \log_{10}(1-\beta) \qquad (6.2.1.)$$

Converting to natural logarithms : $\Delta S = 10 \log_{10} e \ln(1-\beta)$

$$\therefore \ln(1-\beta) = \frac{\Delta S}{10 \log_{10} e}$$

Provided β is small, $\ln(1-\beta) \approx -\beta$

Therefore;

$$\beta \approx \frac{-\Delta S}{10 \log_{10} e} = -0.2303 \Delta S \qquad (6.2.2.)$$

Now, it was shown in section 3.3. that the acoustic impedance is related to β by the expression

$$\beta = 4 \, Re\left[\frac{Z_L}{Z_s}\right]$$

where Z_s is the acoustic impedance of the solid medium and Z_l is the acoustic impedance of the liquid. Re denotes the real part of the complex quantity contained within the brackets.

$$\therefore Re\,[Z_l] = \frac{Z_s}{4}\,\beta \qquad (6.2.3.)$$

The acoustic impedance Z_s is defined thus ; $Z_s = \rho_s v_s$ where ρ_s is the density of the solid medium and v_s is the velocity of sound in that medium , provided that the diameter of the rod is large compared to the wavelength and that rod attenuation is negligible.

$$Re\,[Z_l] = \frac{\rho_s v_s}{4}\,\beta \qquad (6.2.4.)$$

The complex acoustic impedance (Z_l) consists of a real part (R), analogous to acoustic resistance, and an imaginary "acoustic reactance" (X).

$$\text{ie:} \quad Z_l = R + iX \qquad (6.2.5.)$$

$$\therefore R = \frac{\rho_s v_s}{4}\,\beta$$

In substituting for β it must be remembered that the quantity ΔS is referred to an arbitrary zero. Therefore R will also be referred to an arbitrary zero (usually taken to be the value of R at 1.0 Kelvin) and will be denoted by ΔR.

Therefore, substituting for β,

$$\Delta R = -\frac{0.2303}{4} \Delta S \rho_s v_s$$

It is more convenient to express acoustic resistance in terms of R/ρ since this quantity has the dimensions of velocity ;

$$\frac{\Delta R}{\rho} = -\frac{0.2303}{4\rho} \Delta S \rho_s v_s \qquad (6.2.6.)$$

where ρ is the density of the liquid helium. In fact, ρ varies slightly with temperature but this was ignored since the variation is less than one half of one per cent below 1.0 Kelvin. The values of ρ_s and v_s used in the calculations were as follows :

(a) Bismuth germanium oxide; $\rho_s = 9.232 \times 10^3$ kg m^{-3}
(Crystal Technology Inc. data sheet)

$v_s = 1.775 \times 10^3$ m s^{-1}
(from Rehwald (1973))

(b) Quartz; $\rho_s = 2.65 \times 10^3$ kg m^{-3}
(from Neppiras (1973))

$v_s = 5.700 \times 10^3$ m s^{-1}
(from Neppiras (1973))

The density of liquid heliun-3, as a function of pressure, has been measured by Abraham et al (1972) so using these values, and the numerical factors obtained above, the data were replotted as graphs of $\Delta R/\rho$ (in $m\,s^{-1}$) as a function of temperature at various pressures. An example of $\Delta R/\rho$ against temperature at 25.7 bar is shown in figure 6.5.

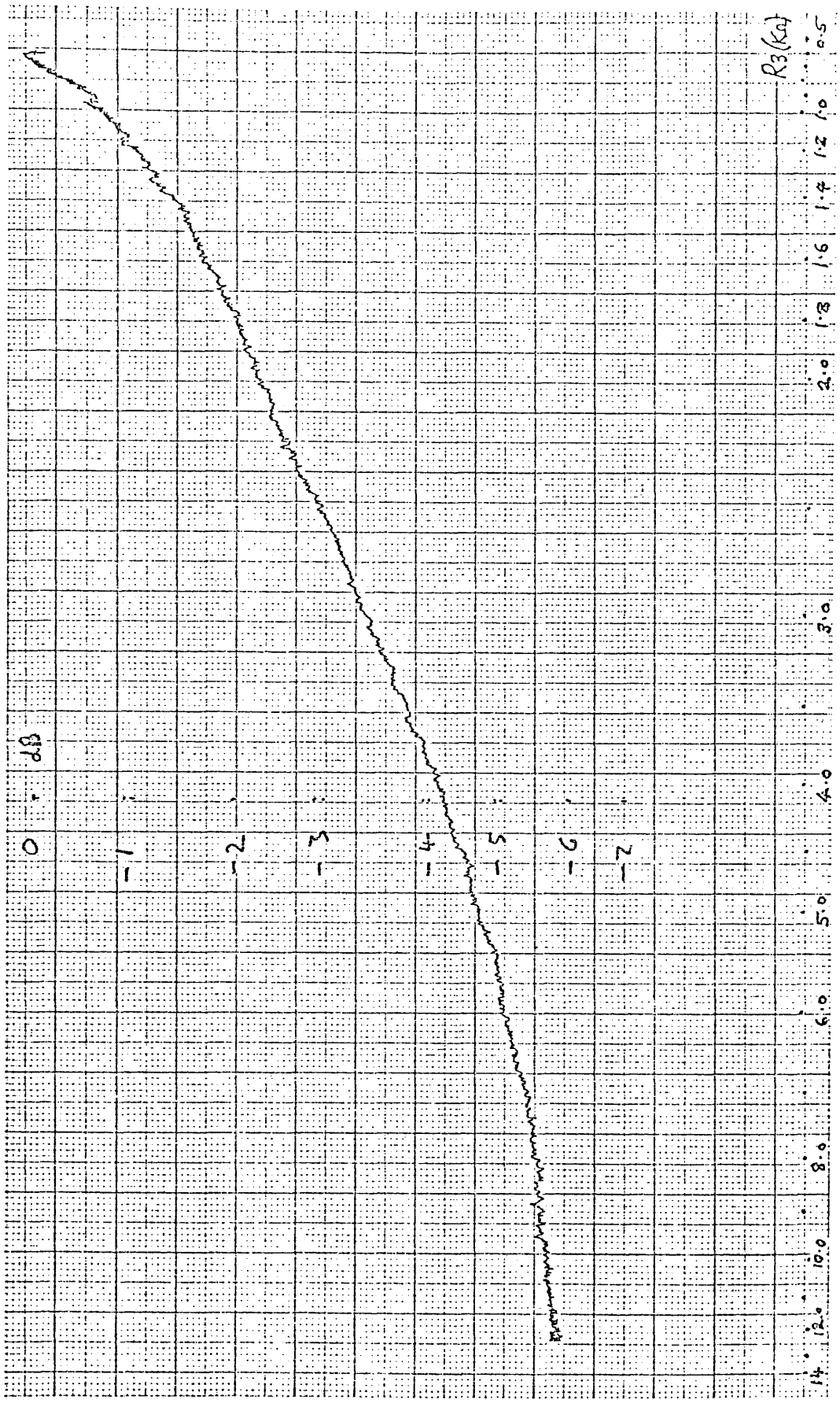

Fig. 6.1 Typical output from 'Boxcar' integrator — transverse waves in ^3He

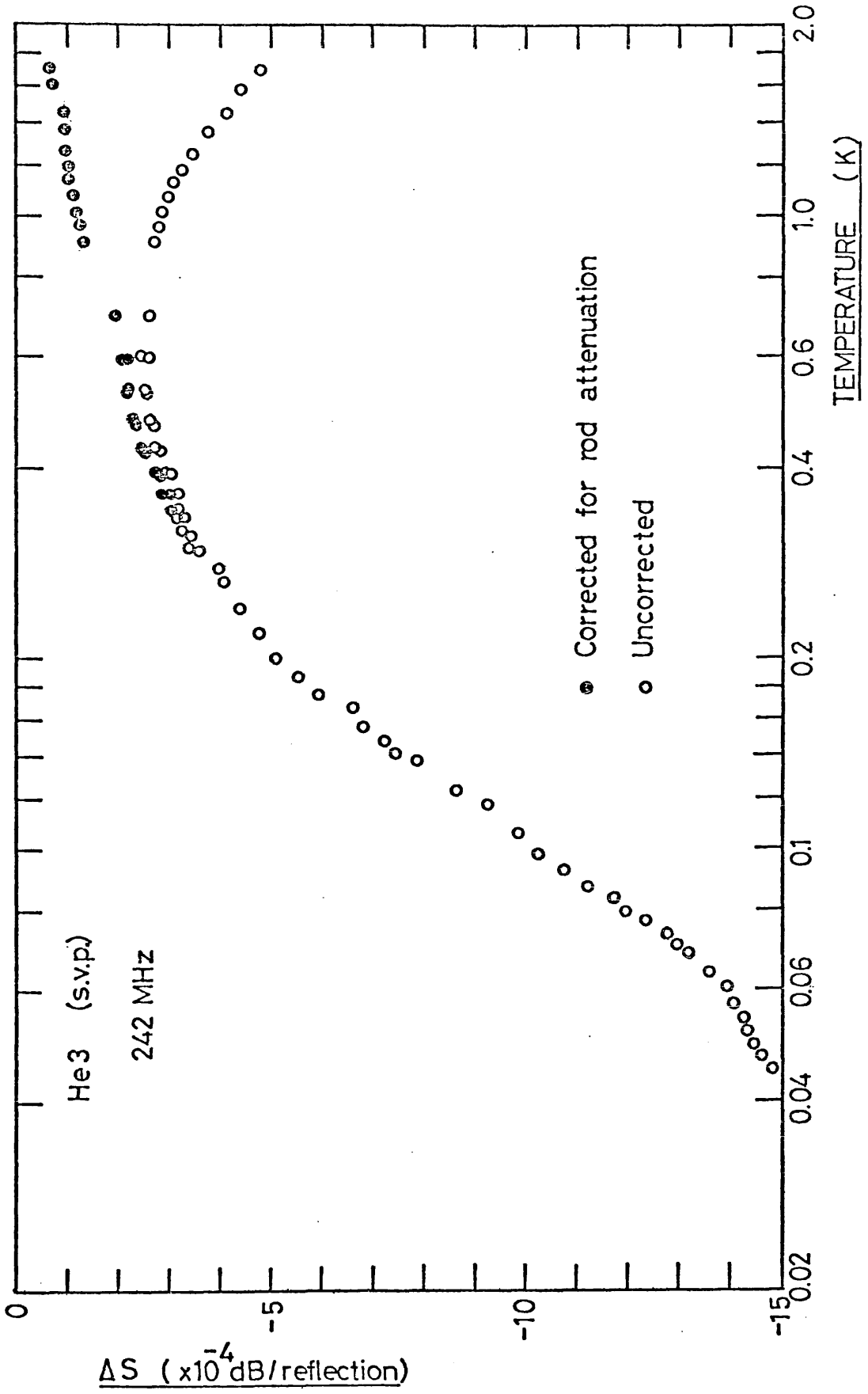

Fig. 6.2 Change in signal height (ΔS) with temperature.

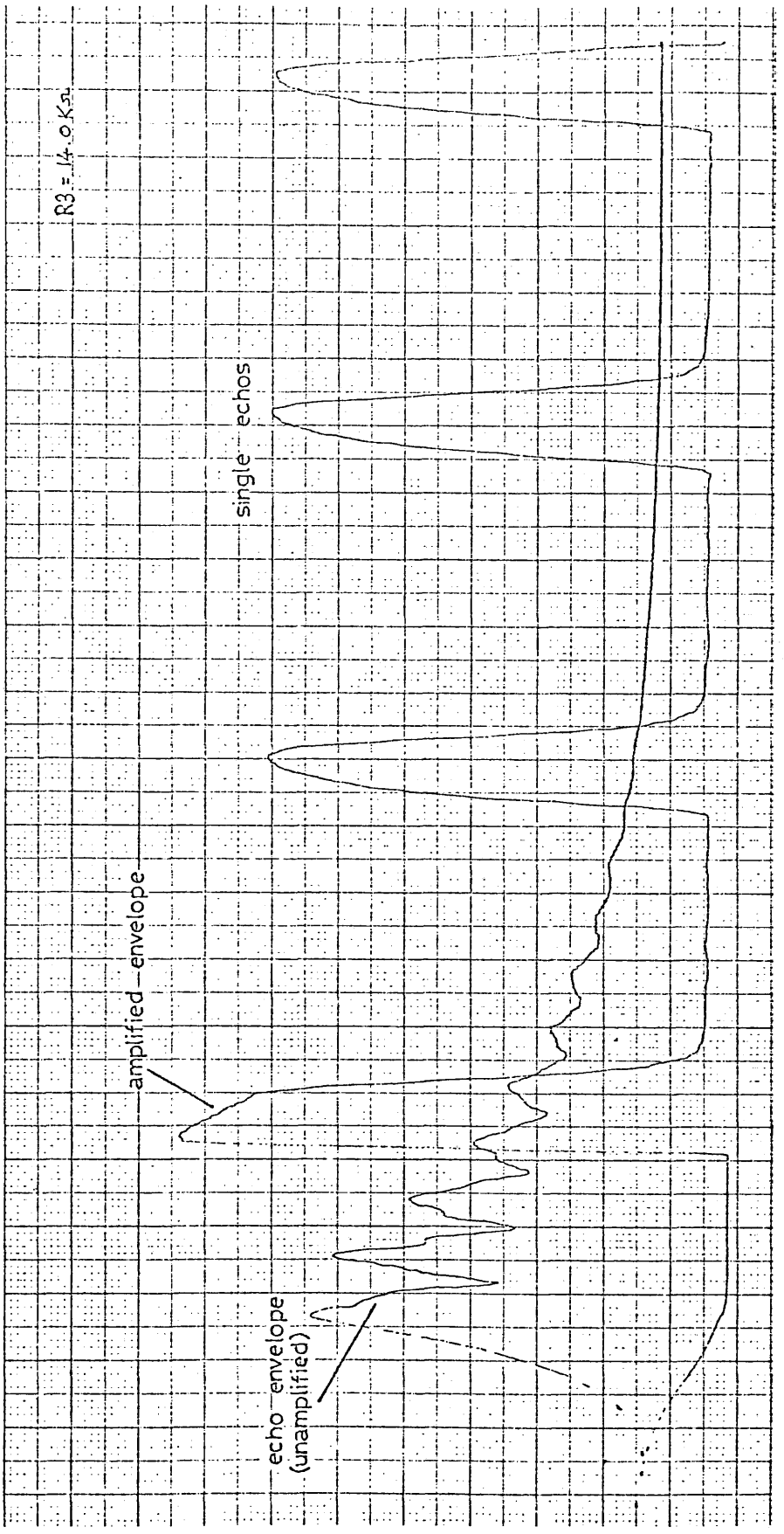

Fig. 6.3 Typical output from 'DL4000' store – transverse waves in ^3He

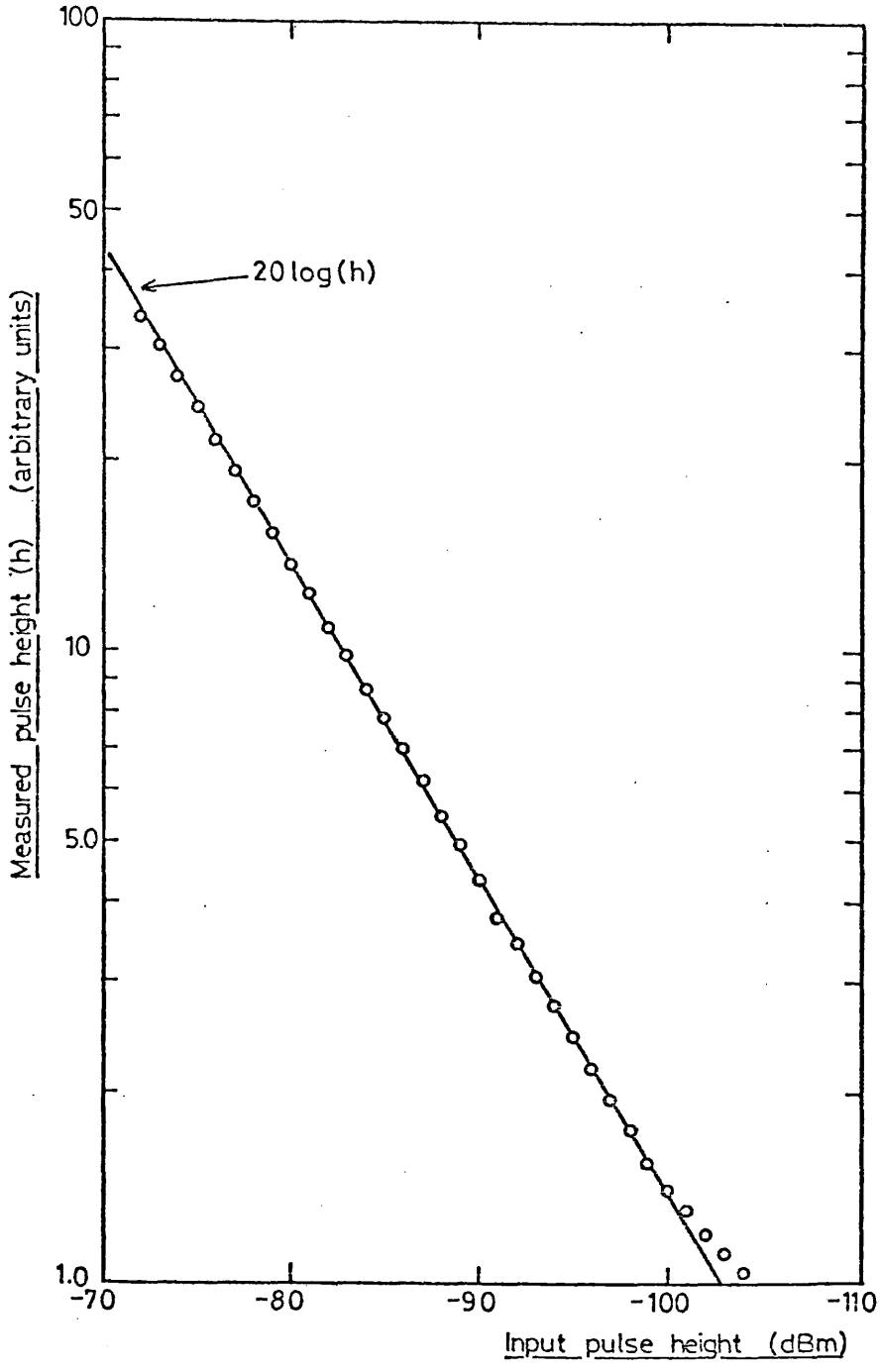

Fig. 6.4 DIODE DETECTOR CALIBRATION

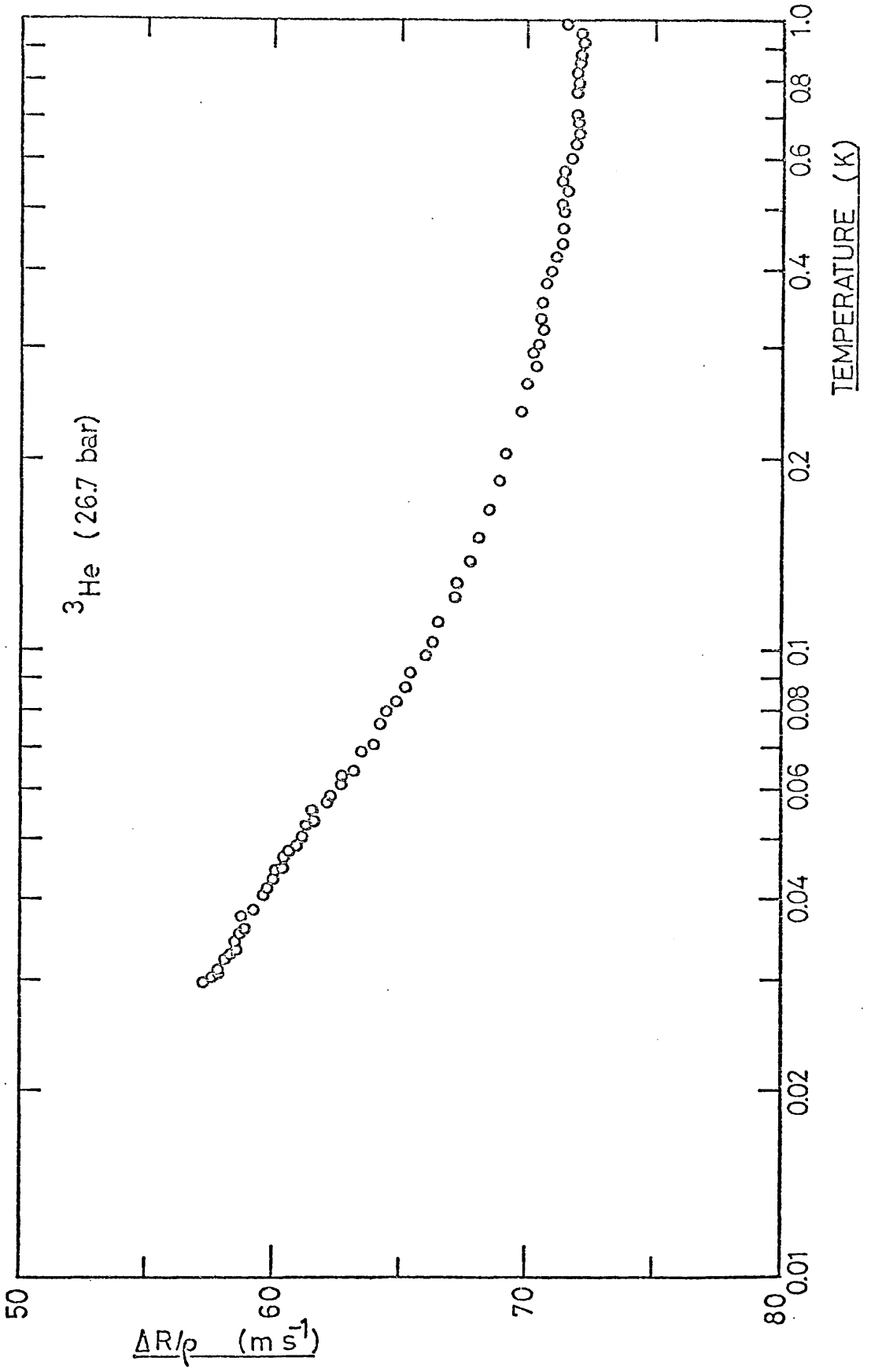

Fig.6.5 Change in acoustic resistance (typical)

6.3. Normalisation of data

For a classical viscous liquid, the transverse acoustic impedance is given by ;

$$Z_o = (R_o + iX_o) = (1 - i)\sqrt{\frac{\eta\rho\omega}{2}} \qquad (6.3.1.)$$

where η is the viscosity of the liquid.

Thus, if only the real part is considered,

$$\frac{R_o}{\rho} = \sqrt{\frac{\eta\omega}{2\rho}} \qquad (6.3.2.)$$

where R_o is the transverse acoustic resistance in the hydrodynamic regime, $\omega\tau \ll 1$.

The viscosity of liquid helium-3 under its saturated vapour pressure has been measured by Black, Hall and Thompson (1971) for temperatures between 0.05 Kelvin and 3.0 K, and they derive the empirical relationship ;

$$\eta = \frac{2.21}{T^2} + \frac{26.3}{T^{1/3}} \quad \mu P. \qquad (6.3.3.)$$

This expression was used with equation (6.3.2.) to calculate R_o/ρ at the s.v.p. The viscosity as a function of pressure has been measured in the temperature range 0.4 K to 1.0 K by McCoy et al (1975) who normalised their

data to those of Black et al (1971). Using these results a set of curves showing R_o/ρ as a function of temperature were plotted at various pressures between zero and 28.0 bar. Our data were normalised by fitting each plot of $\Delta R/\rho$ to the curve of R_o/ρ, at the appropriate pressure, in the temperature range 0.4 K to 1.0 K and the arbitrary scale $(\Delta R/\rho)$ was then replaced by the absolute acoustic resistance,

6.4. Validity of $\omega\tau \ll 1$

Classical viscosity theory is applicable provided that $\omega\tau \ll 1$, where ω is the angular frequency of the disturbance and τ is some relaxation time. Wheatley (1975) quotes values of the viscous relaxation time for helium-3 at pressures from zero to 30 bar, the extreme values being :

$$\tau_\eta T^2 = 1.24 \times 10^{-6} \text{ s (mK)}^2 \text{ at zero pressure}$$
$$\tau_\eta T^2 = 0.73 \times 10^{-6} \text{ s (mK)}^2 \text{ at 30 bar}$$

Thus, at 400 mK, for a disturbance with an angular frequency of 240 MHz, the product $\omega\tau$ is found to be in the range :

$$\omega\tau_\eta = 1.75 \times 10^{-2} \text{ at zero pressure}$$
$$\omega\tau_\eta = 1.03 \times 10^{-2} \text{ at 30 bar}$$

As the temperature increases, $\omega\tau$ falls still further, so we see that at 240 MHz, in the temperature range 0.4 Kelvin to 1.0 K, the condition $\omega\tau \ll 1$ is satisfied for pressures between zero and 30 bar.

The condition is also satisfied at 1048 MHz in the same temperature range, the corresponding values being :

$\omega\tau_\eta = 5.10 \times 10^{-2}$ at zero pressure

$\omega\tau_\eta = 3.00 \times 10^{-2}$ at 30 bar.

CHAPTER SEVEN

7.0. EXPERIMENTAL RESULTS

7.1. 242 MHz transverse waves; liquid helium-3 (0.3 to 28.0 bar)

The results of the above analysis are shown in figures 7.1. to 7.11. The first of these, figure 7.1., shows the qualitative behaviour of the acoustic resistance R/ρ of liquid helium-3 as a function of temperature under the saturated vapour pressure (≈ 0.3 bar). This graph has been plotted twice as a result of the thermometer calibration problem discussed in section 5.5. The upper graph, 7.1.(a), was obtained using the R3 (1972) calibration and the lower graph, 7.1.(b), using the R3 (1977). The resulting difference in the temperature dependence of R/ρ is small and the subsequent experimental results (figures 7.2. to 7.11.) will be shown using the 1972 calibration only. The solid line represents the acoustic resistance calculated from the classical viscosity equation (eqn.(6.3.2.)) using the viscosity data of Black, Hall and Thompson (1971). Our data have been fitted to this curve at 1.0 Kelvin, where the value of R/ρ is calculated to be 5.12 m s^{-1}. A direct measurement of R/ρ, from ΔS, at 1.0 Kelvin, both with and without liquid helium in the cell, agreed with this value although the experimental error in ΔS was rather large due to the change in resonant frequency of the cavity when the liquid was removed.

The measured temperature dependence of R/ρ is well described by the classical expression from 2.0 Kelvin down to 0.2 K at which point it deviates from the curve as the transition from hydrodynamic to collisionless behaviour occurs. Using the values of relaxation time ($\tau_\eta T^2$) given

by Wheatley (1975), the temperature corresponding to $\omega\tau = 1$ was calculated to be 0.043 K at 0.3 bar, and this is indicated by the arrow on the diagram. Below this temperature R/ρ approaches a temperature-independent limit, R_∞/ρ, which will be discussed in detail later.

The remaining diagrams (figures 7.2. to 7.11.) show the temperature dependence of R/ρ for liquid helium-3 at the various pressures indicated. Most of these are the result of a single temperature sweep (warming or cooling, as indicated) but numbers 7.1., 7.2., 7.7., 7.8., and7.11. are composite diagrams which combine the results of two or three different, overlapping runs in each case, taken, of course, at the same pressure. The details of these runs may be found in table I, which follows this section. The temperature corresponding to $\omega\tau=1$ is shown on each graph, these values being calculated from the data given in table V of Wheatley (1975) and shown as a graph of $T_{(\omega\tau=1)}$ against pressure; see figure 7.12. The data at pressures greater than the saturated vapour pressure have been fitted to theoretical curves of R/ρ obtained from the same classical expression (equation 6.3.2.) using the viscosity data of McCoy et al (1975), and are shown as the solid lines on the diagrams between 0.4 K and 1.0 K.

Flowers, Richardson and Williamson (1976) have calculated R/ρ, known by these authors as Z'/ρ, as a function of $\omega\tau$ in the range 0.01 to 10 (ie. between about 0.36 Kelvin and 0.01 K, when converted to temperature, for $\omega/2\pi$ = 240 MHz) using Landau Fermi-liquid theory for helium-3 at a pressure of 23.0 bar. By interpolating their curve of R/ρ versus $\omega\tau$ and converting their ordinate axis to temperature using the data of Wheatley (1975), the theoretical curve shown

in figure 7.13. was obtained. Having first been replotted on corresponding log - log scales, the experimental data were fitted to this curve by aligning the temperatures corresponding to $\omega\tau = 1$ and then fitting the data points to the curve in the low-temperature region (ie. below about 50 mK). In this way the limit of the acoustic resistance, R_∞ / ρ, was determined by extrapolation. The values obtained, however, were found to depend upon the choice of thermometer calibration so the extrapolation was performed using both calibrations in each case. The results are shown in tables II and III, the first being obtained from the R3 (1972) calibration, and the second table from R3 (1977). In each table, the uncertainty quoted in the column labelled "error" is that resulting from data-fitting to which was added a further uncertainty of $\pm 1\%$ to account for errors in the graphical interpolation of the theoretical curve. The overall uncertainty is contained in the column headed "total error". The values of R_∞ / ρ obtained using the R3 (1977) calibration are greater than the corresponding values using R3 (1972) by an average of 4.2%, the greatest difference (5.7%) occuring in the 16.0 bar case, which represents a maximum uncertainty in R_∞ / ρ of $1.32\ \mathrm{m\,s^{-1}}$. The implications of this difference will be discussed in chapter 8.

Figure number	Pressure (bar)	Experimental run number	Date	Temperature range (mK)
7.1	0.3(w)	R 27	18.4.75	1700 - 65
		R 17(b)	14.10.76	230 - 16
7.2	0.3(c)	R 16	20.12.76	430 - 43
		R 17(a)	13.10.76	940 - 31
		R 18(c)	12.11.76	1000 - 92
7.3	5.5(w)	R 20(g)	1.12.76	1580 - 16
7.4	5.5(c)	R 20(c)	26.11.76	1450 - 28
7.5	5.7(w)	R 20(f)	30.11.76	900 - 21
7.6	9.2(w)	R 20(b)	25.11.76	1450 - 18
7.7	16.0(w)	R 18(b)	11.11.76	620 - 15
		R 20(l)	8.12.76	1190 - 110
7.8	21.0(c)	R 17(f)	22.10.76	680 - 25
		R 20(k)	7.12.76	1700 - 174
7.9	25.7(c)	R 17(e)	21.10.76	1000 - 30
7.10	26.2(c)	R 17(k)	13.12.76	880 - 23
7.11	28.0(w)	R 18(a)	10.11.76	370 - 17
		R 20(j)	3.12.76	1450 - 172

(c): cooling
(w): warming

TABLE I Dates of experimental runs

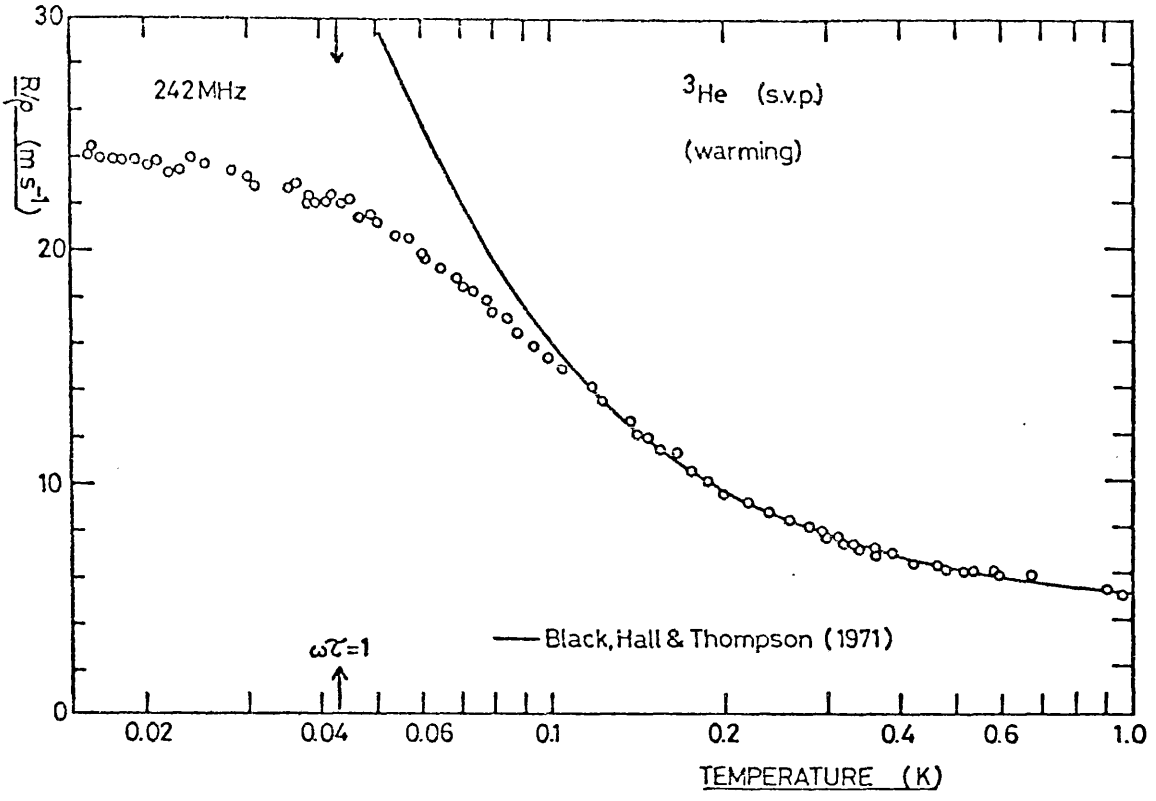

Fig. 7.1(a) Temperature dependence of R/ρ at 0.3 bar (R3(1972) calibration)

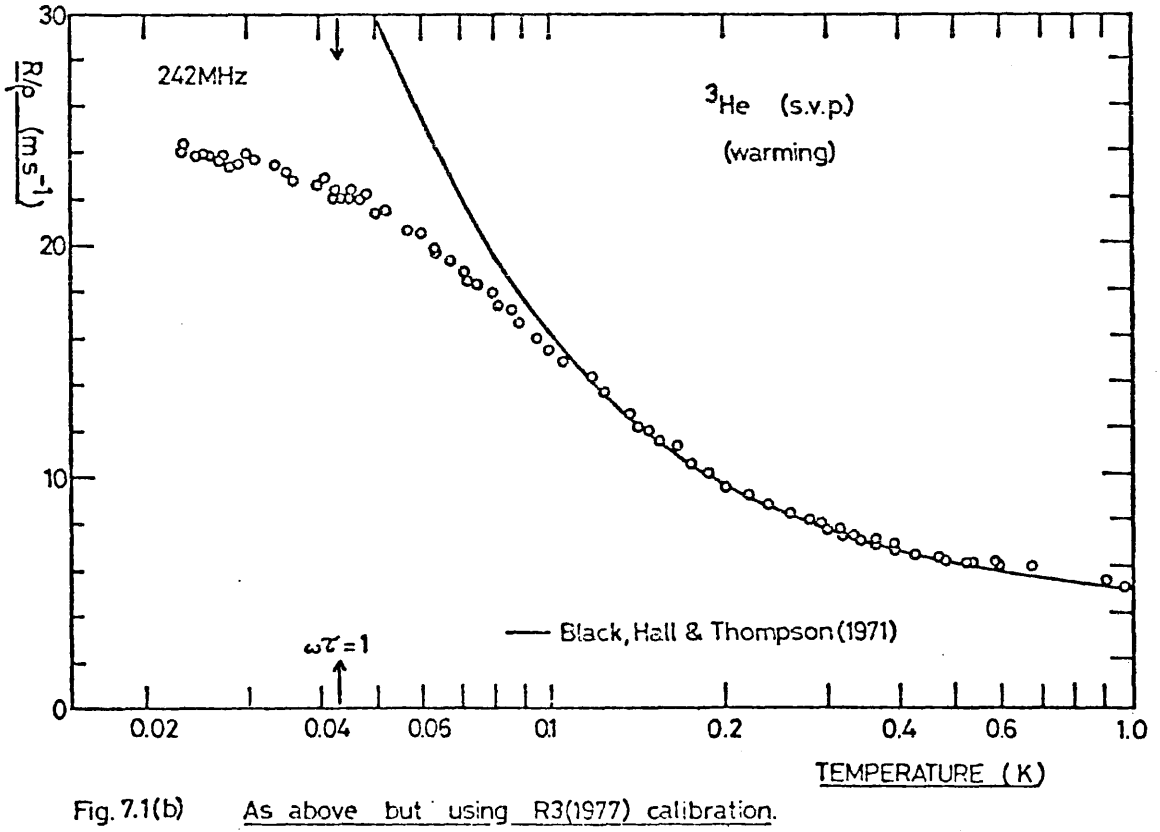

Fig. 7.1(b) As above but using R3(1977) calibration.

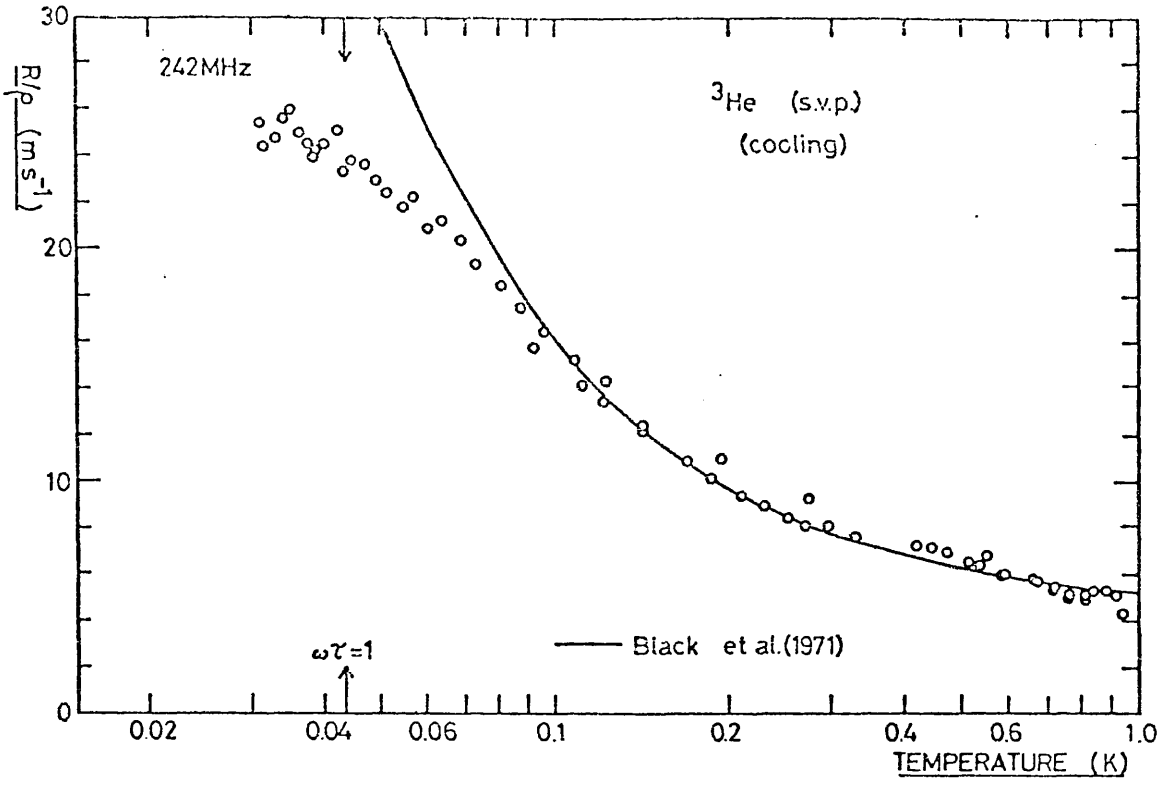

Fig.7.2 Saturated vapour pressure (~0.3 bar)

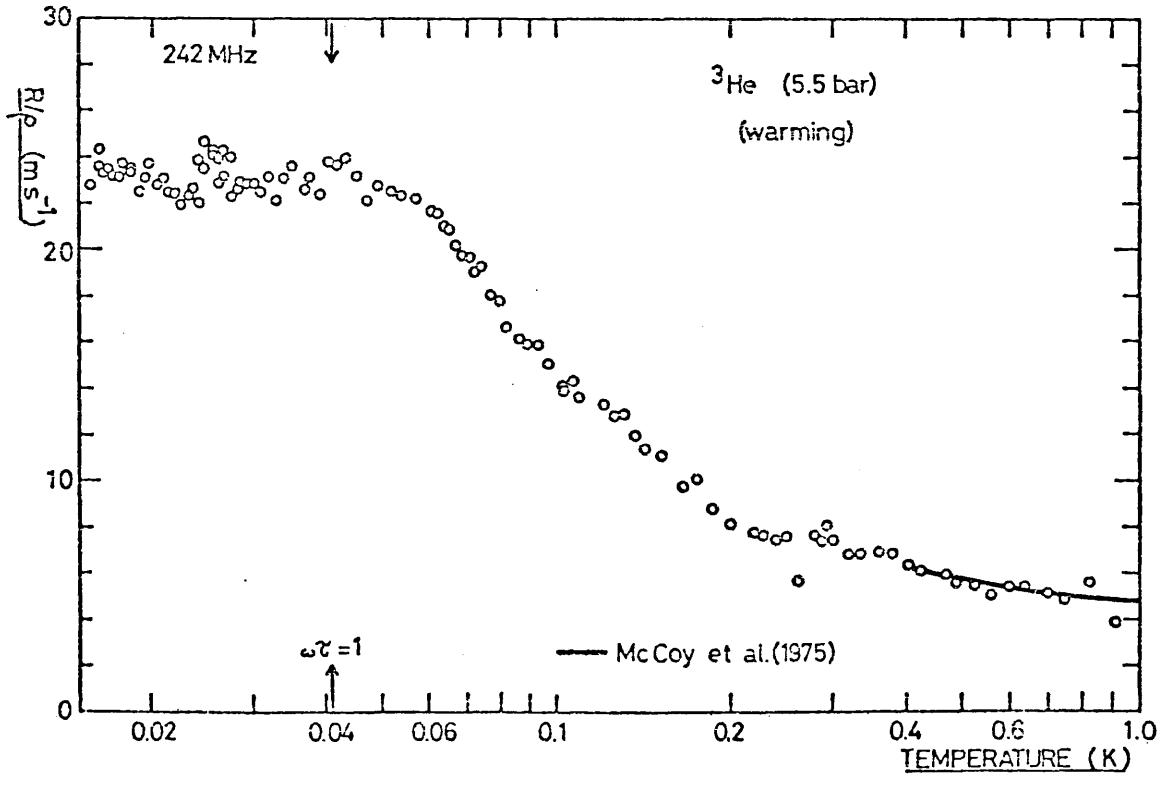

Fig.7.3 5.5 bar

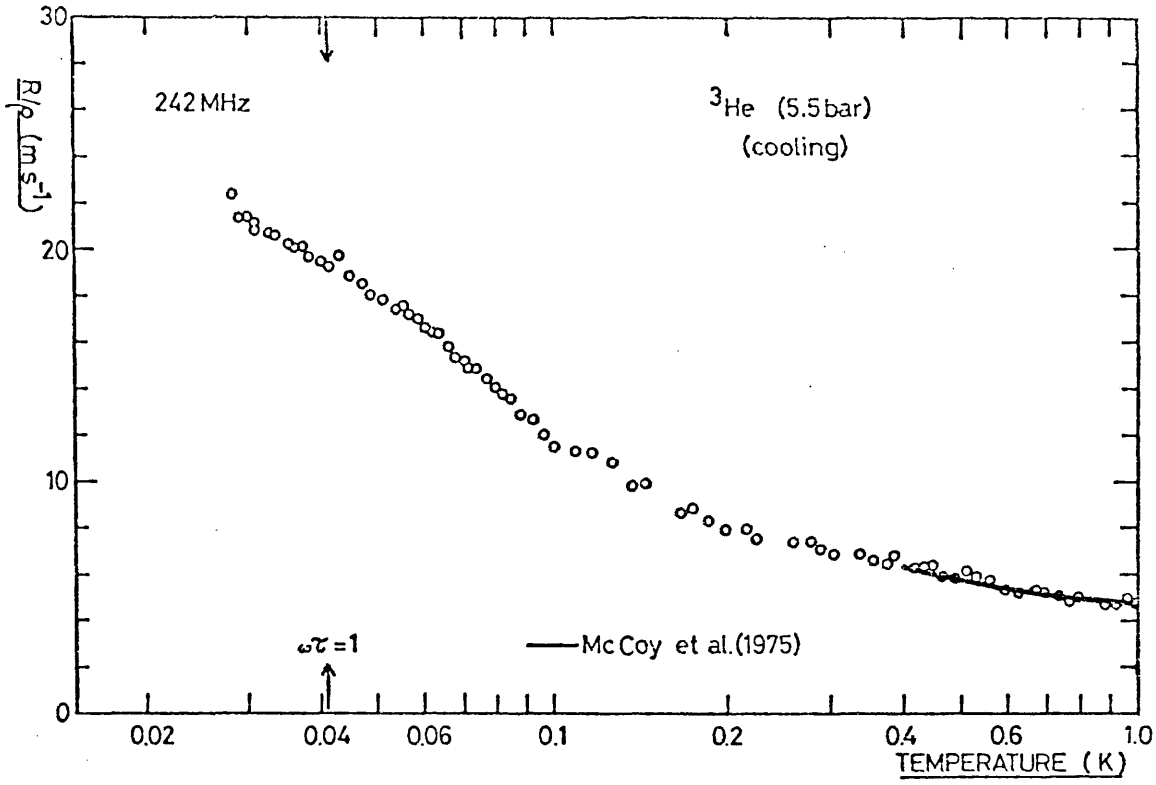

Fig.7.4 5.5 bar

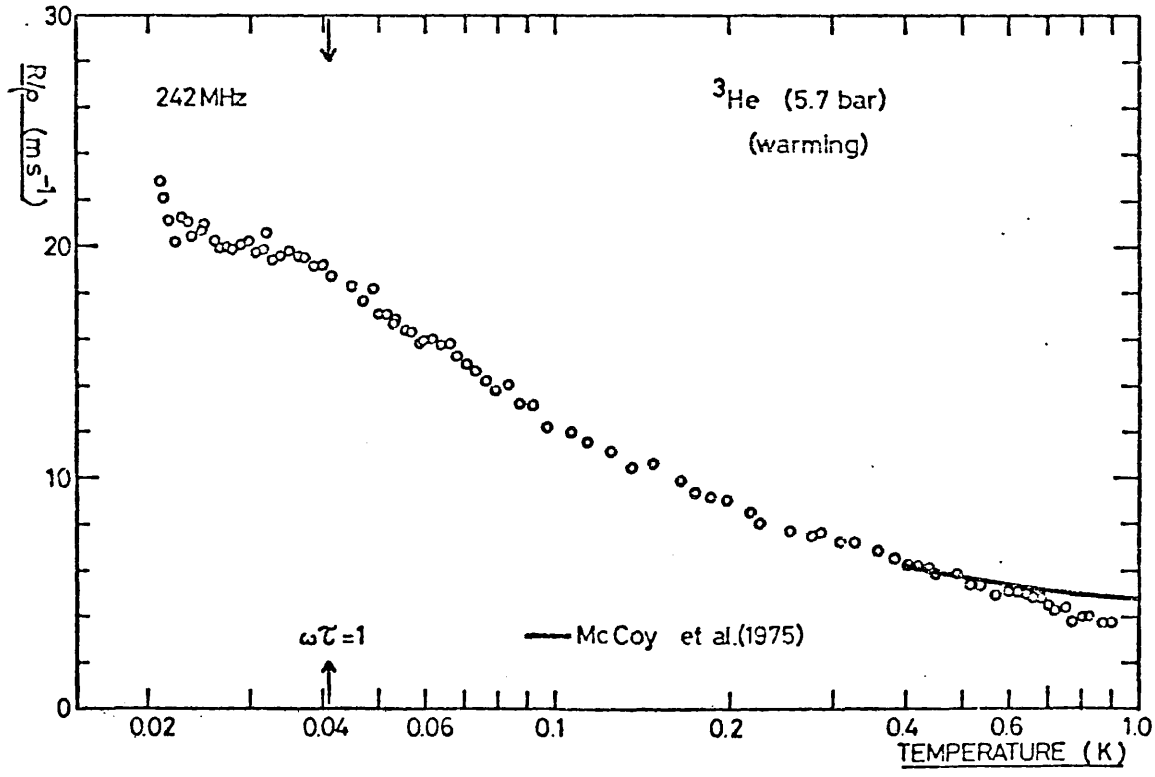

Fig.7.5 5.7 bar

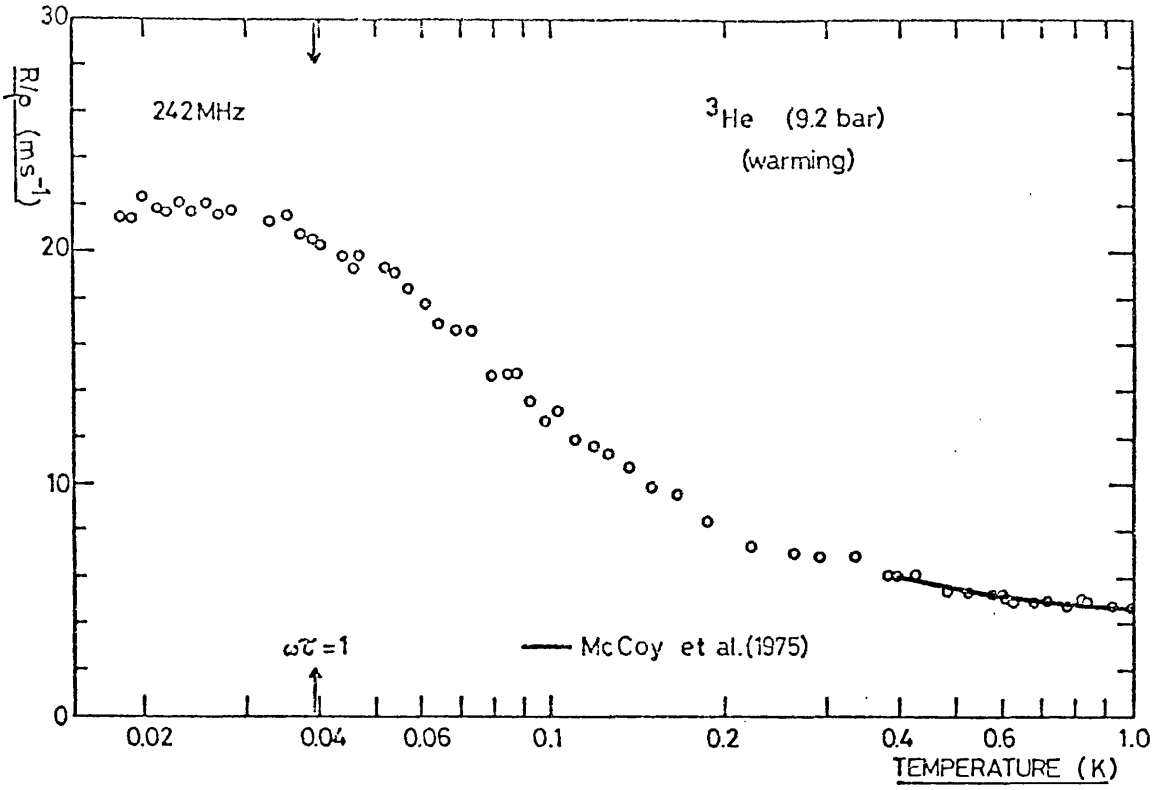

Fig.7.6 9.2 bar

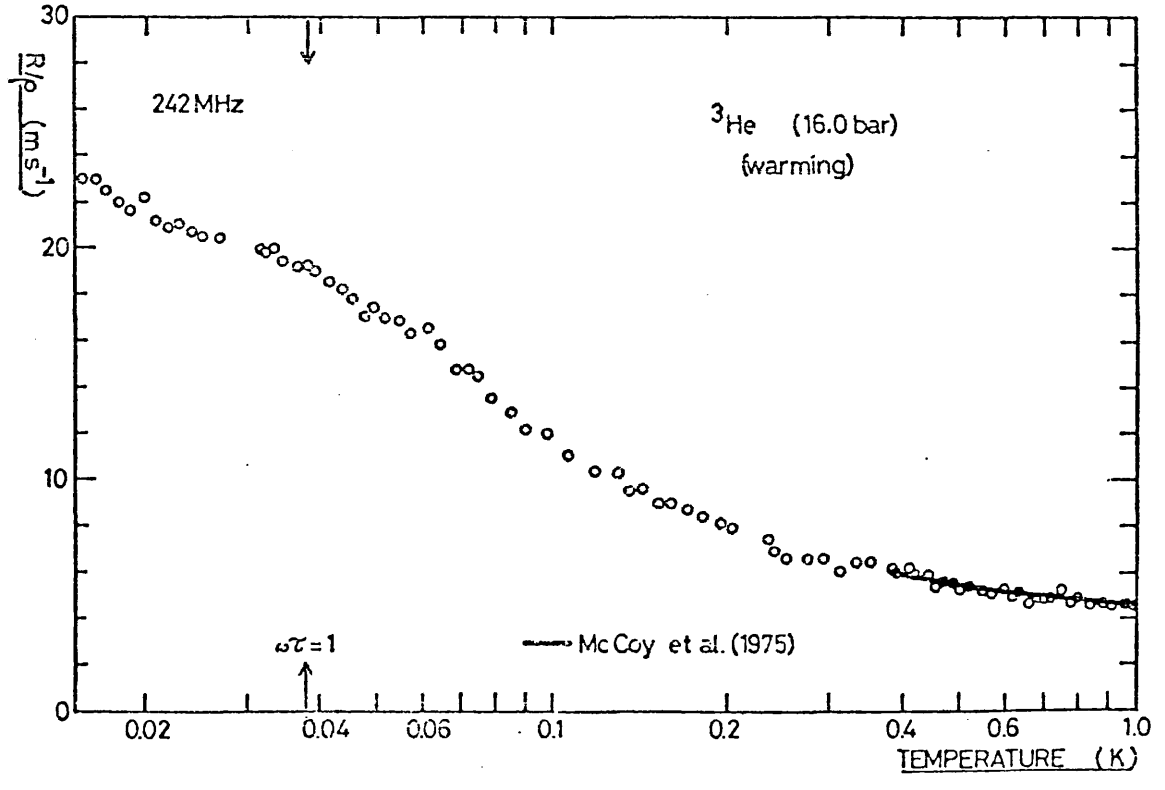

Fig.7.7 16.0 bar

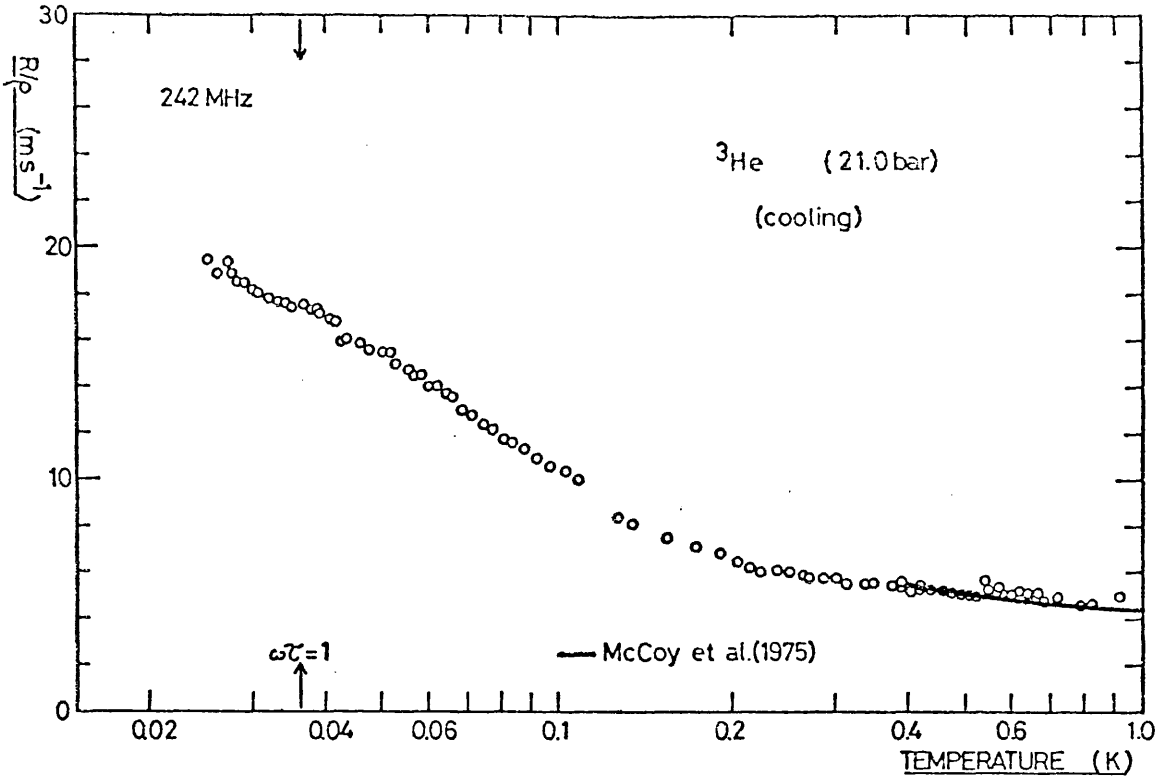

Fig.7.8 21.0 bar

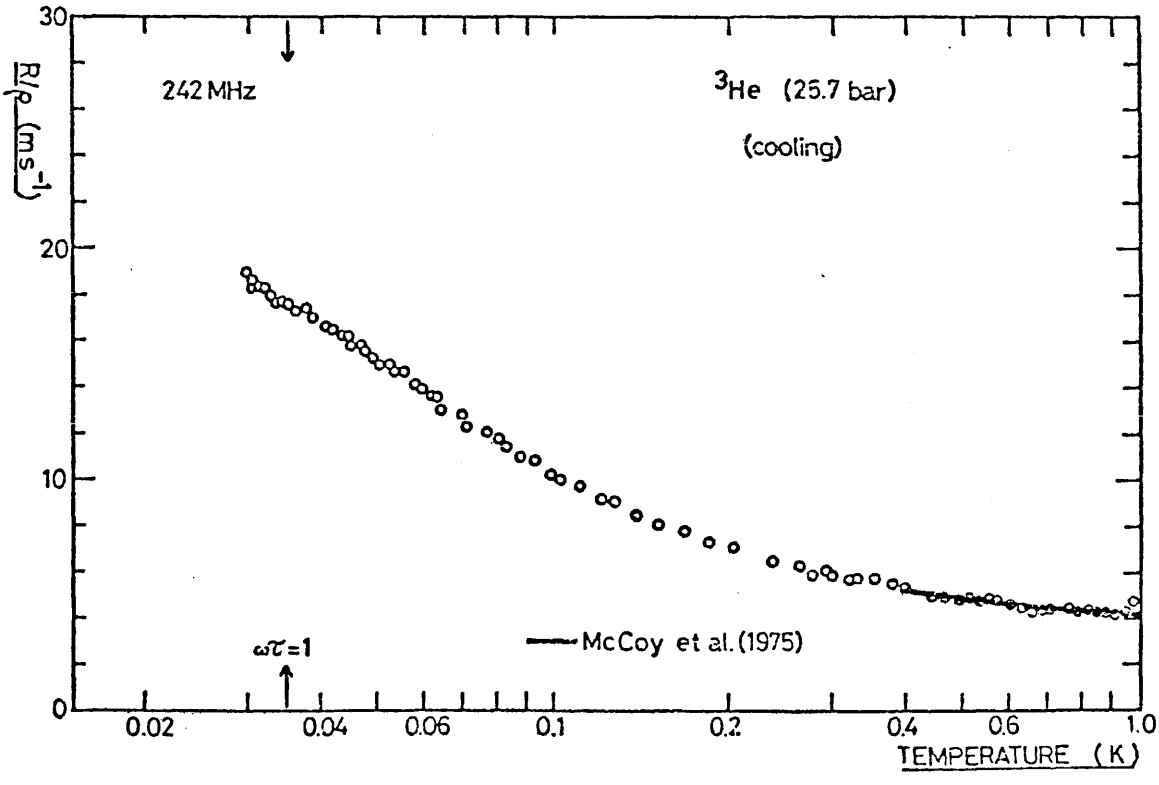

Fig.7.9 25.7 bar

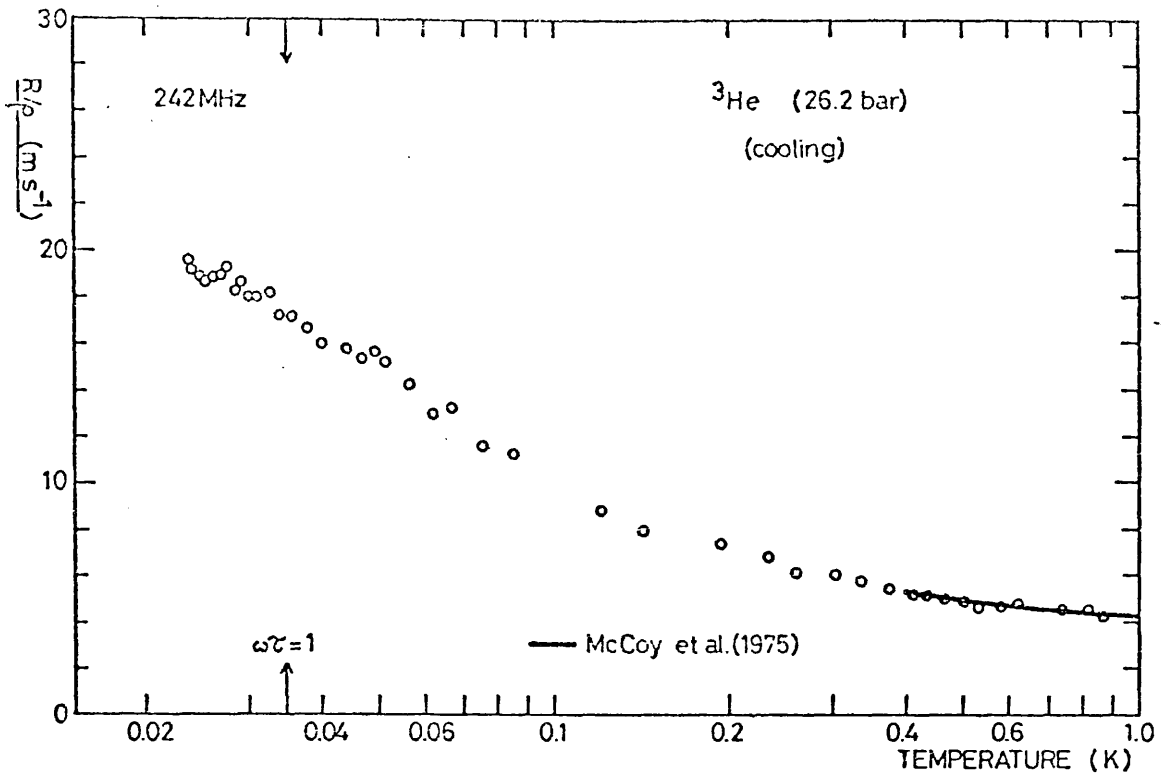

Fig. 7.10 26.2 bar

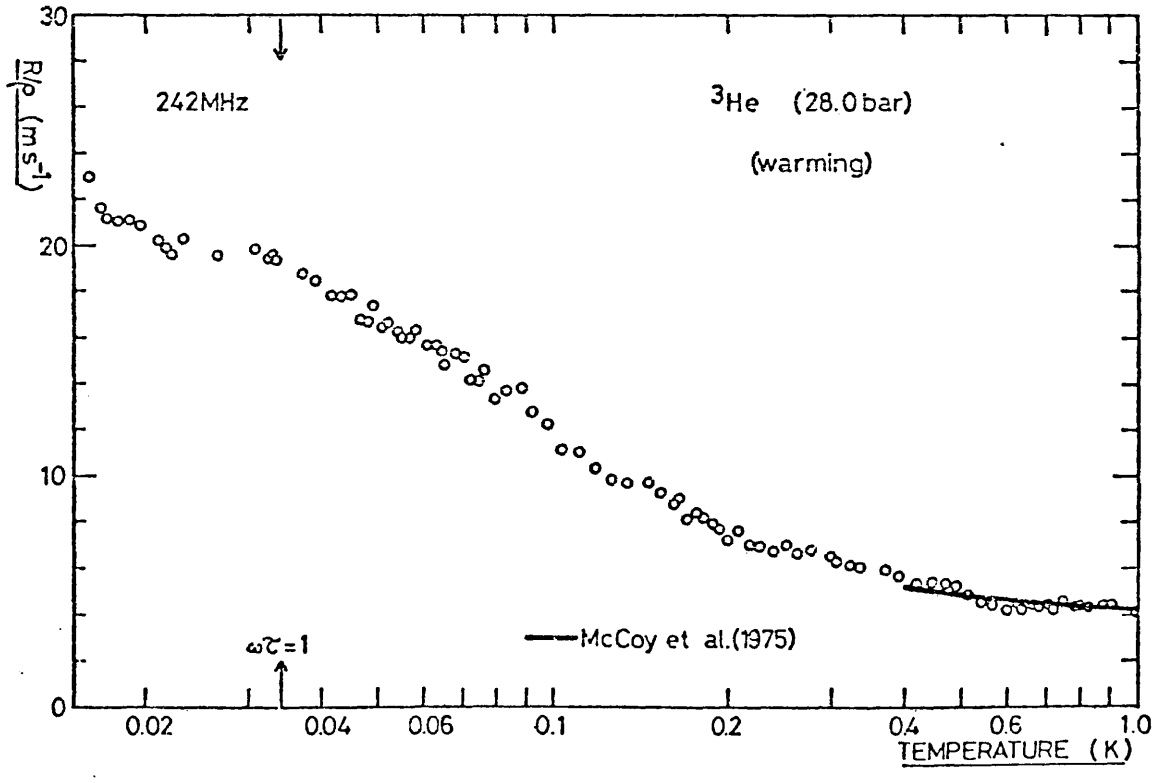

Fig. 7.11 28.0 bar

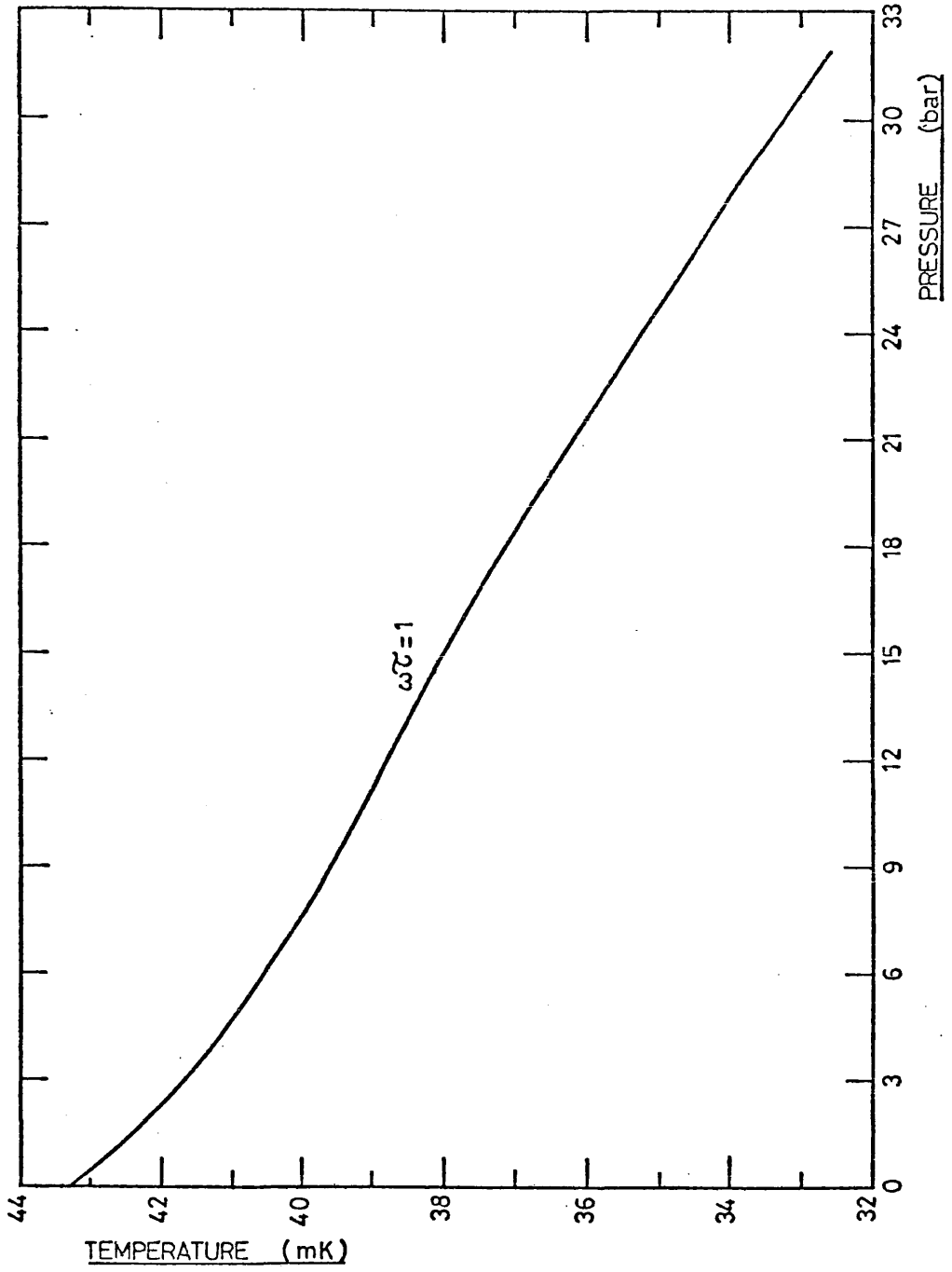

Fig.7.12 Temperature/pressure for $\omega\tau = 1$

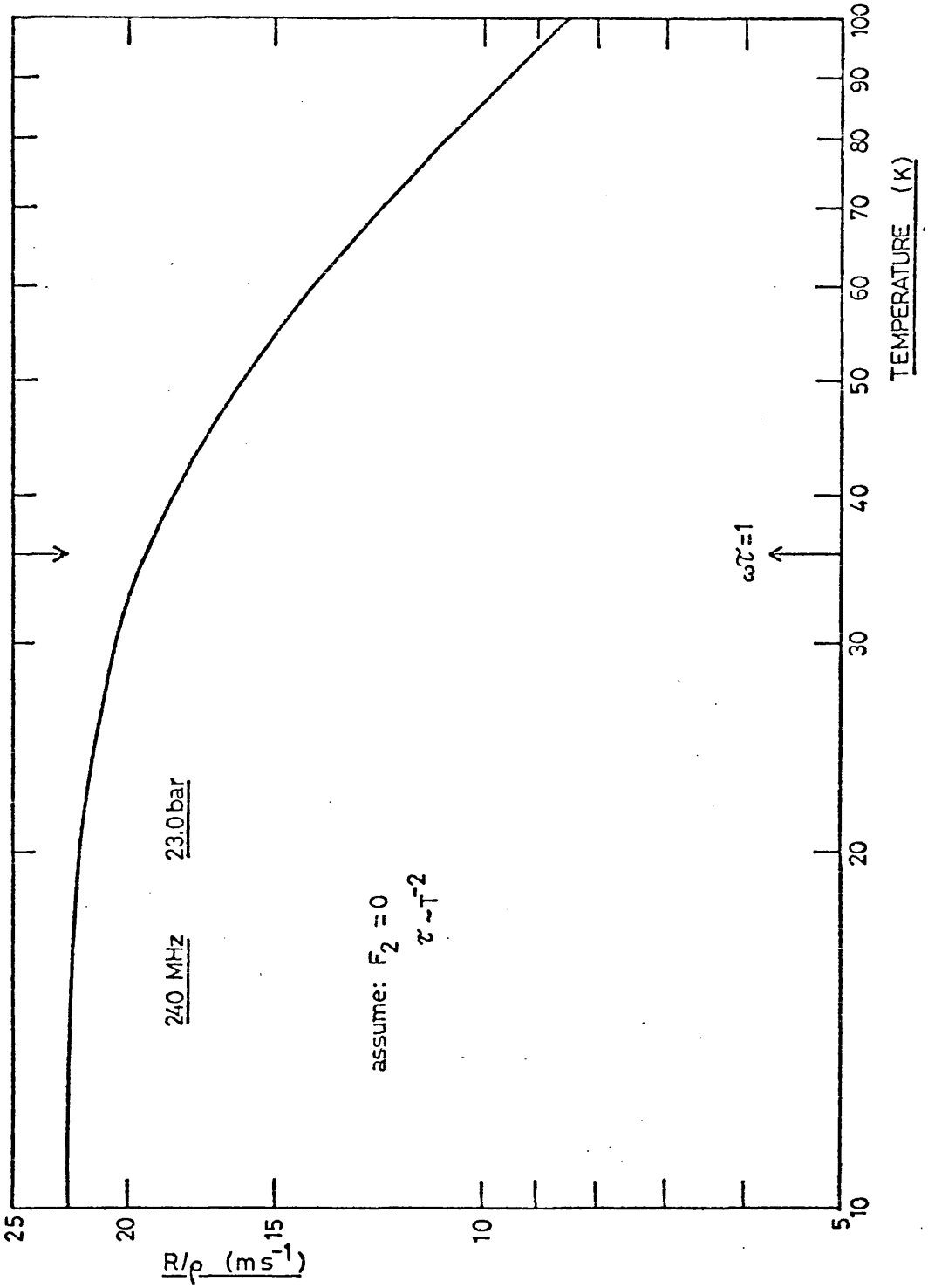

Fig. 7.13 Temperature dependence of acoustic resistance from the theory of Flowers and Richardson.

No.	pressure (bar)	sweep direction	R_∞/ρ ($m\ s^{-1}$)	error	total error
7.1(a)	0.3	warming	24.01	± 0.46	± 0.70
7.2	0.3	cooling	27.19	± 0.75	± 1.02
7.3	5.5	warming	23.43	± 0.62	± 0.85
7.4	5.5	cooling	22.45	± 0.40	± 0.63
7.5	5.7	warming	21.91	± 0.65	± 0.87
7.6(a)	9.2	warming	22.51	± 0.48	± 0.71
7.6(b)	9.2	cooling	22.27	± 0.35	± 0.55
7.7	16.0	warming	21.75	± 0.69	± 0.91
7.8	21.0	cooling	20.09	± 0.35	± 0.55
7.9	25.7	cooling	20.59	± 0.30	± 0.51
7.10	26.2	cooling	20.14	± 0.44	± 0.64
7.11	28.0	warming	21.21	± 0.51	± 0.72

TABLE II Values of R_∞/ρ (using R3(1972) calibration)

No.	pressure (bar)	sweep direction	R_∞/ρ ($m\,s^{-1}$)	error	total error
7.1(b)	0.3	warming	24.53	±0.49	±0.74
7.2	0.3	cooling	28.25	±0.96	±1.24
7.3	5.5	warming	24.04	±0.73	±0.97
7.4	5.5	cooling	23.45	±0.29	±0.52
7.5	5.7	warming	22.40	±0.71	±0.93
7.6(a)	9.2	warming	23.39	±0.37	±0.60
7.6(b)	9.2	cooling	23.48	±0.35	±0.58
7.7	16.0	warming	23.07	±0.82	±1.05
7.8	21.0	cooling	21.10	±0.41	±0.63
7.9	25.7	cooling	21.73	±0.35	±0.57
7.10	26.2	cooling	21.17	±0.56	±0.77
7.11	28.0	warming	22.40	±0.53	±0.75

TABLE III Values of R_∞/ρ (using R3(1977) calibration)

7.2. 242 MHz transverse waves ; liquid helium-4 (s.v.p.)

An experiment to observe the losses into liquid helium-4 was carried out to provide a direct comparison with the previous results. The bomb described in section 4.5. was pressurized to 3.4 bar at room temperature which corresponded to about 0.5 cm^3 of liquid helium-4, under its saturated vapour pressure, at 4.2 Kelvin. This volume of liquid was sufficient to fill the cell completely. The experiment was performed in the same way as the early experiments in liquid helium-3, using a "Boxcar" integrator to average the heights of 39 echos, centred at echo number 2570. Several runs were carried out, both cooling and warming, and the temperature range covered was from 1.75 K to 0.045 K. The raw data was analysed in exactly the same way as the corresponding helium-3 data to yield a curve of energy loss per reflection (ΔS) as a function of temperature and this was converted to change in acoustic resistance $(\Delta R / \rho)$ as described in section 6.2.

The results are shown in figure 7.14. in which the closed circles (●) show the high temperature data corrected for temperature dependent losses in the piezoelectric rod. The energy losses into the liquid appear to be independent of temperature below 0.6 Kelvin and have been set to zero. Above this temperature the energy loss increases due to the viscosity of the liquid helium-4, but increases less rapidly than in the case of helium-3. The solid line (in the 1.0 K to 2.0 K region) shows the loss of energy into the liquid calculated from equation 6.3.2., taking η as the viscosity of liquid helium-4 and ρ as the density of the normal component (ρ_N) of the liquid. Numerical values of $\eta \rho_N$ were taken from the measurements of Tough, McCormick and Dash (1963). Although the temperature

range is limited, the agreement between the calculated values and our data is good and suggests that the losses into helium-4 fall to zero at low temperatures. This result is consistent with the inability of superfluid liquid helium-4 to support a shear stress.

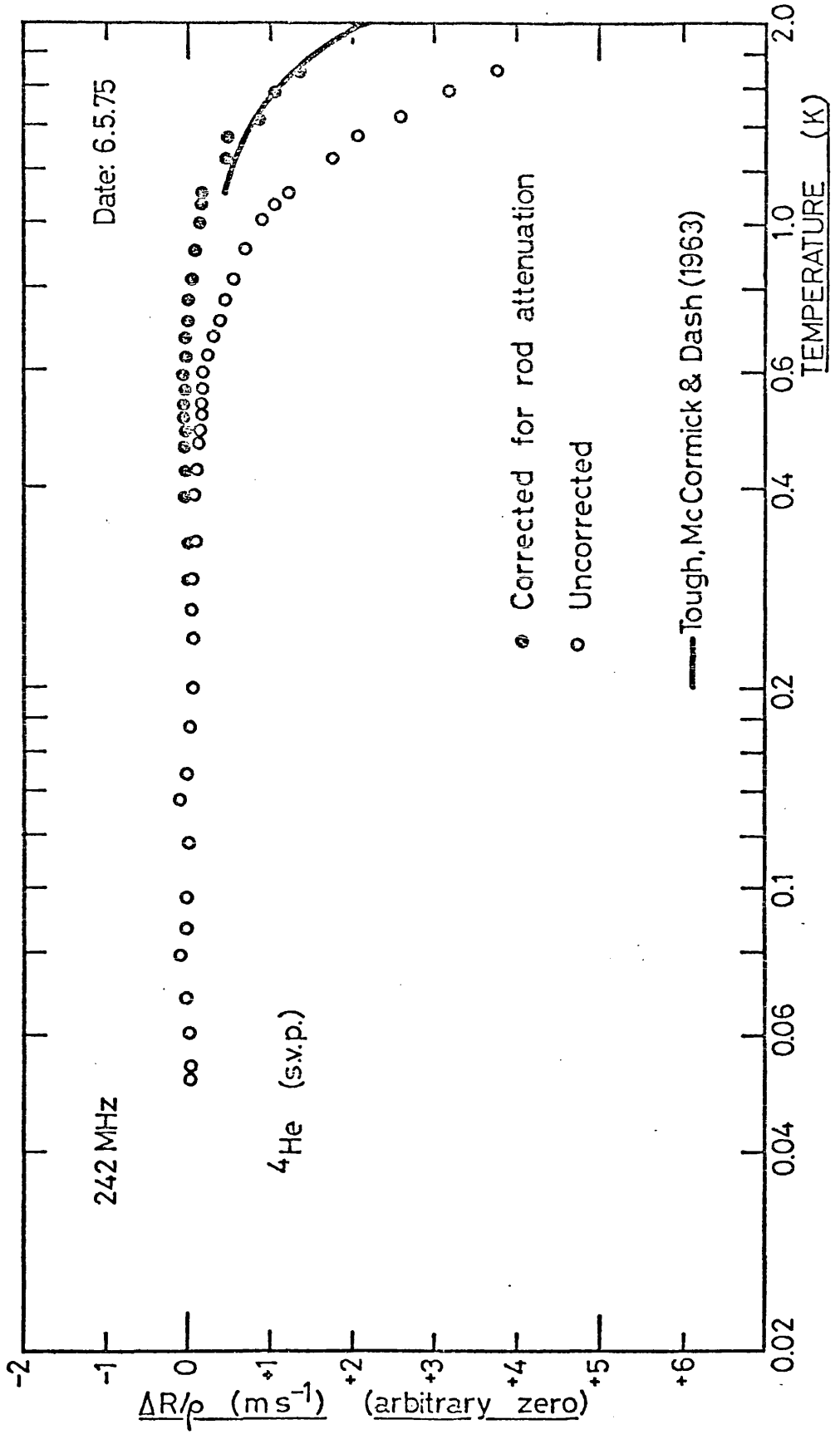

Fig.7.14 Relative acoustic resistance for ^{4}He at 0.3bar.

7.3. 242 MHz transverse waves; helium-3/helium-4 mixture (26.2 bar)

The final set of low-frequency, transverse wave data resulted from the accidental contamination of the helium-3 sample by a small amount of helium-4 due to an imperfect indium seal in the experimental cell. The Boxcar integrator was set to average the heights of three echos, centred at echo number 1490, and the sample was pressurized to 26.2 bar. On cooling the sample the energy losses into the liquid increased as expected in pure helium-3 until, at a particular temperature, sharply defined, the losses suddenly fell to a very low value which remained constant when the temperature was further reduced. This was taken to indicate phase separation in the helium mixture, the liquid helium-4 forming a superfluid film over the surface of the piezoelectric rod and the inner surfaces of the experimental cell, thereby reducing the energy losses into the liquid. This phenomenon has been studied in detail by Borovikov and Peshkov (1976).

Warming the sample from about 43 mK resulted in the chart recorder plot shown in figure 7.15. The transition begins at about 68 mK and is completed by 85 mK, the temperature dependence of the energy loss then follows the pattern expected for pure helium-3. These data were converted in the manner described in section 6.12. to a graph of acoustic resistance (R/ρ) as a function of temperature; figure 7.16. (The high temperature data have been corrected for temperature dependent losses in the piezoelectric rod.) Again, equation 6.3.2. was used to calculate R/ρ over the temperature range 0.4 K to 1.0 K, taking the viscosity of pure liquid helium-3 at 26.0 bar from the data of McCoy et al (1975) and our data were fitted to this curve in the high temperature region. The limiting value of R/ρ at low temperatures was found to be $(1.3 \pm 0.3)\ m\ s^{-1}$.

It has already been shown that the energy losses into pure liquid helium-4 fall to zero at low temperatures due to the inability of the superfluid to support a shear stress. Consequently, the limiting value of acoustic resistance in this case must be due to helium-3 atoms in solution with the film of liquid helium-4. The limiting concentration of helium-3 atoms in a dilute solution has been measured as a function of pressure by Watson, Reppy and Richardson (1970) and extrapolating their data to 26.0 bar, the limiting concentration (X) is about 8.0%. The number density (n_3) of helium-3 atoms is given by :

$$n_3 = \frac{X N_A}{v} \qquad (7.3.1.)$$

where v is the molar volume of the mixture, N_A is Avagadro's number and X is the limiting concentration which is given by :

$$X = \frac{n_3}{n_3 + n_4}$$

(n_4 is the number density of helium-4 atoms).

Now, v may be expressed in terms of v_4 , the molar volume of helium-4, and α , the relative difference in molar volumes of helium-3 and helium-4 atoms, ie :

$$v = (1 + \alpha X) v_4$$

Therefore,

$$n_3 = \frac{X N_A}{v_4 (1 + \alpha X)} \qquad (7.3.2.)$$

Values of v_4 and α as functions of pressure have been published by Watson et al (1970) and extrapolating to 26.0 bar gives values of these factors corresponding to our experimental conditions.

ie : $v_4 = 23.017 \times 10^{-6}\ m^3\ mole^{-1}$; $\alpha = 0.166$

Using equation (7.3.2.) we obtain the number density $n_3 = 2.077 \times 10^{27}\ m^{-3}$

At very low temperatures, the Fermi momentum is given by the expression ;

$$p_F = \hbar (3\pi^2 n_3)^{1/3} \qquad (7.3.3.)$$

Evaluating this equation, using the calculated value of n_3 gives

$$p_F = 4.163 \times 10^{-25}\ kg\ m\ s^{-1}$$

In section 3.8., it was shown that for an assembly of non-interacting Fermions, the acoustic resistance would be given by ;

$$\frac{R}{\rho} = \frac{3}{16}\frac{p_F}{m} \qquad (3.8.2.)$$

where m is the atomic mass of helium-3. However, only the helium-3 atoms contribute to this acoustic resistance so, if ρ_3 is the density of the helium-3 atoms and ρ is the density of the mixture, we have ;

$$\frac{R}{\rho} = \frac{\rho_3}{\rho}\frac{3}{16}\frac{p_F}{m} \qquad (7.3.4.)$$

The density ratio ρ_3/ρ is obtained from the number densities n_3 and n_4 since ;

$$\frac{\rho_3}{\rho} = \frac{3n_3}{3n_3+4n_4}$$

At 26.0 bar, for an eight per cent solution of helium-3 in helium-4 ;

$$\frac{\rho_3}{\rho} = 0.0615$$

Therefore, using the value of m given by Wheatley (1975) of 5.009×10^{-27}Kg we finally obtain the value for the acoustic resistance :

$$\frac{R}{\rho} = 0.96\ ms^{-1}$$

This value compares well with the measured value of (1.3 ± 0.3) m s^{-1} suggesting that the superfluid film surrounding the piezoelectric rod contains helium-3 atoms that behave as a collection of non-interacting Fermions.

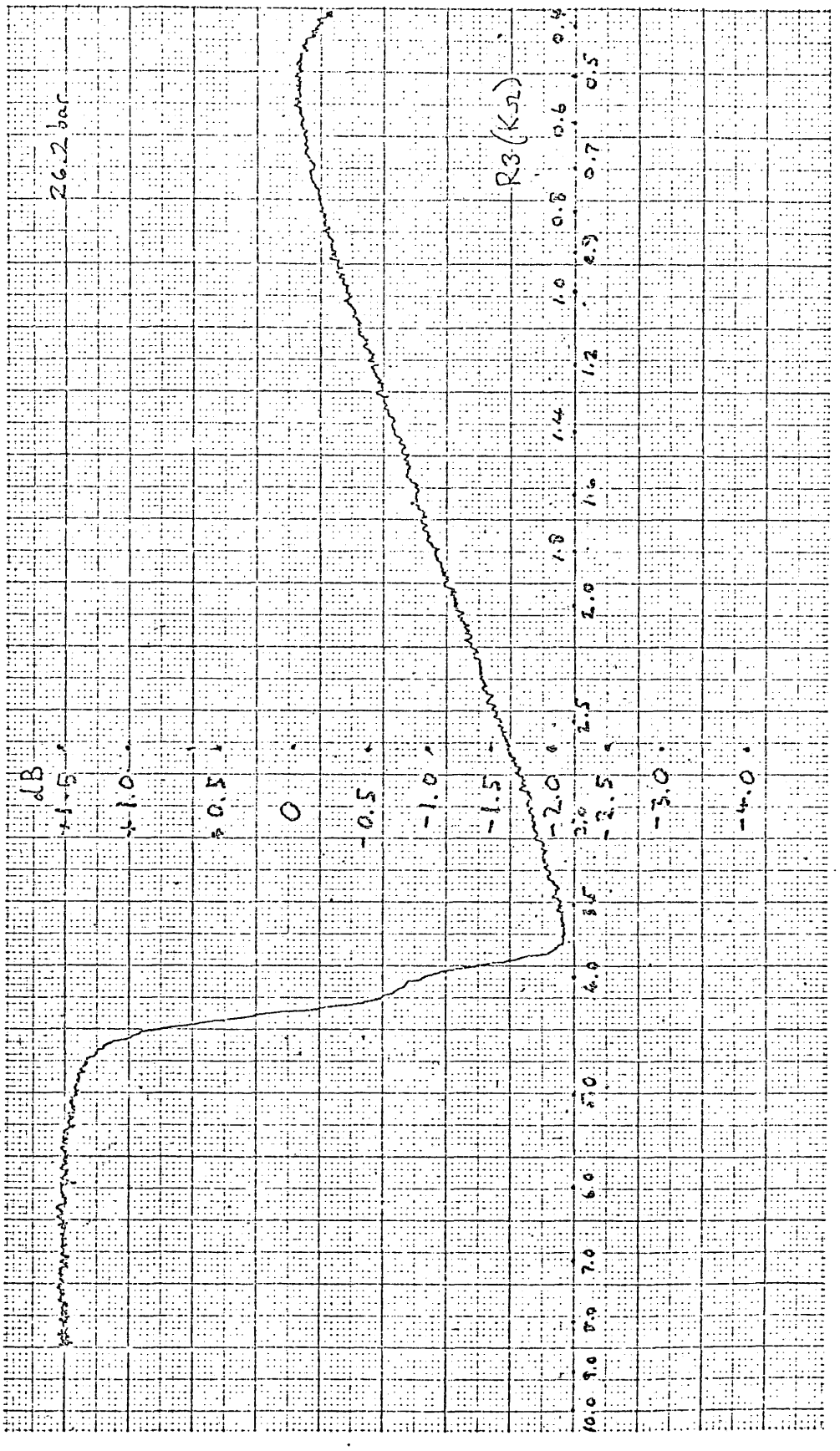

Fig.7.15 Output from 'Boxcar' integrator for $^{3}He-^{4}He$ mixture

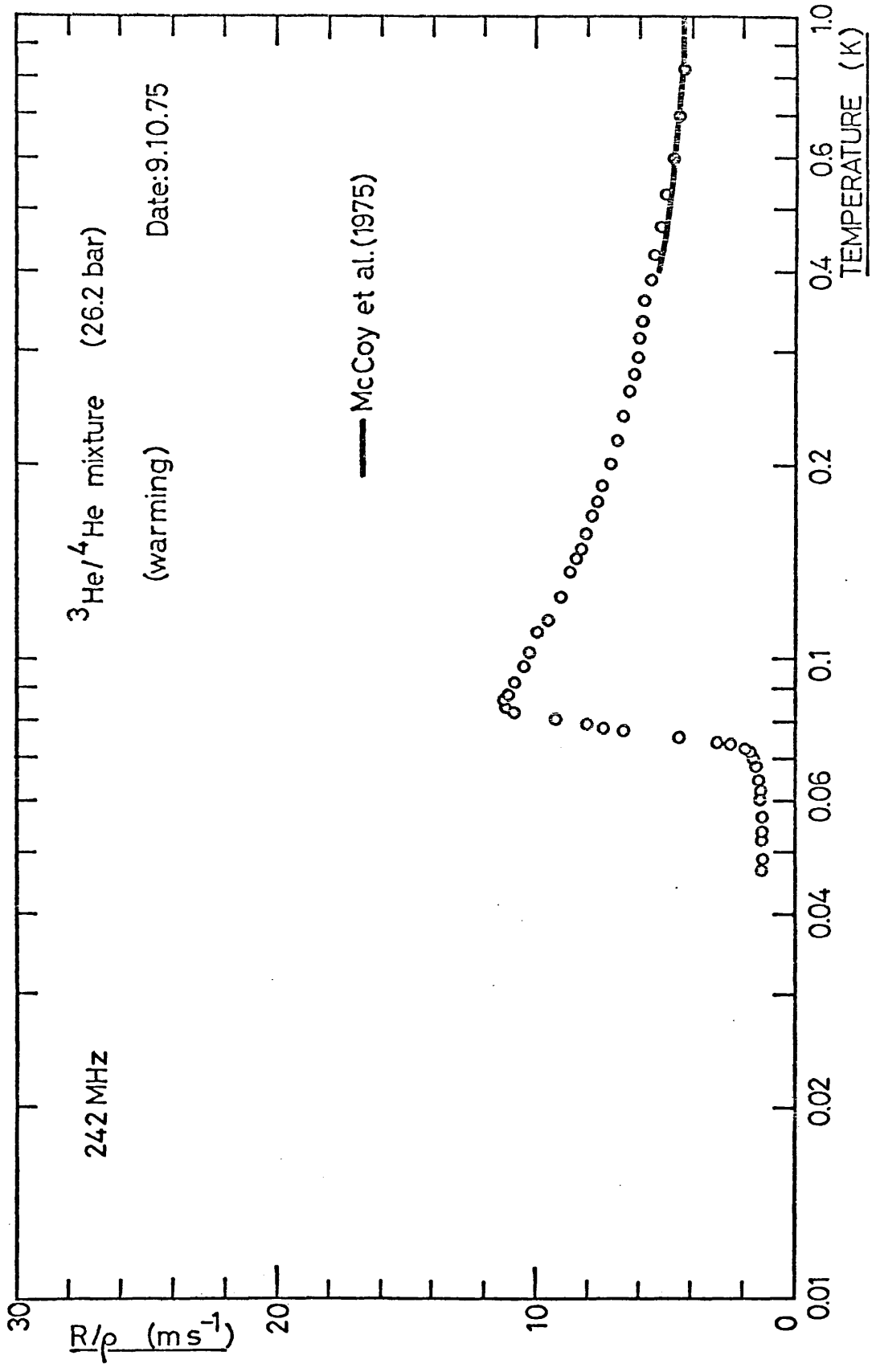

Fig.7.16 Acoustic resistance for $^3He/^4He$ mixture.

7.4. 1048 MHz transverse waves; liquid helium-3 (s.v.p.)

Some measurements of the acoustic resistance of liquid helium-3, under its saturated vapour pressure, were made at 1048 MHz, using the Mark 3 sonic cell described in section 4.2. Ultrasonic attenuation in the piezoelectric material is proportional to the square of the frequency of the wave so the number of echos observed at this frequency was considerably less than the number at 242 MHz. The shape of the echo envelope was also degraded as may be observed in the photograph of the echo train, figure 7.17. To obtain a signal to noise ratio comparable with that of the lower frequency work, a group of four echos centred at echo number 332 was chosen. The relative position of the group is indicated by the bright spot near the middle of the trace in the photograph. This spot actually marks the position of the gate of the Brookdeal "Boxcar" integrator which was used to average the heights of the chosen echos, the output being fed to a chart recorder in the same way as in the low-frequency work. The result of the comparatively small number of reflections was that the energy lost into the liquid was greatly reduced, the total loss of signal in the temperature range 1.0 K to about 50 mK being less than 2.0 dB compared with a loss of as much as 10 dB in the corresponding range in the 242 MHz work. This loss of sensitivity made detailed quantitative analysis of little value in the high frequency case, although the best data did permit an estimate of the change in acoustic resistance to be made. Several runs were performed, both cooling and warming the sample, but useful data were obtained on four runs only (all warming-up runs) the others having to be discarded due to excessive noise on the integrator output. The data obtained in these four runs are shown in figure 7.18., expressed in terms of energy loss into the liquid per reflection (ΔS) as a function of temperature. The zero is arbitrary and the four

sets of data have been fitted together, at constant temperature, to produce the best composite plot. (The error bars are derived from the signal noise in the worst case.)

The temperature dependence of the energy loss at high frequency has the same general form as that at 242 MHz, the losses increasing at high temperatures due to attenuation in the piezoelectric material and increasing at low temperatures as a result of viscous damping in the liquid helium-3. Two of the runs, (b) and (d), show some evidence of a limiting value being approached at low temperatures although run (a) shows no such tendency in the same temperature region. However, this is little more than speculation in view of the uncertainty in the measurement of ΔS. The best data were obtained from run (b) so a quantitative analysis was carried out in this case only, by converting the ΔS measurements into acoustic resistance, $\Delta R/\rho$, by the methods already described. The correction for temperature dependent attenuation in the rod material was calculated, in the absence of experimental data at this frequency, from the experimental results taken at 242 MHz assuming a frequency dependence of ω^2 where ω is the angular frequency of the wave. The results of this analysis are shown in figure 7.19. The solid line in this diagram is a theoretical calculation of R/ρ using the familiar expression for the acoustic resistance of a viscous liquid :

$$\frac{R}{\rho} = \sqrt{\frac{\eta\omega}{2\rho}}$$

where the values of viscosity η calculated from the empirical expression given by Black, Hall and Thompson (1971), see equation (6.3.3.).

The high temperature correction for attenuation in the rod material appears to be rather inadequate above 0.3 Kelvin, so the data have been very tentatively fitted to the theoretical curve between 0.2 K and 0.3 K, where the correction is small. The low temperature data (below 100 mK) were replotted on a log.-log. scale and an estimate of the low-temperature limit, R_∞/ρ, was made by fitting these data to the theoretical curve of Flowers, Richardson and Williamson (1976) and extrapolating, as described in section 7.1. This yielded the result: $R_\infty/\rho = (29.7 \pm 2.7)\,\mathrm{m\,s^{-1}}$. The uncertainty quoted is that associated with the data measurement ($\pm 1.7\,\mathrm{m\,s^{-1}}$) plus an uncertainty of $\pm 1\,\mathrm{m\,s^{-1}}$ due to data-fitting to the theoretical curve at high temperatures. (Compared to these uncertainties, the error in extrapolation was negligible.)

It must be emphasised that the quality of the data was not sufficiently high to allow anything more than speculative conclusions to be drawn about the absolute values, R/ρ and the limiting value of acoustic resistance, R_∞/ρ. However, the change in acoustic resistance between 1.0 Kelvin and the low-temperature (limiting) value does seem, at $(19.1 \pm 1.7)\,\mathrm{m\,s^{-1}}$, to be consistent with the corresponding change measured at 242 MHz; see figure 7.1.

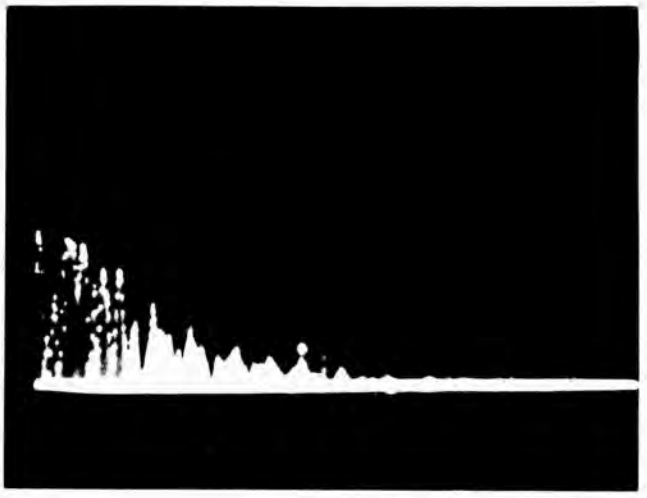

(1 ms cm^{-1} ≈ 100 echo cm^{-1})

Fig.7.17 Echo envelope for transverse waves (1048 MHz) at 0.1K in BGO

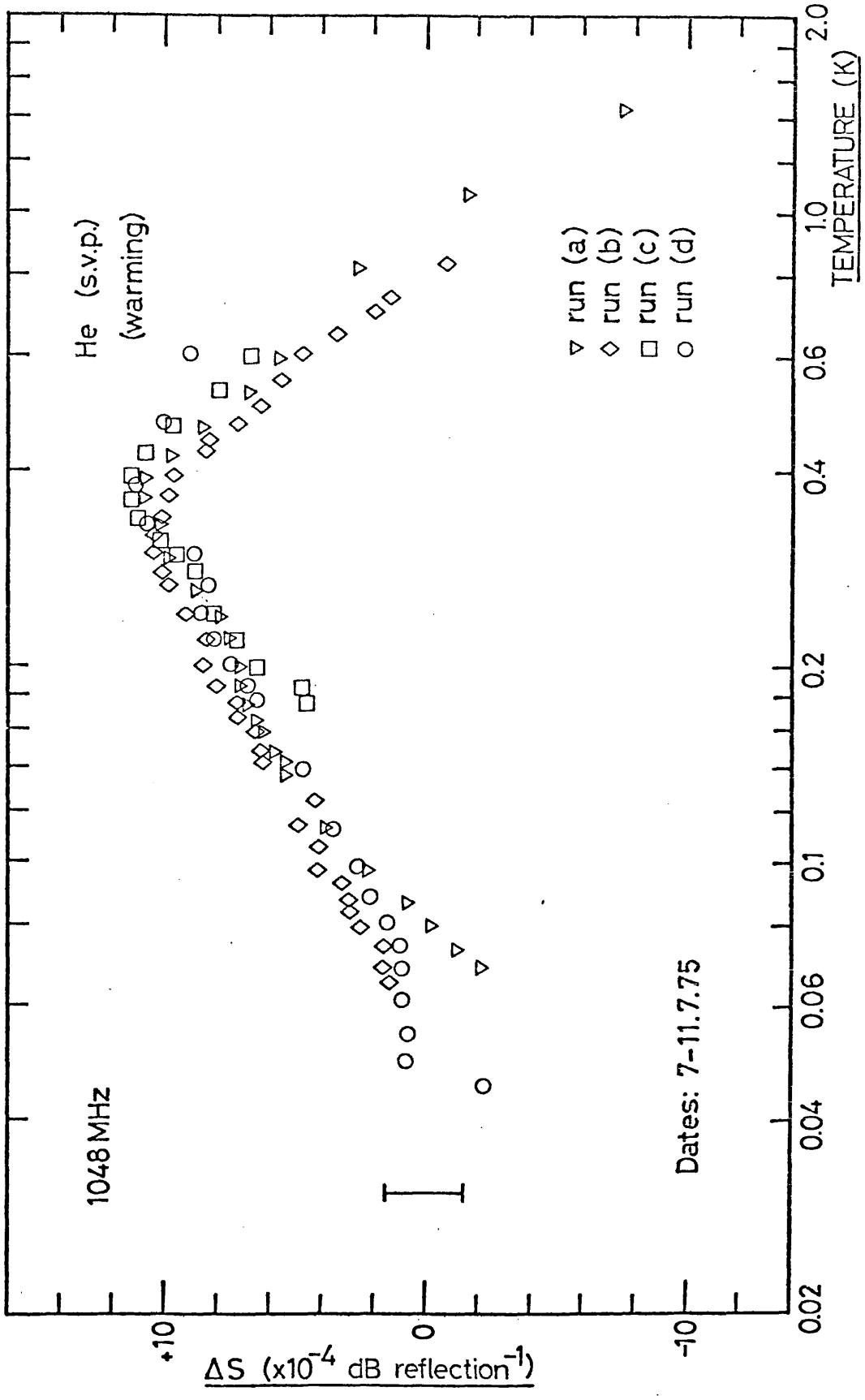

Fig.7.18 Change in signal height (ΔS) at 1048MHz

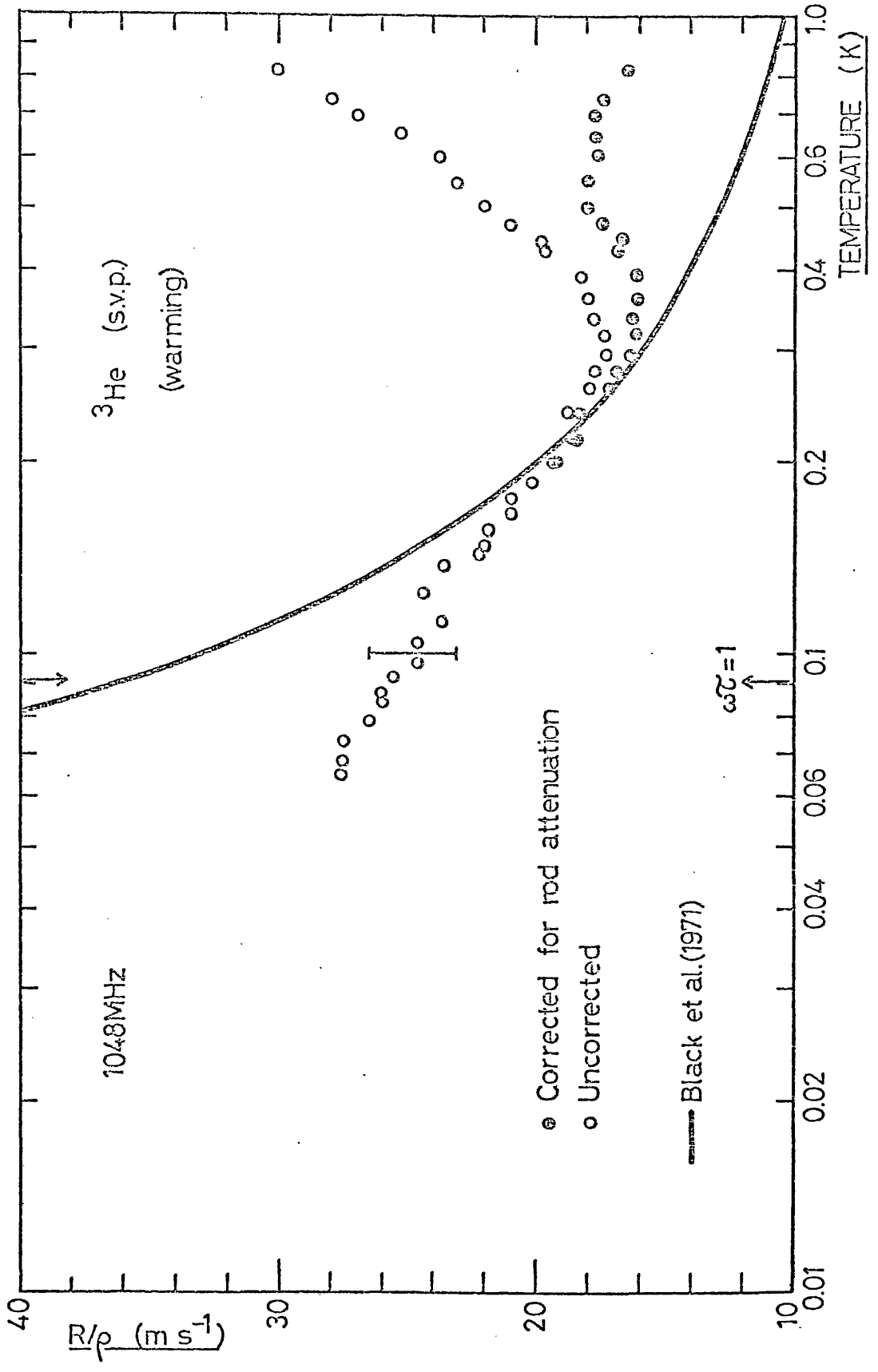

Fig. 7.19 Transverse acoustic resistance for ^{3}He (s.v.p.) (1048 MHz)

7.5. 250 MHz longitudinal waves; liquid helium-3 (s.v.p.)

To complement the transverse-wave work, an experiment was carried out to measure the longitudinal acoustic resistance of liquid helium-3 at the saturated vapour pressure which would help to explain the discrepancy between the measured values of Keen, Matthews and Wilks (1965) and the theoretical predictions of Brooker (1964 and 1967), see section 3.3. The experimental method was the same as that used in the transverse work except that a rod of X-cut quartz was used to generate the longitudinal waves. The high attenuation in this material resulted in an echo train even shorter than that of the preceding section, the echo group studied being centred at echo number 165, and the energy loss into the liquid over the temperature range 0.5 K to about 20 mK was therefore less than 0.3 dB. The measurement of such a small change in an already low-level signal (ie. of the order of -80 dBm) would have proved impossible without the sophisticated data-processing system that became available towards the end of this work. This system, incorporating the "Datalab" DL 4000 digital store was basically that described in section 4.4. except that, rather than the data being outputin an analogue fashion to a chart recorder, they were stored in digital form on magnetic tape cartridges by means of a "Perex" Perifile recorder. Each datum point stored consisted of the signal heights of the first 160 echos (the echo envelope), followed by a detailed scan of the next ten echos as described in section 4.4.3. (about ninety channels were available for each of these echos). The digital information stored was processed, using a computer, as described below.

The mean echo height was obtained by taking the average of the heights of ten echos (numbers 160 to 169, inclusive), each of which was itself the

average of twenty-one channels of the transient recorder (that is, the channel corresponding to the peak of the echo, plus the ten channels to either side). The mean echo height was then converted to decibel units and scaled to account for any variations in the amplitude of the r.f. input pulse. This scaling was performed by comparing the mean echo height with the heights of the first few echos, for which the losses into the liquid are very small and may be considered temperature independent. Normalising the data to the mean echo height at the lowest temperature reached yielded the change in signal (in dB) which, when divided by the number of reflections suffered by the mean echo number of the group (ie. 329), gave ΔS in decibel per reflection as a function of temperature. The acoustic resistance was calculated from equation 6.2.6. using the values for ρ_s and v_s appropriate to X-cut quartz, obtained from Neppiras (1973). A single experimental run only was performed in which the sample was warmed from about 19 mK (using R3 (1972) calibration) to 0.6 Kelvin, and the results are plotted as a graph of acoustic resistance (R/ρ) against temperature; figure 7.20. It should be noted that the high temperature data have not been corrected for losses in the piezoelectric rod, unlike the previous cases, and that the measured acoustic resistance is referred to an arbitrary zero. The values of R/ρ indicated on the vertical axis refer to the solid line (see below) to which our experimental data have been fitted.

In spite of the various averaging processes involved in the analysis, there is considerable scatter associated with the data points which gives rise to an uncertainty of about $\pm 2\,\mathrm{m\,s^{-1}}$ in the acoustic resistance. However, a small increase in R/ρ may be observed as the temperature decreases and this change is estimated to be about $(5.5 \pm 2.0)\,\mathrm{m\,s^{-1}}$. For comparison,

the solid line in the diagram is the theoretical change in longitudinal acoustic resistance for liquid helium-3 at the saturated vapour pressure, calculated by Brooker (1964 and 1967) for $F_2^S = 0$, to which our data have been fitted at $\omega\tau = 1$. The predicted change in R/ρ (that is, $\Delta(Z/\rho)$ in Brooker's notation) is 6.0 m s^{-1} if F_2^S is set to zero, the limiting value at low temperature being 189.4 m s^{-1}. This prediction is calculated using a value of F_1^S of 5.64 (taken from Anderson, Reese and Wheatley (1963)), which is slightly lower than the value given by Wheatley (1975) of $F_1^S = 6.04$ at zero pressure. However, Brooker asserts that any uncertainty in F_1 will not affect the shape of the curve, or the magnitude of the change in acoustic resistance, but only the value of the zero-sound limit, R_∞/ρ. (If the more recent value for F_1 is used, the zero-sound limit is reduced by about 0.1 m s^{-1}.)

Brooker (1967) has also calculated the effect of non-zero values of the Landau parameter F_2^S on the acoustic resistance and we find that a value of $F_2^S = -0.5$ reduces the predicted change in R/ρ to 5.5 m s^{-1}, the value observed in this experiment. If the uncertainty in R/ρ is expressed as an uncertainty in F_2^S, we may tentatively suggest that our observed change in longitudinal acoustic resistance implies the value $F_2 = -0.5 \pm 2.0$.

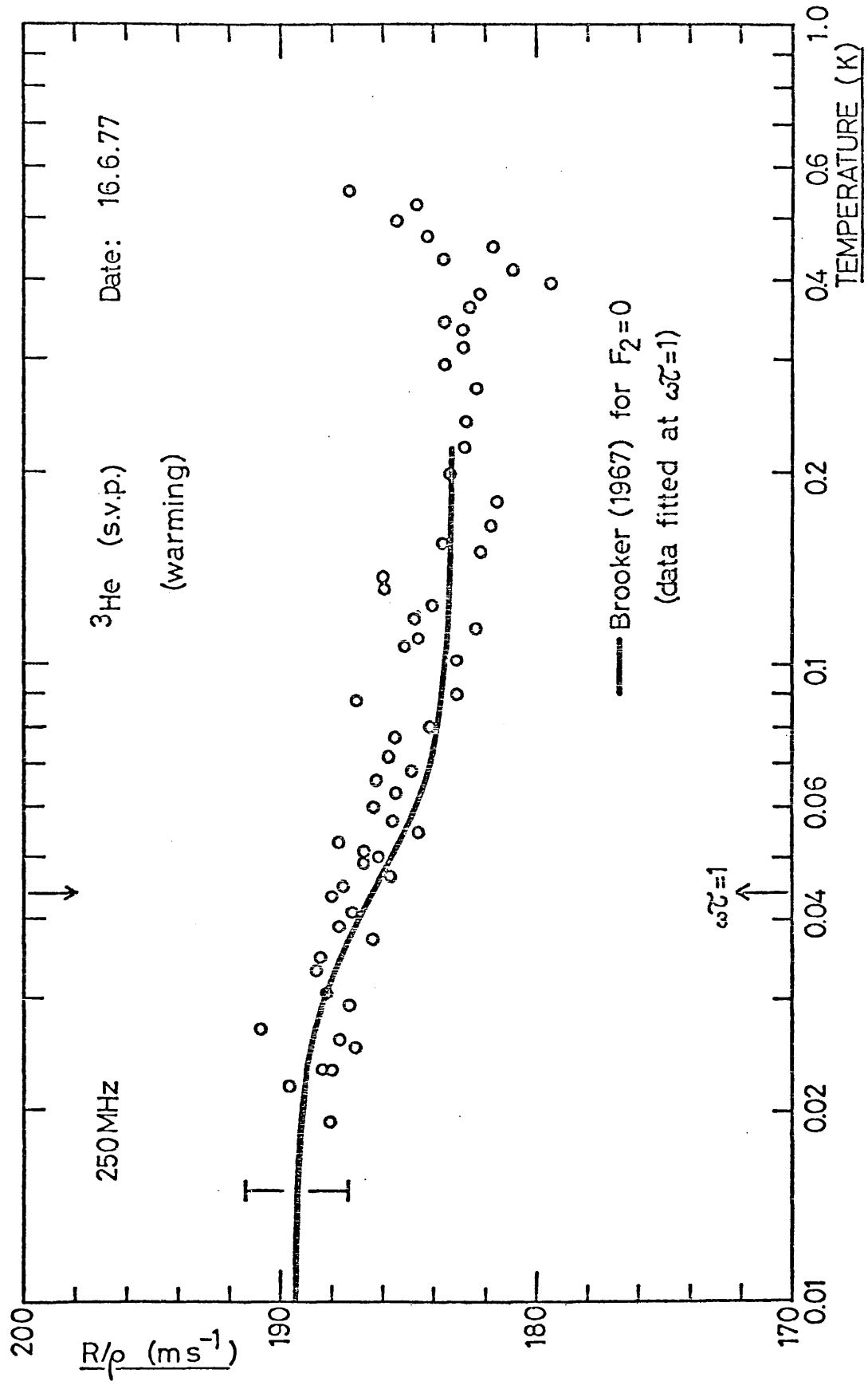

Fig. 7.20 Longitudinal acoustic resistance of ^{3}He (s.v.p.)

CHAPTER EIGHT

8.0. DISCUSSION AND CONCLUSIONS

8.1. Zero sound and transverse acoustic impedance

The transverse acoustic impedance of a normal Fermi liquid has been calculated as a function of temperature by both Fomin (1968) and Flowers et al (1976) with the Landau parameter $F_2^S=0$, and by Flowers and Richardson (1978) in the case of $F_2^S \neq 0$ and their methods have been outlined in chapter 3. The important conclusion that may be drawn from these calculations is that the complex acoustic impedance contains contributions of comparable magnitude from both single particle excitations and transverse zero sound (collective) modes. Since both contributions become independent of temperature in the collisionless limit, a qualitative study of the temperature dependence of the transverse acoustic impedance cannot alone provide evidence of the existence of transverse zero sound. The contributions have been separated, however, in the theory of Flowers and Richardson (1978) for the case $F_2^S \neq 0$, which, in the zero sound limit $(\omega\tau \to \infty)$, reduce to equations (3.5.5.) and (3.5.6.) (Section 3.5.) for the total acoustic impedance and equation (3.6.2.) (Section 3.6.) for the contribution to the impedance resulting from zero sound alone. These equations have been solved numerically, by AJ Cooper, for $F_2^S = -1, 0, +1$ over the range of F_1^S values corresponding to pressures from 0 bar to 30 bar. The computation employed solutions to the dispersion relation obtained by applying Newton's method to the approximate solutions shown earlier in figure 2.3. Figure 8.1. shows the results of these calculations. The solid lines represent the total acoustic resistance R_∞ / ρ, in the collisionless limit, as a function

of pressure for the F_2^S values indicated and the broken lines represent the corresponding zero sound contributions, R_∞^c/ρ. The data points (o) and (●) represent the measured values of acoustic resistance in the collisionless limit obtained from our helium-3 data (cooling and warming, respectively,) see table II. (The measured values of R_∞/ρ differed slightly when the calibration R3 (1977) was used; therefore a similar graph, figure 8.2., shows the values obtained using the later calibration, taken from table III.)

Both of the graphs show that, with the exception of one point at 0.3 bar, which will be discussed later, all our data points fall within the limits $-1 < F_2^S < +1$, implying that F_2^S is small at all pressures. In view of the experimental error associated with each point, any further conclusions about F_2^S must be somewhat speculative, but it seems likely that, from figure 8.1., F_2^S is approximately zero at low pressure, falling to about -1.0 ± 0.5 at pressures greater than about 12.0 bar. The second graph, figure 8.2., in which the values of R_∞/ρ were obtained using the unconfirmed 1977 temperature calibration, shows that F_2^S may be slightly positive at low pressures ($F_2^S \approx 0.5$) decreasing to about -0.5 ± 0.5 at about 27.0 bar. From the theoretical curves, we see that provided $F_2^S \geqslant -1$, the acoustic resistance at pressures greater than about 15.0 bar is dominated by the zero sound contribution, so we may be confident that transverse zero sound has been observed at these pressures. The existence of this mode at low pressure is much less certain and a discussion of the evidence will be found in the next section.

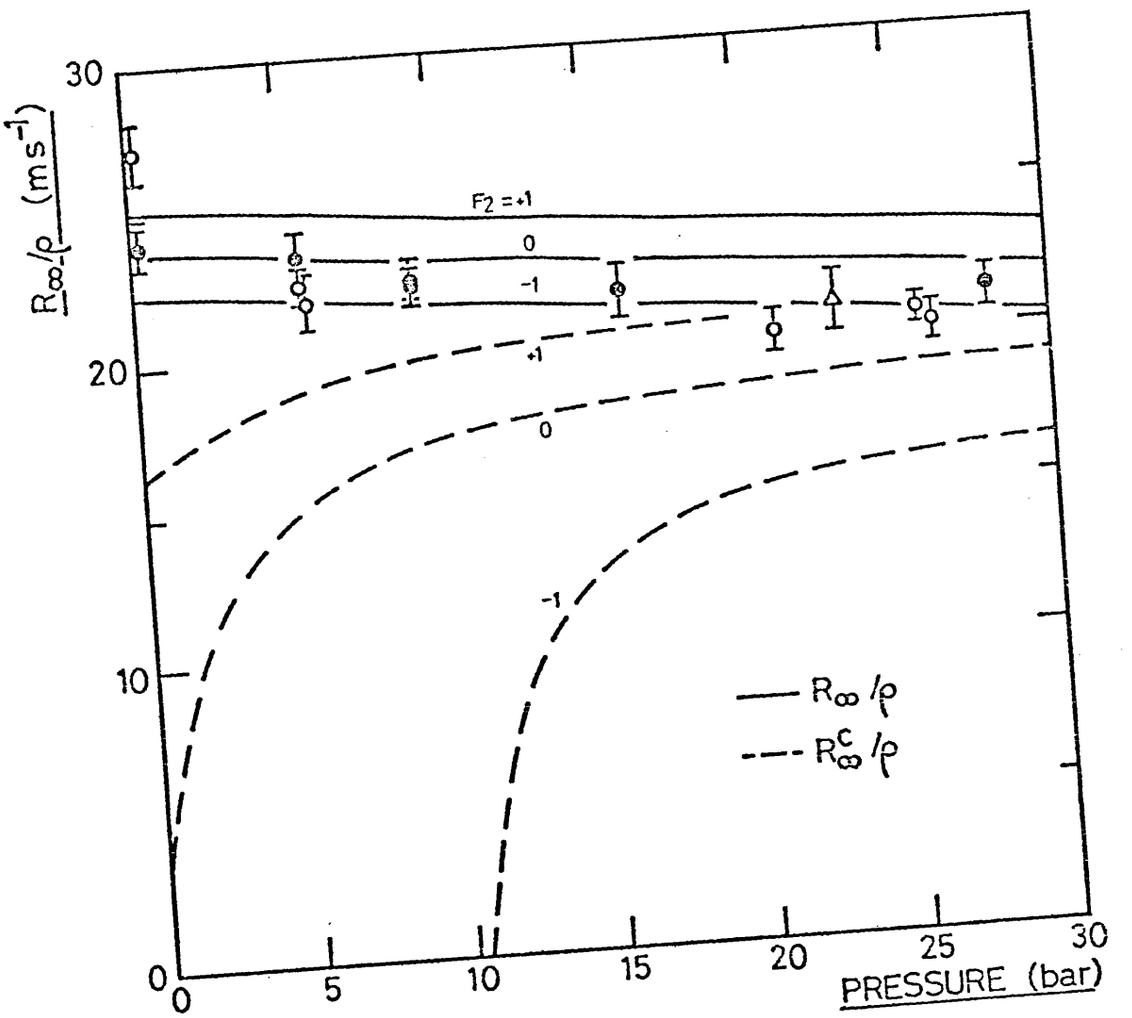

Fig. 8.1 R_∞/ρ against pressure — R3(1972)

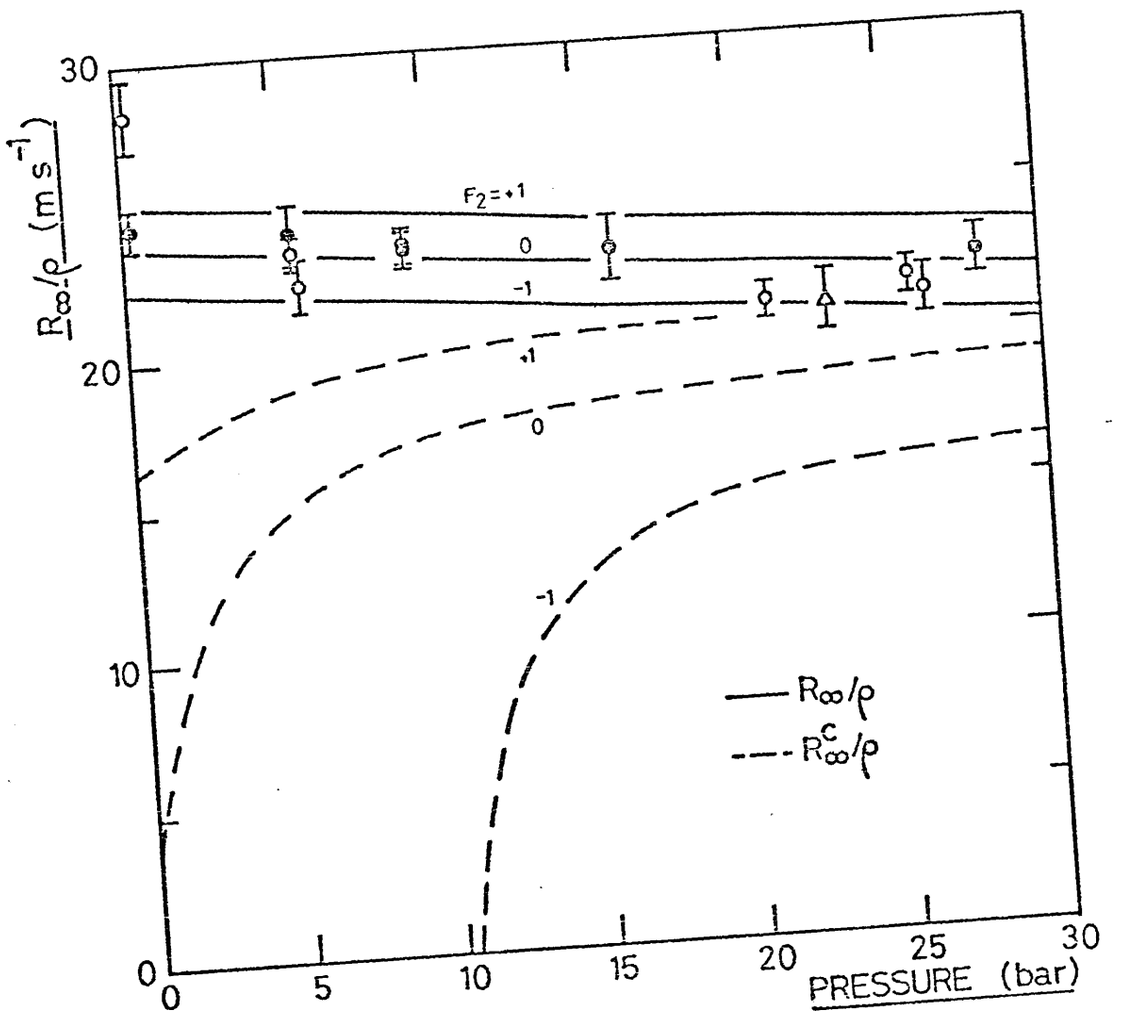

Fig. 8.2 R_∞/ρ against pressure — R3(1977)

8.2. F_2^S at low pressure

The dispersion relation for transverse zero sound in the limit $\omega\tau \to \infty$, as derived by Brooker (1964 and 1967) is :

$$(1-s^2)\left\{\frac{s}{2}\ln\left(\frac{s+1}{s-1}\right)-1\right\}+\frac{1}{3} = \frac{2}{F_1+\left(\frac{3F_2 s}{1+F_2/5}\right)}$$

(provided that $F_l = 0$ for $l > 2$), where s is the ratio of the transverse wave velocity (c_t) to the Fermi velocity, v_F. Now, for transverse zero sound to be an identifiable mode, distinguishable from the single particle excitations also produced by a transversely oscillating boundary, the velocity of the wave must exceed that of the single particles which, being close to the Fermi surface, will be approximately equal to v_F. Therefore, taking $s = 1$ as the limit of existence of the wave, the first term of the dispersion relation vanishes to leave the condition for the existence of transverse zero sound:

$$F_1 + \frac{3F_2}{1+F_2/5} > 6 \qquad (2.6.4.)$$

By equating the two sides of this expression a relationship between F_1 and F_2 is obtained which determines the limiting values of these parameters when transverse zero sound first appears. Thus :

$$F_2 = \frac{-(1-F_1/6)}{1/5 - 1/6(F_1/5+3)}$$

which may be solved to give F_2 as a function of F_1. If F_2 is set to zero, $F_1 = 6$ which is the condition for the existence of transverse zero sound obtained by Abrikosov and Khalatnikov (1959) for infinite $\omega\tau$, and by Lea et al (1973) for all values of $\omega\tau$. We note that F_2 falls as F_1 is increased and that for $F_1 < 6$, F_2 is positive. In the case of liquid helium-3, the values of F_1 given by Wheatley (1975) indicate that F_2 will be negative at all pressures since $F_1 = 6.04$ at zero pressure. However, if F_1 is reduced by about five per cent, as suggested by Wölfle (1976), F_2 is slightly positive at low pressures becoming negative for pressures in excess of about 0.7 bar. Therefore taking Wheatley's value of F_1 at zero pressure with a five per cent uncertainty, we find that F_2 may be expected to fall within the range -0.11 to +0.09, providedthat $S = 1$; that is, $F_2^S \approx 0 \pm 0.1$ at zero bar.

In our calculations of the transverse acoustic impedance, the F_1 values quoted by Wheatley (1975) were used and the transverse zero sound condition (equation (2.6.4.)) was incorporated by setting the zero sound contribution to zero when the condition was not fulfilled. (Under these circumstances, S was set to 1.) Consequently, in figures 8.1. and 8.2. the zero sound contribution to the acoustic impedance (R_∞^c/ρ) is seen to increase from zero at zero pressure (ie. $F_1^S \approx 6.0$) for $F_2^S = 0$, and from zero at some finite pressure for $F_2^S < 0$. We further see that, if F_2^S is positive, a contribution to transverse zero sound will exist, even at the lowest pressures. Unfortunately, it is not possible to differentiate between wave and single particle contributions by means of transverse acoustic impedance experiments so the existence of transverse zero sound remains unclear at low pressures. However, we may draw some conclusions about the parameter F_2^S from the total acoustic resistance (R_∞/ρ) which is represented by the solid lines in figure 8.1. for the F_2^S values -1, 0 +1.

Limiting values of (R_∞/ρ) at the saturated vapour pressure (approx, 0.3 bar) were determined from two sets of data, the lower value being obtained from data collected by warming the sample at this pressure, figure 7.1.(a), and the higher value from measurements taken whilst cooling at the same pressure, figure 7.2. (Both sets of data were the combined results of two separate runs.) It is clear that the limiting values obtained from these data are not in agreement. A possible reason for the discrepancy could have been poor thermal contact between the liquid helium-3 and the resistance thermometer which would result in an apparently more rapid change in acoustic resistance during cooling than during the warming-up run. Extrapolation to the low-temperature limit would therefore yield an erroneously high value of R_∞/ρ, particularly in view of the high temperature from which the extrapolation was made (approx. 30 mK). However, similar comparisons between cooling and warming at higher pressures (for example 5.5 and9.2 bar) do not show this degree of inconsistency.

When the two values of R_∞/ρ at 0.3 bar are compared with the theoretical estimate of acoustic resistance, figures 8.1. and 8.2., we see that the higher value implies that F_2 is of the order of 3 or 4. Such a value would require the presence of a large zero sound contribution and a wave velocity that exceeds v_F by a factor of about 1.25 (that is; $s \approx 1.25$). Now, our data indicate, with a fair degree of consistency, that at higher pressures F_2 if probably in the range -0.5 to -1.0 which implies, by a numerical solution to the dispersion relation, that $s \approx 1.1$ (see graphical solutions to dispersion relation, figure 2.3.). Consequently, if we are to accept both the low pressure value $F_2 \approx 4$, and the high pressure value $F_2 \approx -0.5$, we are then forced to accept that the velocity of transverse zero sound decreases with increasing pressure, in direct contradiction to the theory.

Alternatively, if we take the transverse zero sound wave velocity to be constant (at, say, $1.1\,v_F$), this puts an upper bound on the value of F_2 at low pressure which is found to be about +1.5 at 0 bar. We therefore conclude that the probable value of F_2^S at low pressure is in the range 0 to +1.0. If the higher measurement is ignored we may take the average of the values indicated by the two graphs (figures 8.1. and 8.2.) to obtain a probable value of F_2^S at the saturated vapour pressure; ie. $F_2^S \approx 0.4 \pm 0.5$. This is now consistent with a zero sound wave velocity roughly equal to the Fermi velocity, at low pressure, suggesting that the transverse zero sound contribution is very small (and difficult to identify) at these pressures.

This estimate of F_2^S may be compared with that obtained from the longitudinal zero sound experiments performed by Abel, Anderson and Wheatley (1971) at 0.32 bar. Although their own analysis ignores the effects of F_2, Brooker (1964 and 1967) has estimated its magnitude from their measurements of wave velocity, peak attenuation and relaxation time and finds that $F_2^S = 0 \pm 4, 0$ and +0.6 respectively (no uncertainties being given in the last two cases). We note that our estimate of F_2^S at 0.3 bar is in good agreement with these values. However, if our transverse acoustic impedance results at low pressure are compared with the longitudinal impedance data of Keen, Matthews and Wilks (1965), as discussed by Brooker (1964 and 1967), we find no area of agreement, and the suggestion that $F_2^S \approx 14.8$ at 0 bar is still unexplained. Furthermore, our unfinished attempt to repeat their longitudinal measurements failed to reproduce their results but rather tended to confirm our own suggestion by revealing a change in acoustic resistance corresponding to $F_2^S \approx -0.5 \pm 2.0$. (The large uncertainty associated with this value reflects the somewhat speculative nature of the data.)

An expression relating F_2^S to the thermal conductivity and shear viscosity of liquid helium-3 has been produced by Nettleton (1976). By fitting this expression to the thermal conductivity data obtained by Anderson, Salinger and Wheatley (1961) and by Abel, Johnson, Wheatley and Zimmerman (1967), Nettleton estimates F_2^S to have the values -0.338 and-0.563 respectively. No uncertainties are quoted and the author concludes only that F_2^S is less than zero. We note here that these results provide further evidence, obtained independently, that F_2^S is approximately zero at low pressures.

8.3. F_2^S at high pressure

A direct comparison may be made between this work, at high pressures, and that of Roach and Ketterson (1976), who reported the first observation of transverse zero sound in March 1976. Both real (R/ρ) and imaginary (X/ρ) components of the complex acoustic impedance were measured as functions of temperature, at pressures between 2.0 and 28.9 bar and at frequencies ranging from 12.0 to 108.0 MHz. The measurements were made by observing the ringing of an AC - cut quartz disc transducer, immersed in liquid helium-3, when the excitation energy was removed. Their published data show, at 23.0 bar, an increase in R/ρ of about 19.0 m s^{-1}, the low temperature limiting value (R_∞/ρ) being (21.0 $\pm$ 1.0) m s^{-1}. (This is indicated in figures 8.1. and 8.2., thus : Δ). The temperature dependence of the acoustic resistance was similar to that observed in our experiments. Roach and Ketterson also noticed a peak in X/ρ corresponding to the increase in R/ρ and these two features, taken together, were considered by the authors to be proof of the existence of transverse zero sound. Their experiment independently measured the attenuation in

propagation of the wave by means of a transmission technique in which two transducers were separated by a distance of only twenty-five micrometre. The measured attenuation coefficients were compared with theoretical estimates obtained from the dispersion relation (equation 2.6.1.) for various values of F_2^S and the best agreement was reached with $F_2^S = +1.5$ at 2.0 bar, falling to -1.0 at 28.9 bar.

Their conclusions were criticised by Flowers, Richardson and Williamson (1976) on the grounds that only a quantitative analysis of acoustic impedance data, in which the contribution from single particle excitations is also considered, could be taken as proof of the existence of transverse zero sound. They performed such an analysis on the data and found that, whilst the measured temperature dependence of R/ρ could be fitted to the theory, the temperature dependence of the imaginary part, X/ρ could not be so fitted. Furthermore, the value of F_2^S at 23.0 bar indicated by the limiting value of the acoustic resistance ($F_2^S = -1.0 \pm 0.5$) was not consistent with that indicated by the attenuation data at this pressure. Comparing these results with our own we find that the value $F_2^S = -1.0 \pm 0.5$ at 23.0 bar, obtained from the real part of the acoustic impedance is in good agreement with our value at this pressure (that is, $F_2^S \approx -1.0 \pm 0.5$ using the R3(1972) calibration and $F_2^S \approx -0.5 \pm 0.5$ using R3 (1977)). see p169 We also observe that the total change in F_2^S is rather less than that suggested by the attenuation data of Roach and Ketterson (1976). That F_2^S might be expected to fall with increasing pressure is contrary to the pressure dependence predicted by Ostgaard (1969), and also to the known behaviour of the symmetric Landau parameters F_0^S and F_1^S, but follows from the condition for the existence of transverse zero sound (equation 2.6.4.) where the wave velocity is put

equal to the Fermi velocity; ie. $S = 1$. By differentiating the dispersion relation (in the limit $\omega\tau \to \infty$), Nettleton (1977) shows that, for constant wave velocity $(S \geq 1)$, F_2^S always decreases with increasing F_1^S. Therefore, provided that the ratio of transverse wave velocity to the Fermi velocity (S) is only weakly dependent upon pressure, F_2^S always falls as the pressure is increased.

Recent work on the superfluid phases of liquid helium-3 has included a number of longitudinal zero sound experiments at high pressures. Wölfle (1976) has considered some of these and has produced further estimates of F_2^S which do not seem consistent with the negative values mentioned above. For example, measurements of the velocity of longitudinal zero sound in normal liquid helium-3 near the superfluid transition have been made by Paulson, Johnson and Wheatley (1973) at 32.2 bar, and by Ketterson et al (1975) at 29.3 bar. Wölfle has calculated values of F_2^S from these results and finds that in the first case, $F_2^S = 0.5 \pm 0.3$ and, in the second, $F_2^S = 1.0 \pm 0.5$. Similar calculations using data collected in the superfluid "B" phase by Paulson et al (1973) at 19.6 bar and by Roach et al (1975) at 21.0 bar, show that, in both cases, $F_2^S \approx 0.4$. Wölfle has also pointed out that the values of m^* quoted by Wheatley (1975) may be overestimated at high pressures so the above values of F_2^S were obtained using m^* values about four per cent lower than those used in our calculations. However, using Wölfle's value at 21.0 bar $(m^*/m = 4.9)$ reduces our estimate of F_2^S at this pressure to about -1.2 which increases the discrepancy between our results and these positive F_2^S values.

8.4. Estimates of F_2^S using "Sum Rule"

The Pauli Exclusion Principle requires that the forward scattering amplitude for two Fermions of the same spin must vanish. The scattering amplitude may be expressed in terms of the Landau parameters, as discussed by Baym and Pethick (1976), which are therefore constrained by the "forward scattering sum rule" :

$$\sum (A_l^S + A_l^A) = 0 \qquad \text{where} \qquad A_l^i = F_l^i \left(1 + \frac{F_l^i}{2l+1}\right)^{-1}$$

The Landau parameters F_0^S, F_1^S and F_0^A are all quite well known and have been tabulated, as functions of pressure, by Wheatley (1975). (Note that Wheatley denotes the first assymmetric parameter by Z_o where $Z_o = 4F_0^A$.)

The parameter F_1^A is difficult to determine experimentally. Dy and Pethick (1969) have estimated values at zero pressure by comparing their exact calculation of the scattering amplitude with the thermal capacity data of Abel et al (1967) and the spin diffusion data of Anderson et al (1961) and then adjusting F_1^A to provide the best agreement. They obtain the results $F_1^A = -0.46 \pm 0.14$ and $F_1^A = -0.39 \pm 0.14$ from these data, where the errors quoted include only the contributions resulting from curve fitting. Their method is slightly unsatisfactory in this particular application because they set the Landau parameters F_l^i to zero for $l \geq 2$; but if this point is ignored and their F_1^A values are put back into the sum we obtain values for F_2^S of -0.30 ± 0.15 and -0.38 ± 0.15 respectively. (Being close to zero, these results retrospectively justify the omission of $F2^S$ in the calculation of F_1^A.)

Taking the average of these values we obtain $F_2^S = -0.34 \pm 0.15$ which is in reasonable agreement with our result and with the other estimates at low pressure.

The spin-echo experiments of Corruccini et al (1972) allow F_1^A to be determined directly by using an expression for the gyromagnetic ratio, obtained by Leggett and Rice (1968), in which F_0^A is the only other Landau parameter involved. The method therefore avoids any arbitrary assumptions about the other Landau parameters. The values obtained in their experiments were : $F_1^A = -0.15 \pm 0.3$ at 0 bar and $F_1^A = +0.2 \pm 0.6$ at 27.0 bar. When these results are used, the forward scattering sum rule yields F_2^S values of -0.6 ± 0.3 and -0.9 ± 0.3 at 0 and 27 bar respectively. The low pressure result is rather more negative than the other estimates (although not unrealistically so) but the value at high pressure agrees well with our estimate of $F_2^S \approx -1.0$ at 27.0 bar.

The various estimates of F_2^S obtained from the forward scattering sum rule are, then, broadly consistent with our estimates from experimental data and indicate that F_2^S is probably negative, decreasing from a little less than zero at zero pressure to about -1.0 as the melting pressure is approached. Estimates from the sum rule are slightly suspect in that it is necessary to set all the higher Landau parameters to zero (in our case, $F_l^S = 0$ for $l \geq 3$ and $F_l^A = 0$ for $l \geq 2$). However, the magnitudes of the Landau parameters are thought to decrease as l increases, therefore since F_1^A and F_2^S are small, it seems likely that the contributions to the sum from higher parameters may be ignored without casting serious doubts on the estimates obtained.

8.5. Concluding remarks

The principal objective at the start of this work was to make the first experimental observations of transverse zero sound in liquid helium-3 by studying the temperature dependence of the acoustic resistance. As mentioned in section 7.3., the first reported observation of this mode was made, in March 1976, at the Argonne National Laboratory, Illinois, by PR Roach and JB Ketterson, who identified changes in both the real and imaginary parts of the acoustic impedance with the propagation of transverse zero sound. Their measurements of the attenuation of this mode cover range of pressures from 2.0 to 28.9 bar, but the published data on the acoustic impedance are limited to a single value of pressure ; 23.0 bar. Since the theoretical predictions about transverse zero sound indicated a considerable dependence upon pressure, it was felt that our work, although concerned only with the real component of the impedance, could yield valuable information both to confirm the result of Roach and Ketterson and to provide new data at low pressures. It was satisfying to obtain good agreement at 23.0 bar with these authors but the low-pressure data were not sufficient to clarify the situation near the saturated vapour pressure. Furthermore, the uncertainty in the value of effective mass, mentioned in section 8.3., somewhat clouds the issue and it seems doubtful whether any firm conclusions about the low pressure behaviour of transverse zero sound will be possible until this value has been firmly established. At present we must restrict our conclusions concerning the existence of the transverse mode to pressures greater than about 12.0 bar where the acoustic resistance observed is too large to be accounted for without a considerable contribution due to transverse zero sound.

The estimation of the Landau parameter F_2^S from the acoustic resistance data has already been discussed in some detail and it seems clear that the inclusion of this parameter is necessary for quantitative evaluation of the data. However, this raises the question of the importance of successive parameters in the series. Fomin (1976) has suggested that, if the series cannot be limited to the first two harmonics (ie. F_0^S and F_1^S), then several more terms must be considered since the inclusion of F_2^S only does not necessarily lead to a more precise result. At present, no experiments have been proposed by which additional symmetrical Landau parameters may be measured and, in view of the already uncertain values of F_1^A and F_2^S, the calculation of further parameters from the sum rule would be a fruitless exercise.

It would seem to be more profitable to concentrate work, in the immediate future, on the precise evaluation of F_2^S since this may resolve some of the conflicts that still remain between experiment and theory, and between the various experiments themselves. Perhaps the most outstanding of these inconsistencies is the very high value of F_2^S implied by the longitudinal acoustic impedance measurements of Keen et al (1965). It was hoped that some firm evidence would be obtained from this work but technical problems with the refrigerator prevented all but a single preliminary run using a rather poor piezo electric crystal. However, as shown in section 7.5., in this run we did not observe a change in the longitudinal acoustic impedance of anything like the magnitude of that observed previously. Another problem, also unexplained, is that longitudinal zero sound experiments generally indicate positive values of F_2^S whereas transverse wave experiments seem to imply a negative value for this parameter (see Dobbs (1977)). Again it may prove necessary to include Landau parameters of higher order to resolve this conflict.

Although Landau Theory has explained many aspects of the behaviour of interacting Fermi systems, there is still a great deal of work yet to be done before the theory can be used to fully explain the acoustic phenomena observed in liquid helium-3; the extension of these various experiments into the superfluid phases of the liquid will surely prove to be a fruitful field of study. The results of the work here presented, although not entirely clear due to the unsatisfactory thermometer calibration, have provided some evidence for the existence of transverse zero sound and, it is hoped, made a worthwhile contribution towards the greater understanding of the Fermi liquid.

April 1978

K. J. BUTCHER

Acknowledgements

It is a pleasure to record my thanks to the many people who have helped me in this work, particularly my supervisor, Professor ER Dobbs, for his help and encouragement, and to Dr MJ Lea for his constant attention to every aspect of this project, both experimental and theoretical.

For technical assistance I wish to thank Mr AK Betts for his help with the electronics, particularly the design and construction of the devices described in section 4.4., and Mr AOT Le Mottee for his assistance in operating and maintaining the dilution refrigerator. The sonic cells, and numerous other items, were the results of the experience, skill and patience of the Departmental Workshop Technicians, Mr FA Grimes and Mr AW King.

I am also indebted to my friends and fellow students, Alan J Cooper, for his calculation of the transverse acoustic impedance, and Patrick Retz for many useful discussions, and to the Departmental Secretary, Miss Franklin and her staffor their help in the preparation of this thesis. I would also thank the New Scientist for permission to reproduce the photograph that forms the frontispiece.

Finally, I gratefully acknowledge the financial support of the Science Research Council in the form of a Research Studentship.

References

Abel WR, Anderson AC and Wheatley JC	Phys.Rev.Lett.17, 129 (1971)
Abel WR, Johnson RT, Wheatley JC and Zimmerman W	Phys.Rev.Lett.18, 737 (1967)
Abraham BM, Chung D, Eckstein Y, Ketterson JB, Roach PR	J Low Temp.Phys. 6, 521 (1972)
Abraham BM, Eckstein Y, Ketterson JB, Kuchnir M, Vignos J	Phys.Rev. 181, 347 (1969)
Abrikosov AA and Khalatnikov IM	Rep.Prog. in Phys. 22, 343 (1959)
Anderson AC, Reese W, Sarwinski RJ Wheatley JC	Phys.Rev.Lett.7, 220 (1961)
Anderson AC, Reese W, Wheatley JC	Phys.Rev. 130, 495 (1963)
Anderson AC, Salinger GL, Wheatley JC	Phys.Rev.Lett.6, 443 (1961)
Andres K and Bucher E	J Low Temp.Phys. 16, 479 (1974)
Baym G and Pethick C	in "The Physics of Liquid and Solid Helium" eds: Bannermann KH and Ketterson JB (Wiley, New York(1976))
Bekarevich IL and Khalatnikov IM	Sov.Phys.(JETP), 27, 1010 (1968)
Berglund PM, Collan HK, Ehnholm GJ, Gylling RG, Lounasmaa OV	J Low Temp.Phys.4, 605 (1971)
Betts DS	"Refrigeration and Thermometry below One Kelvin" (Sussex Univ. Press, UK (1976))
Betts DS, Brewer DF, Hamilton RS	J Low Temp.Phys. 14, 331 (1974)
Betts DS, Edmonds DT, Keen BE, Matthews PW	J Sci.Instr. 41, 515 (1964)
Black MA, Hall HE, Thompson K	J Phys.C, 4, 129, (1971)
Black WC, Roach WR, Wheatley JC	Rev.Sci.Instr. 35, 587 (1964)
Boghosian C, Meyer H, Rives JE	Phys.Rev. 146, 110 (1966)
Bömmel H and Dransfeld K	Phys.Rev.Lett. 1, 234, (1958)
Borovikov AP and Peshkov VP	Sov.Phys.(JETP), 43, 156 (1976)
Brooker GA	D.Phil.Thesis, Univ.of Oxford (1964)

Brooker GA	Proc.Phys.Soc. 90, 397 (1967)
Corruccini LR, Clarke JS, Mermin ND, Wilkins JW	Phys.Rev. 180, 225 (1969)
Corruccini LR, Osheroff DD, Lee DM, Richardson RC	J Low Temp.Phys., 8, 229 (1972)
Dobbs ER	Proc.ULT Hakone Symposium (1977)
Dy KS and Pethick CJ	Phys.Rev. 185, 373 (1969)
Flowers EG and Richardson RW	Phys.Rev.B, 17, 1238 (1978)
Flowers EG, Richardson RW, Williamson SJ	Phys.Rev.Lett., 37, 309 (1976)
Fomin IA	Sov.Phys. (JETP), 27, 1010 (1968)
Fomin IA	JETP Letters, 24, 77 (1976)
Gates E	Proc.IEEE, 52, 1129 (1964)
Gavoret J	Phys.Rev.A, 137, 721 (1965)
Harley RT, Gustafson JC, Walker CT	Cryogenics, 10, 510 (1970)
Hudson RP, Marshak H, Soulen RJ, Utton DB	J Low Temp.Phys, 20, 1 (1975)
Keen BE, Matthews PW, Wilks J	Proc.Roy.Soc. A 284, 125 (1965)
Ketterson JB, Roach PR, Abraham BM, Roach PD	in "Quantum Statistics and the Many Body Problem" eds: Trickey SB, Kirk WP, Dufty JW (Plenum, New York (1975))
Kirby IJ and Wilks J	J.Phys.A, 4, 426 (1971)
Landau LD	Sov.Phys. (JETP), 3, 920 (1957)
Landau LD	Sov.Phys. (JETP), 5, 101 (1959)
Lawson DT, Gully WJ, Goldstein S, Richardson RC, Lee DM	J Low Temp.Phys. 15, 169 (1974)
Lea MJ, Birks AR, Lee PM, Dobbs ER	J Phys.C., 6, L226 (1973) (a)
Lea MJ, Tepley N, Dobbs ER	J Phys.E., 6, 268 (1973) (b)
Leggett AJ and Rice MJ	Phys.Rev.Lett., 20, 586 (1968)

Lounasmaa OV	"Experimental Principles and Methods below 1K"(Academic Press, London (1974))
McCoy RJ, Steinback M, Lyden JK, Guernsey RW	Proc. LT 14 (Helsinki) 1, 80, (1975)
McSkimin MJ	J.Acoust.Soc. ofAm., 28, 484 (1956)
Nava R and Rodriguez M	Phys.Rev.B., 4, 4512 (1971)
Neppiras EA	J.Phys.E., 6, 952 (1973)
Nettleton RE	J Low Temp.Phys., 24, 275 (1976)
Nettleton RE	J Low Temp.Phys., 26, 277 (1977)
Oda Y, Fujii G, Nagamo H	Cryogenics, 14, 323 (1974)
Ostgaard E	Phys.Rev., 187, 371 (1969)
Paulson DN, Johnson RT, Wheatley JC	Phys.Rev. Lett., 30, 829 (1973)
Redwood M	J.Acoust.Soc. of Am., 31, 442 (1959)
Rehwald W	J.App.Phys., 44, 3017 (1973)
Richardson RW	Private communication
Roach PR, Abraham BM, Kuchnir M, Ketterson JB	Phys.Rev.Lett., 34, 711 (1975)
Roach PR and Ketterson JB	Phys.Rev.Lett., 36, 736 (1976)
Robinson FNH	J.Sci.Instr., 36, 481, (1959)
Sherman RH	Proc.LT10 (Moscow), 1, 188 (1966)
Spencer EG, Lenzo PV, Ballman AA	Proc.IEEE, 55, 2074 (1967)
Tough JT, McCormick WD, Dash JG	Phys.Rev., 132, 2373 (1963)
Watson GE, Reppy JD, Richardson RC	Phys.Rev., 188, 384 (1970)
Wheatley J	Rev.Mod.Phys., 47, 415 (1975)
Wilks J	"The Properties of Liquid and Solid Helium" (Clarendon,Oxford (1967))
Wölfle P	Phys.Rev.B., 14, 89 (1976)
Zeller RC and Pohl RO	Phys.Rev.B., 4, 2029 (1971)

Abbreviations

Phys.Rev.Lett.	Physical Review Letters
J Low Temp.Phys.	Journal of Low Temperature Physics
Phys.Rev.	Physical Review
Rep.Prog. in Phys.	Reports on Progress in Physics
Sov.Phys.(JETP)	Soviet Physics (JETP)
J.Sci.Instr.	Journal of Scientific Instruments
J.Phys.	Journal of Physics
Rev.Sci.Instr.	Review of Scientific Instruments
Proc.Phys.Soc.	Proceedings of the Physical Society of London
Proc.IEEE	Proceedings of the Institute of Electrical and Electronics Engineers
Proc.Roy.Soc.	Proceedings of the Royal Society
J.Acoust.Soc. of Am.	Journal of the Acoustical Society of America
J.App.Phys.	Journal of Applied Physics
Proc. LT10	Proceedings of the Tenth International Conference on Low Temperature Physics (Moscow)
Proc. LT14	Proceedings of the Fourteenth International Conference on Low Temperature Physics (Helsinki)
Rev.Mod.Phys.	Review of Modern Physics

Communications on Physics 2 59–63 (1977)

The transverse acoustic impedance of normal liquid ^{3}He †

M. J. Lea, K. J. Butcher and E. R. Dobbs
Department of Physics, Bedford College, University of London,
Regent's Park, London NW1 4NS

Received 11 January 1977

The transverse acoustic impedance of liquid ^{3}He has been measured at 240 MHz at pressures from 0·3 to 28 bar in the temperature range 0·015 to 1·0 K. The measurements verify the existence of transverse zero sound in liquid ^{3}He at the higher pressures and enable the Landau parameter F_2^s to be determined.

The existence of a transverse zero sound mode in a Fermi liquid was originally postulated by Landau [1] and predicted in liquid ^{3}He by Brooker [2] and Fomin [3]. A necessary condition for the existence of the transverse zero sound mode is [2]:

$$F_1^s + 3F_2^s(1 + F_2^s/5)^{-1} > 6, \tag{1}$$

if $F_{l>2}^s = 0$, where F_l^s are the symmetric Landau parameters. Most of the experimental properties of normal liquid ^{3}He have been successfully explained by Landau's theory with finite values of only F_0^s, F_1^s and F_0^a, as discussed by Wheatley [4], who uses the alternative notation of $Z_l/4$ for F_l^a, the asymmetric Landau parameters. Recent measurements of the transverse acoustic properties of liquid ^{3}He by Roach and Ketterson [5] have indicated that finite values of F_2^s may be required to account for their data. If $F_2^s \neq 0$, then clearly the condition in *Equation* 1 must be satisfied for the transverse zero sound to exist, whereas with $F_2^s = 0$ it could exist at all pressures in liquid ^{3}He. We show here that F_2^s is much less than F_1^s and discuss the existence of the transverse zero sound mode over the pressure range 0 to 28 bar.

Experimentally transverse zero sound should be generated by a transversely oscillating surface immersed in normal liquid ^{3}He, provided $\omega\tau \gg 1$, where ω is the angular sound frequency and τ a quasi-particle relaxation time. We have measured the transverse acoustic impedance of liquid ^{3}He at 240 MHz at various pressures from 0·3 to 28 bar over the temperature range 1·0 K to 15 mK. At the lower temperatures we have obtained data in the collisionless limit. We generated a short pulse ($\approx 2\,\mu$s) of transverse ultrasound in a piezoelectric rod immersed in liquid ^{3}He, by placing one end of the rod in a resonant r.f. cavity, following the method originally used for measuring the longitudinal acoustic impedance, as described by Wilks [6]. The sound pulse propagates in the rod, producing a series of echoes. The Nth echo represents a sound pulse which has undergone $(2N-1)$ reflections at a solid/liquid interface. By measuring changes in the relative amplitudes of the first and Nth

† Work supported by the Science Research Council, with a grant and a studentship.

echoes, we have determined the fractional power loss per reflection, ΔS, from the sound pulse into the liquid ^{3}He. ΔS is directly related to the real part R (acoustic resistance) of the transverse acoustic impedance, $Z = R + iX$, of the helium :

$$\Delta S = 4R/R_s,$$

when $R \ll R_s$, where $R_s = \rho_s v_s$ is the rod's transverse acoustic impedance ; ρ_s is the density, and v_s is the velocity of sound, in the rod. The condition $R/R_s \ll 1$ is well satisfied for liquid ^{3}He, the maximum value of R/R_s being about $1{\cdot}2 \times 10^{-4}$, which corresponds to $\Delta S \approx 2 \times 10^{-3}$ dB. Consequently, many echoes are required to obtain a measurable change in echo amplitude due to the liquid helium. Below 4·2 K over 3000 echoes could be seen ; the measurements reported here were made on the 1200th echo, although ΔS was independent of echo number. Further details of the experiment and the data acquisition techniques used will be published elsewhere.

Measurements of the temperature dependence of R/ρ at 0·3 and 28 bar from 0·015 K to 1·0 K are shown in *Figure* 1. The density ρ of the liquid ^{3}He at $T = 0$ K was taken from [4], without allowing for the small temperature dependence of ρ which is less than 0·5% below 1 K [7]. The data points above 0·4 K have been corrected for a small temperature-dependent ultrasonic attenuation in the rod, which was measured separately and varied from

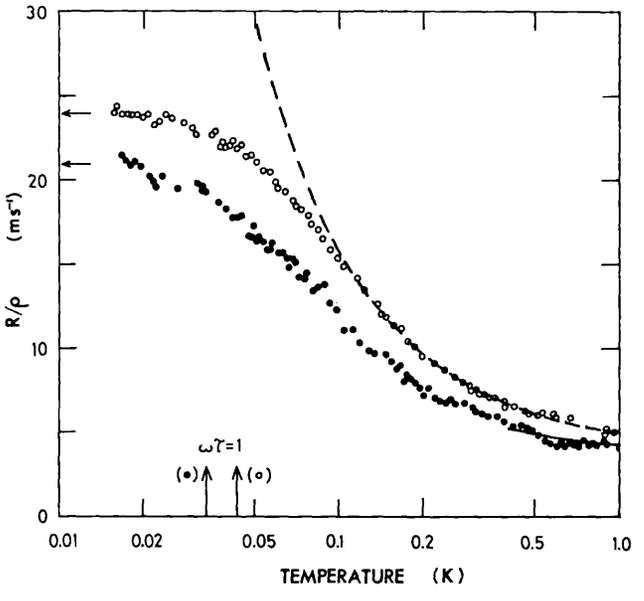

Figure 1 The temperature dependence of the transverse acoustic resistance of ^{3}He, R, measured at 240 MHz and at pressures of 0·3 bar (o) and 28·0 bar (•). The resistance is plotted as R/ρ, where ρ is the density of the liquid. The dashed line is calculated from the viscosity data of Black, Hall and Thompson [8] and the solid line similarly from McCoy *et al.* [9]. The measurements of R were fitted to each of these lines at 1·0 K. The low temperature limits (R_∞) are denoted by arrows on the ordinate scale.

0·18 ms^{-1} at 0·4 K to 2·6 ms^{-1} at 1·0 K when expressed as a correction to R/ρ. The measurements of R/ρ were taken relative to their value at 1·0 K ; the absolute values of R/ρ at 1·0 K were calculated from measurements of the viscosity η of liquid ^{3}He, using

$$R_0 = (\eta\rho\omega/2)^{1/2}, \tag{2}$$

where R_0 is the transverse acoustic resistance of the liquid in the hydrodynamic limit, $\omega\tau \ll 1$. *Figure* 1 shows R_0/ρ calculated from the semi-empiric formula for η given by Black, Hall and Thompson [8] for liquid ^{3}He under its s.v.p. above 0·05 K :

$$\eta = \frac{2{\cdot}21}{T^2} + \frac{26{\cdot}3}{T^{1/3}}. \qquad (\mu P) \tag{3}$$

The data at 0·3 bar in *Figure* 1 have been fitted to these calculations at 1·0 K where $R/\rho = 5{\cdot}12$ ms^{-1}. Direct measurements of R/ρ at 1·0 K from ΔS with and without liquid helium in the cell agree with this value, although the experimental error in ΔS, due to the detuning of the resonant cavity when the liquid is removed, is rather large. The measured temperature dependence of R/ρ at 0·3 bar is well described by *Equation* 2 from 0·2 to 2·0 K, as shown in *Figure* 1. At higher pressures, the measurements could be fitted to values of R/ρ derived from the viscosity data of McCoy *et al.* [9]. Below 0·1 K R/ρ

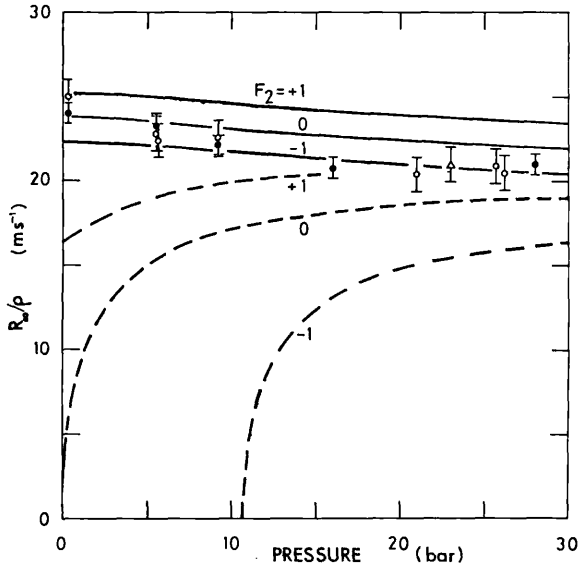

Figure 2 The pressure dependence of the transverse acoustic resistance of liquid ^{3}He at 240 MHz in the collisionless limit, R_∞, expressed as R_∞/ρ. Data were obtained by (*a*) warming from about 16 mK (●) and (*b*) cooling to about 25 mK and extrapolating to 16 mK (○). The measurement of Roach and Ketterson [5] at 23·0 bar is also shown (Δ). The results are compared with graphs computed from Flowers and Richardson [12] for $F_2 =$ 1, 0, −1 ; the solid lines are R_∞/ρ and the dashed lines are the parts ($R_\infty{}^c/\rho$) due to transverse zero sound.

deviates from the classical expression as the transition from the hydrodynamic to the collisionless regime occurs. We estimate that $\omega\tau = 1$ at 0·043 K for 0·3 bar and 0·034 K for 28 bar, from the value of $\tau_\eta T^2$ given in [4]. At the lowest temperature R/ρ tends to a temperature independent limit R_∞/ρ. Measurements were taken at various pressures up to 28·0 bar and the qualitative dependence of R/ρ on T was the same in all cases. *Figure* 2 shows the limiting values of R_∞/ρ versus pressure as derived from our data, and also the value $R_\infty/\rho = 21 \pm 1$ ms^{-1} at 23 bar from [5]. It can be seen that R_∞/ρ is only slightly pressure dependent, decreasing from 24 ± 1 ms^{-1} at low pressure to 21 ± 1 ms^{-1} at 28·0 bar.

The transverse acoustic impedance Z of a normal Fermi liquid has been calculated by Fomin [**10**] and by Flowers *et al.* [**11**] with the Landau parameter $F_2^s = 0$. Recently Flowers and Richardson [**12**] have derived Z as a function of $\omega\tau$, F_1^s and F_2^s. They show that R contains contributions of comparable magnitude from both single particle excitations and the transverse zero sound modes. Both these contributions to R become independent of temperature in the collisionless limit and so the temperature dependence of R/ρ, observed both by Roach and Ketterson and by ourselves, is not conclusive evidence for transverse zero sound. Its presence can, however, be inferred from a quantitative comparison of theory with the measurements of R. Flowers *et al.* [**11**] found that the measured temperature dependence of R/ρ at 23 bar [**5**] fitted the theory and obtained $F_2^s = -1{\cdot}0 \pm 0{\cdot}5$ from the limiting value R_∞/ρ. The temperature dependence of X/ρ, on the other hand, could not be fitted to the theory.

To analyse our data we have used the expressions (which are too complex to reproduce here) given by Flowers and Richardson [**12**] to calculate R_∞/ρ as a function of pressure for various values of F_2^s, using the values for the density ρ, the Fermi velocity v_F and F_1^s given in [**4**]. *Figure* 2 shows the calculations of both total R_∞/ρ and that part (R_∞^c/ρ) due to the transverse zero sound, for $F_2^s = 1$, 0, -1. Our data points all fall within these limits so clearly F_2^s is small at all pressures. Within our experimental errors, as shown in *Figure* 2, $F_2^s \simeq 0$ at low pressures, but above 12 bar $F_2^s = -1{\cdot}0 \pm 0{\cdot}5$, in agreement with the values derived by Flowers *et al.* [**11**] for 23 bar. We thus find that F_2^s decreases as the pressure rises, but our total change in F_2^s is somewhat less than that suggested in [**5**]. However, Fomin [**10**] has pointed out that if F_2^s is necessary then Landau parameters $F_{l>2}^s$ might be required. The theory also assumes that the scattering of quasi-particles from the solid surface is perfectly diffuse ; if the scattering were specular, then R would be zero in the collisionless regime. Experiments on the thermal conductivity of liquid ^{3}He have confirmed [**13**] that in Vycor glass the specular reflection coefficient is zero. We conclude that for $p > 12$ bar, R_∞ is dominated by the transverse zero sound, but that at low pressures the uncertainty in F_2^s implies a similar uncertainty in the existence of transverse zero sound.

Nettleton [**14**] has derived $F_2^s = -0{\cdot}34$ and $-0{\cdot}56$ from two sets of thermal conductivity data at low temperatures and zero pressure. The Landau parameters are constrained by the sum rule [**15**] :

$$\sum_l \frac{F_l^s}{1 + F_l^s/(2l+1)} + \sum_l \frac{F_l^a}{1 + F_l^a/(2l+1)} = \sum_l A_l^s + \sum_l A_l^a = 0. \qquad (4)$$

If we use the values of F_0^s, F_1^s and F_0^a given in [4] and assume that F_2^s and F_1^a are the only other significant Landau parameters, then we find that $(A_2^s + A_1^a)$ varies from $-0{\cdot}86$ at 0 bar to $-0{\cdot}64$ at 27 bar. F_1^a is difficult to determine experimentally but has been estimated variously (see [15]) as $-0{\cdot}46 \pm 0{\cdot}14$, $-0{\cdot}39 \pm 0{\cdot}14$, $-0{\cdot}15 \pm 0{\cdot}3$ at 0 bar and $+0{\cdot}2 \pm 0{\cdot}6$ at 27 bar. The sum rule would then give respectively $F_2^s = -0{\cdot}30 \pm 0{\cdot}17$, $-0{\cdot}38 \pm 0{\cdot}16$, $-0{\cdot}62 \pm 0{\cdot}26$ at 0 bar and $-0{\cdot}9 \pm 0{\cdot}4$ at 27 bar. These estimates are in reasonable agreement with the present measurements and with all other experimental data, with the sole exception of the measurements of longitudinal acoustic impedance. Brooker [2] found that the measurements of Wilks and his co-workers [6] in the collisionless limit could only be fitted to Landau theory with F_2^s of 3·4 at 12·55 atm and 14·8 at zero pressure. These anomalously large values of F_2^s suggest that a different explanation must be found for the longitudinal impedance data, especially as the longitudinal transmission data [16] is consistent with $F_2 \simeq 0$ at 0·3 bar. Our conclusions are based on the correctness of Table V of Wheatley [4] and Wölfle [17] has pointed out that the m^* values given there may be an overestimate at high pressures. He calculated, for example, from other experimental data that at $p = 21$ bar, $F_2^s = 0{\cdot}4$, but if we use his lower value of $m^*/m = 4{\cdot}9$ at 21 bar, our value of F_2^s becomes $-1{\cdot}2$ instead of $-1{\cdot}0$, well within our experimental error.

Acknowledgments

We are grateful to A. K. Betts, F. A. Grimes, A. W. King and A. O. T. le Mottee for technical assistance and to A. J. Cooper for computer calculations. We would like to thank D. S. Betts, J. P. R. Bolton, I. A. Fomin and P. M. Lee for helpful discussions.

References

1 Landau L D *Zh Eksp Teor Fiz* **32** 59 (1957) (*Sov Phys JETP* **5** 101 (1957)).
2 Brooker G A D Phil thesis University of Oxford (1964) ; *Proc Phys Soc* **90** 397 (1967).
3 Fomin I A *Zh Eksp Teor Fiz* **54** 1881 (1968) (*Sov Phys JETP* **27** 1010 (1968)).
4 Wheatley J C *Rev Mod Phys* **47** 415 (1975).
5 Roach P R and Ketterson J B *Phys Rev Lett* **36** 736 (1976).
6 Wilks J *The Properties of Liquid and Solid Helium* (Clarendon, Oxford, 1967).
7 Boghosian C, Meyer H and Rives J E *Phys Rev* **146** 110 (1966).
8 Black M A, Hall H E and Thompson K *J Phys C* **4** 129 (1971).
9 McCoy R J, Steinback M, Lyden J K and Guernsey R W *Proc 14th Intern Conf Low Temp Phys* (North Holland, Amsterdam, 1975) **1** 80.
10 Fomin I A *Pis'ma Zh Eksp Teor Fiz* **24** 90 (1976).
11 Flowers E G, Richardson R W and Williamson S J *Phys Rev Lett* **37** 309 (1976).
12 Flowers E G and Richardson R W. To be published.
13 Betts D S, Brewer D F and Hamilton R S *J Low Temp Phys* **14** 331 (1974).
14 Nettleton R E *J Low Temp Phys* **24** 275 (1976).
15 Baym G and Pethick C in Bennermann K H and Ketterson J B (Eds) *The Physics of Liquid and Solid Helium* (Wiley, New York, 1976).
16 Abel W R, Anderson A C and Wheatley J C *Phys Rev Lett* **17** 74 (1966) ; Wheatley J C *Prog Low Temp Phys* Vol 6 77 (1970).
17 Wölfle P *Phys Rev* **B14** 89 (1976).